Old Dominion University Research Foundation

DEPARTMENT OF AEROSPACE ENGINEERING
COLLEGE OF ENGINEERING & TECHNOLOGY
OLD DOMINION UNIVERSITY
NORFOLK, VIRGINIA 23529

LARGE ANGLE MAGNETIC SUSPENSION TEST FIXTURE

Principal Investigator: Colin P. Britcher

Final Report
For the period ended October 31, 1995

Prepared for
National Aeronautics and Space Administration
Langley Research Center
Hampton, VA 23681-0001

Under
NAG-1-1056
Nelson J. Groom, Technical Monitor
FDCD-Spacecraft Controls Branch

November 1995

DEPARTMENT OF AEROSPACE ENGINEERING
COLLEGE OF ENGINEERING & TECHNOLOGY
OLD DOMINION UNIVERSITY
NORFOLK, VIRGINIA 23529

LARGE ANGLE MAGNETIC SUSPENSION TEST FIXTURE

Principal Investigator: Colin P. Britcher

Final Report
For the period ended October 31, 1995

Prepared for
National Aeronautics and Space Administration
Langley Research Center
Hampton, VA 23681-0001

Under
NAG-1-1056
Nelson J. Groom, Technical Monitor
FDCD-Spacecraft Controls Branch

Submitted by the
Old Dominion University Research Foundation
P.O. Box 6369
Norfolk, Virginia 23508-0369

November 1995

ACKNOWLEDGMENTS

In lieu of a final report for the research project entitled "Large Angle Magnetic Suspension Test Fixture" for the period April 1, 1995 through October 31, 1995, a compilation of three reports are included herein. The three reports are: 1) "Design and Implementation of a Digital Controller for a Magnetic Suspension and Vernier Pointing System," by Daniel J. Neff, submitted as his Master's thesis, August 1995; 2) "Influence of Eddy Currents on the Dynamic Characteristics of Magnetic Suspensions and Magnetic Bearings," by Colin P. Britcher, submitted for consideration by the IEEE Transactions on Control System Technology, submitted September 1995; 3) "Design and Implementation of a Digital Controller for a Magnetic Suspension and Vernier Pointing System," by Daniel J. Neff and Colin P. Britcher, submitted for presentation at the 3rd International Symposium on Magnetic Suspension Technology, December 1995. The work for this project was supported by the NASA Langley Research Center through NAG-1-1056, Nelson J. Groom, Technical Monitor, FDCD-Spacecraft Controls Branch, NASA Langley Research Center, Mail Stop 161.

Design and Implementation of a Digital Controller for a Magnetic Suspension and Vernier Pointing System

By

Daniel J. Neff
B.S. August 1992, Mechanical Engineering
Old Dominion University

A Thesis Submitted to the Faculty of Old Dominion University in Partial Fulfillment of the Requirements for Degree of

MASTER OF SCIENCE
AEROSPACE ENGINEERING
Old Dominion University
August, 1995

Approved by

Colin P. Britcher (Director)
Colin P. Britcher
Brett A. Newman
Brett Newman
Jen K. Huang
Jenkuang Huang

Abstract

This thesis will present the study of an Annular Suspension and Pointing System (ASPS) developed in the mid 1970's for space viewing experiments. In the early 1970's, a need was established to develop a multi-purpose experiment mounting platform. The first prototype of the ASPS was developed for NASA Langley Research Center by Sperry Flight Systems (now Honeywell Satellite Systems). The prototype was delivered to NASA Langley in 1983, but was never assembled due to a shift in priorities. In late 1992 the ASPS hardware was loaned to Old Dominion University (ODU) in hopes that the system would be recommissioned. The ASPS consists of several sub-systems, but the Vernier Pointing Assembly (VPA) that utilizes magnetic suspension to provide noncontacting isolation and vernier pointing of the payload is the main focus of this research. Modification of the magnetic actuators, also referred to as the Magnetic Bearing Assemblies (MBA), a component of the VPA, has been made in such a way that the system can now be tested in a one-g environment without the elaborate testing fixture (a gravity offload). Development of new up-to-date control hardware and software has been achieved. Verification of the hardware design has been performed by fully controlling the iron rotor in five degrees-of-freedom using a proportional plus derivative controller. This thesis will give a brief description of the existing systems, and will cover the steps taken to develop the new hardware and software that controls the Vernier Pointing Assembly of the ASPS.

Acknowledgments

I think the best way to thank everyone that made this possible is to start at the beginning. First I would like to thank my parents for giving me the opportunity to go to college. I will be forever indebted to them. Next I would like to thank Robert Ash for insisting that I pursue a graduate degree and for giving me a wonderful teaching assistantship job to get me started. I would like to say that I enjoyed working with Colin Britcher, and I would like to thank him for giving me this challenging research project; and also for all his help over the semesters. I would like to thank Jen Huang and Brett Newman for reviewing my work. Last but not least I would like to thank all my friends that have supported me through out my seven year tour at ODU.

This project was supported by NASA grant NAG-1-1056, technical monitor Nelson J. Groom.

Table of Contents

List of Tables

List of Figures

Chapter 1

Introduction

The Annular Suspension and Pointing System (ASPS) is a precision payload pointing system designed for use aboard the space shuttle. In the early 1970's, NASA's Earth-Orbital Systems Technology group established a need to develop a multi-purpose experiment mounting platform to meet the needs of solar, stellar, and earth viewing experiments planned for the 1980's. The ASPS concept evolved, with the objective of meeting this need. The prototype used in this process was developed for NASA Langley Research Center by Sperry Flight Systems (now Honeywell Satellite Systems). The prototype was delivered to NASA Langley Research Center in 1983, but was never assembled due to a shift in priorities. In late 1992 the ASPS hardware was loaned to Old Dominion University with the intention that the system would be recommissioned.

1.1 General Description of ASPS

The ASPS consists of several systems, the Payload Mounting Plate, the Vernier Pointing Assembly, two Coarse Gimbal Assemblies, a Mounting and Jettison Assembly, a Control Electronics Rack, Balance and Testing Fixture, and assorted connection hardware, as shown in Figure 1.1. The payload mounting plate forms a removable base plate for mounting and aligning experiments prior to installation on the ASPS. The Vernier Pointing Assembly (VPA) contains the annular iron rotor that supports the payload mounting plate. The annular rotor has a cross-section of an L shape. The vernier pointing assembly also contains a roll axis drive, also referred to as the roll torque motor, which provides unlimited rotational motion about the payload's longitudinal axis, in other

words, the axis perpendicular to the payload plate. Finally, the vernier pointing assembly contains five magnetic actuators (magnetic coils) that provide attractive magnetic forces to suspend the annular iron rotor in five degrees-of-freedom. The magnetic actuators are also referred to as the Magnetic Bearing Assemblies (MBA). The axial magnetic bearing

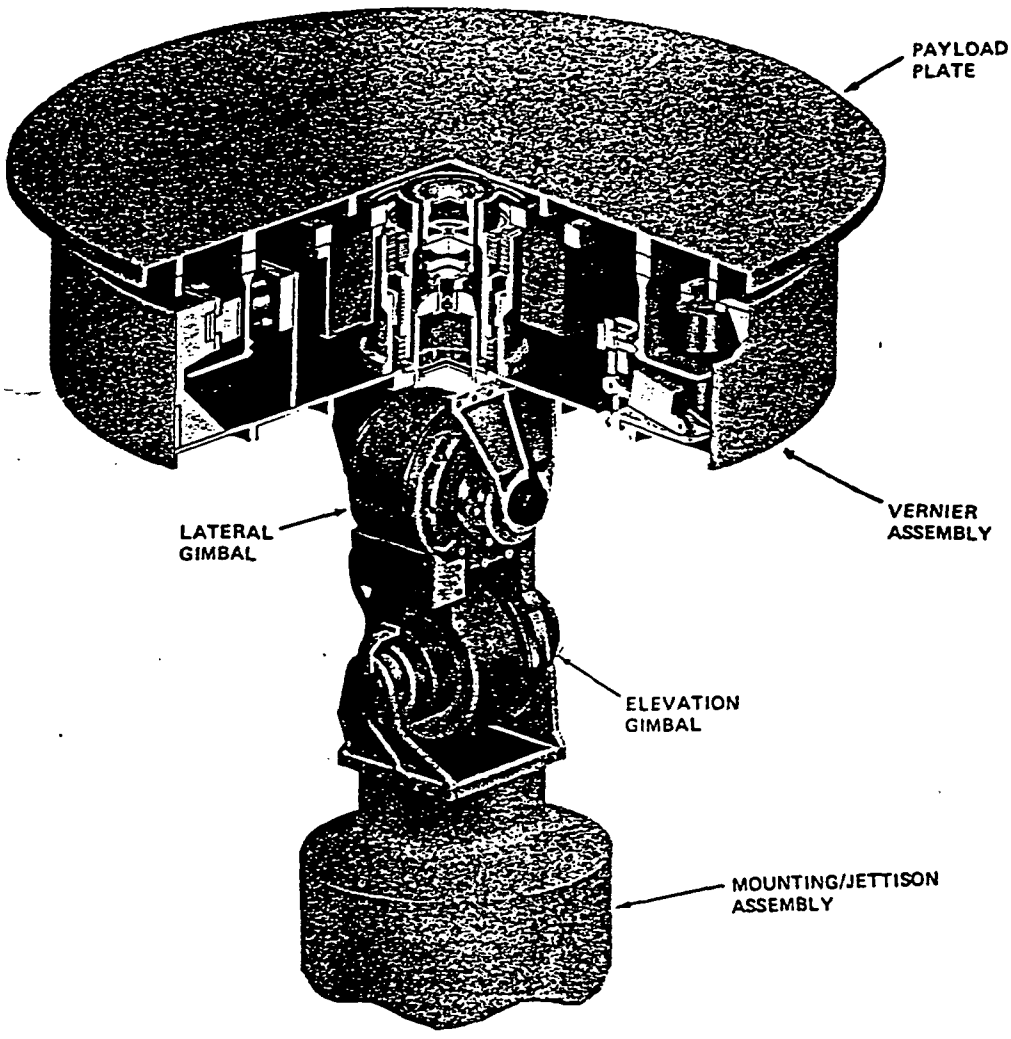

Figure 1.1 Annular Suspension and Pointing System

assemblies controls the payload rotation of $\pm .75$ degrees about axes in the plane parallel to the payload mounting surface, and also the vertical displacements of the payload. The radial magnetic bearing assemblies control the centering of the payload about the axis

normal to the payload mounting surface. The two coarse gimbal assemblies are stacked to form an elevation and a lateral gimbal pair. Design of the gimbal mounting bracket and gimbal mounting structure is such that it provides a mechanically limited travel of ± 100 degrees (from vertical) along the lower elevation gimbal axis, and ± 60 degrees about the upper lateral gimbal axis. The mounting and jettison assembly supports the coarse gimbals and also contains pyrotechnics to jettison the ASPS (and payload) in the event of a multiple failure which prevents stowage in orbit. The control electronics rack is an assembly of analog circuits made up of power amplifiers and data acquisition to control the vernier pointing assembly. The power amplifiers supply power to the magnetic bearing assemblies and the roll torque motor. The balance and testing fixture is a gravity off-load used to simulate a zero-gravity environment. The apparatus consists of a counter-balancing system to unload the payload mounting plate and vernier pointing assembly in an attempt to simulate orbiter conditions.

Magnetic suspension is utilized in the vernier pointing assembly to provide noncontacting isolation and vernier positioning of the payload. Three axial magnetic bearing assemblies provide axial translation and vernier pointing about the transverse axis, and two radial magnetic bearing assemblies provide radial centering of the annular iron rotor. Proximity sensors associated with each magnetic bearing assembly measure the position of the suspended rotor. This information can then be fed back to the controller to provide a force/displacement characteristic for each magnetic actuator. The proximity sensors are also combined together to determine the orientation of the payload. The focus of this research will be on the vernier pointing assembly and its components.

1.2 Hardware Status

At the beginning of this research the hardware had not even been looked at for several years. When the hardware was delivered to ODU it was partially disassembled. Reassembly of some of the components was difficult due to the lack of documentation.

The vernier pointing assembly, the controls electronics rack , and the testing and balancing fixture were the only systems loaned to ODU. The other components that were mentioned were not fully developed, or are in use at a different location. The vernier pointing assembly was basically complete. The controls electronics rack was missing the main power supply, and some of the electronic cards were not functioning properly. Also, there was not much documentation of the control system to be found. The Balance and Testing fixture was present, but most of its components were disassembled for storage and transportation. This system has not been reassembled at this time. The control electronics rack has been replaced with new up-dated hardware, and the vernier pointing assembly has been recommissioned.

1.3 Project Goals

The main focus of this research was to concentrate on recommissioning the vernier pointing assembly. The first goal was to develop the necessary hardware and software to be able to convert the system from an analog controller to a digital controller. The next goal was to implement a proportional plus derivative controller using the new digital processor. The final goal was to magnetically suspend the annular iron rotor against gravity in five degrees-of-freedom.

1.4 Thesis Outline

The organization of this thesis is as follows. Chapter 2 will give a detailed description of the multiple systems that make up the ASPS. As mentioned in the introduction the vernier pointing assembly is the main focus of this thesis. The design of the vernier pointing assembly is given in Section 2.2. The other sections in Chapter 2 are dedicated to describing the other systems that make up the ASPS. Chapter 3 is included to give a comparison between the two different types of control. The original approach of

controlling the vernier pointing assembly used an analog computer; the new approach is to use a digital processor. Again this chapter is to give the reader a brief understanding of the old and new design approaches. Chapter 4 will cover some of the previous design changes made to the ASPS. Chapter 5 is devoted to developing a mathematical model of the systems that make up the controller and plant of the system. Two methods of determining the force to gap relationship are used to verify correctness of the mathematical model. The method of developing the PD controller is also covered in this chapter. Chapter 6 covers the steps taken in developing the new controller hardware and software used to suspend and control the rotor in five degrees-of-freedom. Chapter 7 shows some experimental results to demonstrate that the system works. Then some concluding remarks and recommendations for future work are given in Chapter 8.

Chapter 2

Component Description

This chapter will give more detail of each of the major components of the Annular Suspension and Pointing System (ASPS). The ASPS, shown in Figure 2.1, is a precision payload pointing system designed for use on the space shuttle. Experiments of virtually any size may be accommodated by mounting the experiment to the payload mounting plate. The magnetic actuators were sized to accept payloads weighing up to 600 kg with a center of mass positioned up to one and one half a meter above the payload mounting plate [1]; however the magnetic actuators have since been modified to work in a gravity environment as will be discussed shortly. The ASPS consists of a payload mounting plate, a vernier pointing assembly, two coarse gimbal assemblies, a mounting and jettison assembly, a control electronics rack, balance and testing fixture, and assorted connection hardware. The vernier pointing assembly is the main focus of this research and will be discussed in more detail in section 2.2.

2.1 Payload Mounting Plate

The experiment attaches directly to the removable payload mounting plate. The payload mounting plate is a 965.2 mm diameter and 22.2 mm thick machined aluminum structure which normally mounts to the vernier pointing assembly. The weight of the payload plate is 12.02 kg. In the event that the vernier pointing assembly is not necessary during flight the payload mounting plate can be mounted directly to the gimbal mounting platform. Attachment of the payload mounting plate to the vernier pointing assembly is

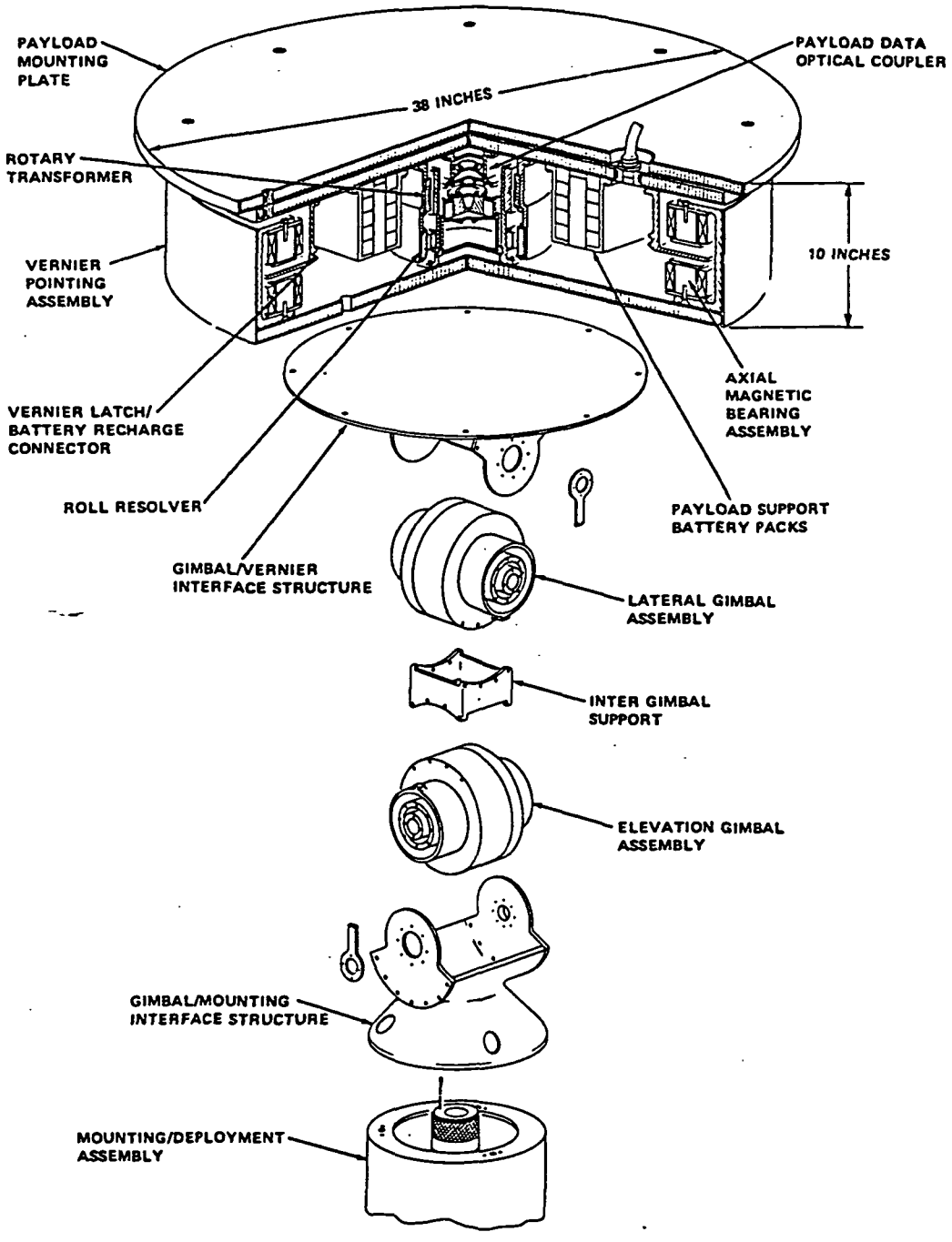

Figure 2.1 ASPS Component Breakdown

via a series of twelve 1/4-20 fasteners spaced at 30 degree intervals around the annular iron rotor of the vernier assembly.

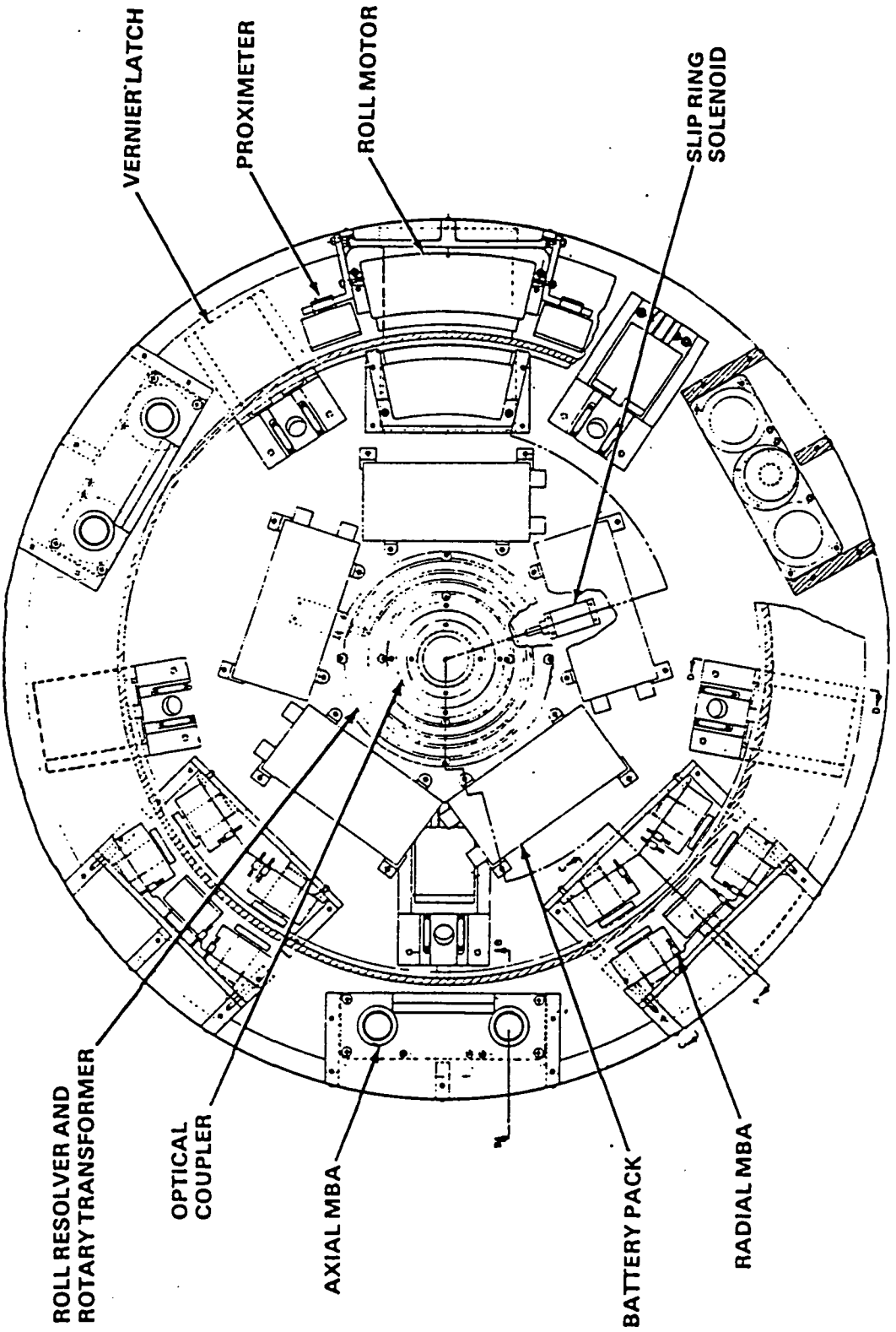

Figure 2.2 The Vernier Pointing Assembly

2.2 Vernier Pointing Assembly

The vernier pointing assembly provides the ASPS with its high resolution pointing capability. The vernier pointing assembly is made up of an annular iron rotor, three axial magnetic bearing assemblies, two radial magnetic bearing assemblies, roll motor, seven proximity sensors, five vernier latches, roll resolver, rotary transformer, and battery packs as shown in Figure 2.2. The battery pack system was not fully developed and is explained in more detail in reference [1]. The three axial magnetic bearing assemblies, two radial magnetic bearing assemblies and roll motor actively control the six degrees-of-

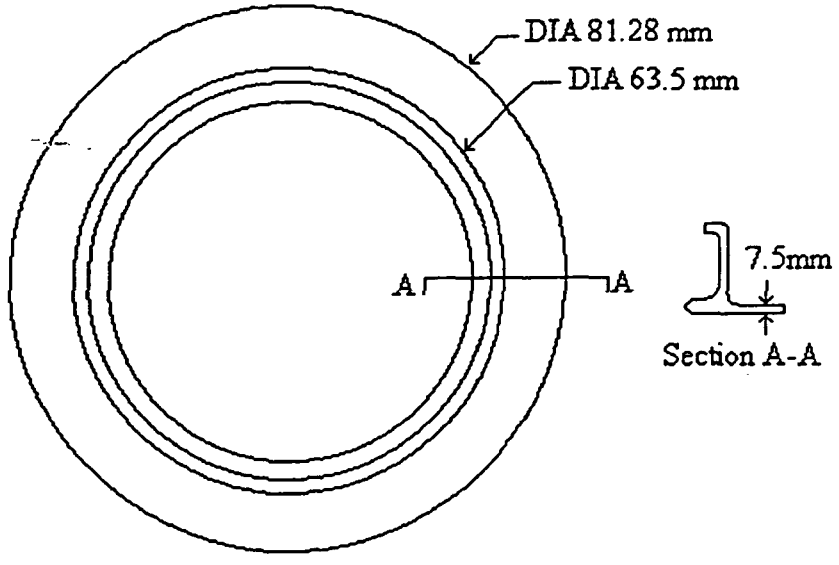

Figure 2.3 Dimensions of iron rotor.

freedom of the annular iron rotor. The dimensions of the rotor are shown in Figure 2.3 and also in Appendix A. The three axial magnetic bearing assemblies control axial translation and angular rotation of the payload about two axis. The axial magnetic bearing assemblies are spaced at 120 degree intervals about the vernier baseplate. The two radial magnetic bearing assemblies control the lateral position of the payload. The radial magnetic bearing assemblies are located 90 degrees apart and are ± 45 degrees from the

reference magnetic bearing assembly. The roll motor controls the sixth degree-of-freedom about the axis perpendicular to the payload plate. The roll motor is located directly opposite the reference magnetic bearing assembly. The annular iron rotor is magnetically suspended in the transverse and lateral directions by the magnetic bearing assemblies. The axial magnetic bearing assemblies react against the radial flange and the radial magnetic bearing assemblies react against the cylindrical surface of the annular iron rotor. The displacements of the rotor are sensed by proximity sensors. Each axial and radial magnetic bearing assembly has a pair of proximity sensors incorporated into its design. The roll motor has two paired proximity sensors to assist in compensating for torque produced by the roll motor. The roll motor is a segmented two-phase solid iron rotor ac linear induction motor which controls the roll about the axis perpendicular to the payload plate.

2.2.1 Magnetic Bearing Assembly

The electrical and mechanical descriptions of the magnetic bearing assembly for both the axial and radial assemblies are contained in Figures 2.4 and 2.5. The force capacity of the axial and radial magnetic bearing assemblies were ± 28.9N* and ± 14.2N respectively. The operating range of the axial and radial assemblies were ± 5.6mm and 5.1mm respectively. The magnetic actuators consist of a wire-wound magnetic coil and a core material manufactured out of 50% Nickel-Iron. The magnetic coils for the axial and radial magnetic bearing assemblies are made up of two windings each. The axial and radial magnetic coils are wound with 810 ± 1 turns of #20 AWG, HML insulated copper wire and 863 ± 1 turns of #22 AWG, HML insulated copper wire respectively. As previously stated the axial magnetic bearing assemblies react against the horizontal of the iron rotor which runs circumferentially under the payload mounting surface at a

*The axial MBA's have had the gap modified from a nominal gap of 7.6mm to 4.31mm in order to suspend the rotor in a one-g enviornment.

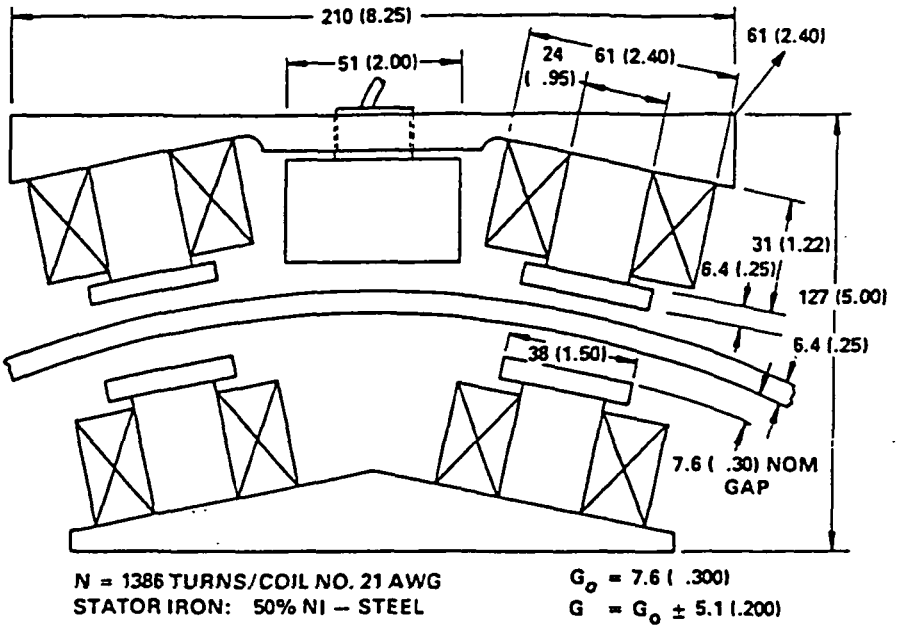

Figure 2.4 Radial magnetic bearing assembly.

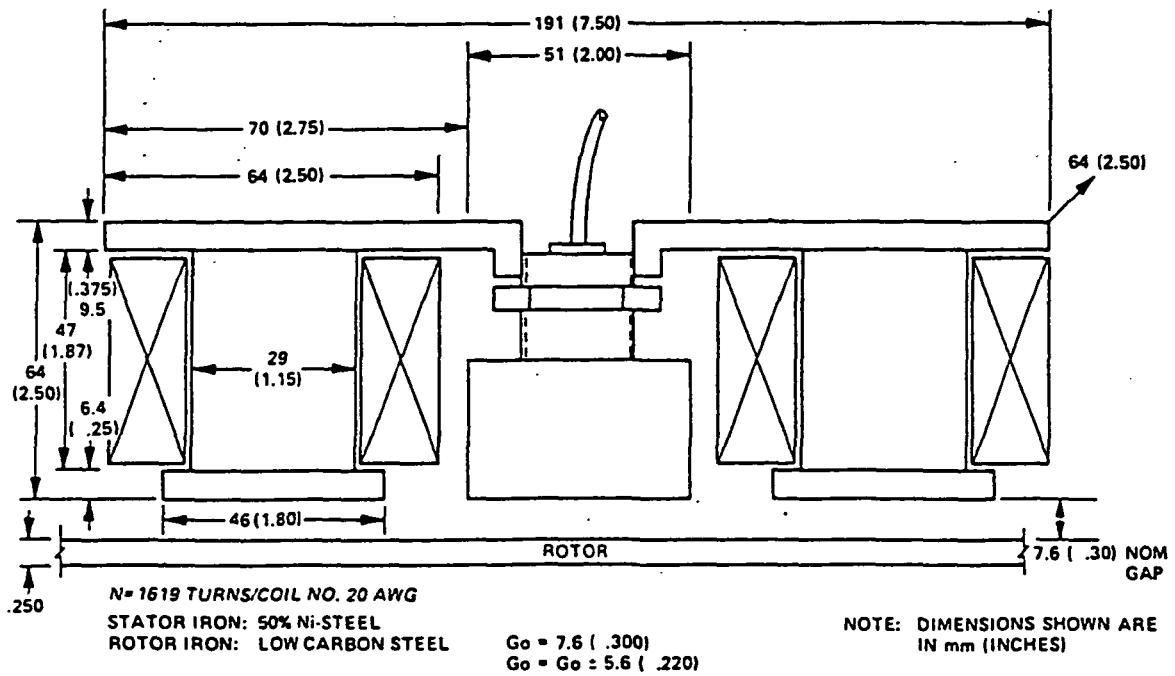

Figure 2.5 Axial magnetic bearing assembly.

radial distance of .362 meters. The radial magnetic bearing assemblies are spaced 90 degrees apart and provide radial centering of the iron rotor. Each axial and radial magnetic bearing assembly are paired with a proximity sensor to provide gap compensation for centering the payload. Appendix A contains more information about the detail dimensions of the magnetic bearing assemblies.

2.2.2 Proximity Sensors

The proximity sensors used on the ASPS were developed by Kaman Instrumentation. These noncontacting position sensors use the principle of impedance

PARAMETER	DESCRIPTION
RANGE:	25.4mm (1.01 IN)
LINEARITY:	<.2 PERCENT FULL SCALE
BANDWIDTH:	20 KHz
REPEATABILITY:	.05%
NOISE:	<.3 MILLIVOLTS
SENSITIVITY:	ADJUSTABLE UP TO .254V/M (10V/INCH)
OPERATING TEMP RANGE:	−55° C TO +75° C
INPUT POWER:	±12 VDC, 70 MA
SENSOR DIMENSIONS:	
OUTER DIAMETER:	50.8mm (2.000 IN.)
LENGTH:	32.4mm (1.274 IN.)
VENDOR:	KAMAN SCIENCES CORPORATION
TARGET MATERIAL:	NICKEL

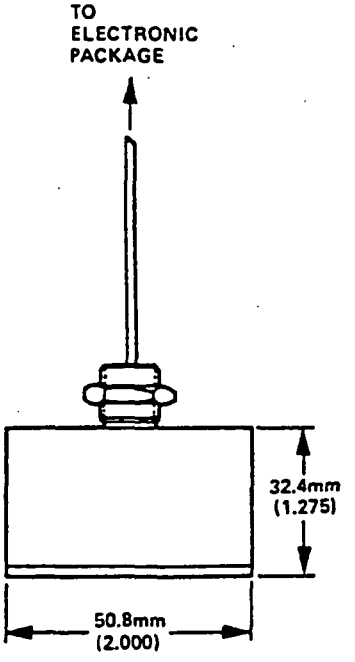

Table 2.1 Proximity sensor characteristics.

caused by eddy currents that are induced in the conductive target by the sensor coil. Table 2.1 is a list of sensor characteristics. The coil in the sensor is driven by a 10 MHz crystal-controlled oscillator. Excitation of the sensor coil generates an electromagnetic field that couples with the target. The gap between the sensor and target affects the strength of the electromagnetic coupling. The changing gap causes the impedance of the coil to vary,

which unbalances the bridge network in the electronic package. The magnetic bearing assemblies use two sensors one on each side of the iron rotor. The signals from each sensor are then differenced and converted into an analog signal. The electronic package is mounted on the vernier pointing assembly under the radial magnetic bearing assembly. The electronic assembly consists of an oscillator and demodulator card. Appendix B shows the wiring diagram and parts list for each card.

2.2.3 Roll Motor

The roll motor used on the ASPS is an AC Linear Induction motor that works on the principle that the flux wave generated in the stator sets up circulating currents in the iron rotor which in turn generate a counter-flux field lagging the stator-flux field and thereby generates torque [1]. The motor design also contains proximity sensors to permit compensation for the radial attractive forces produced in the two motor segment windings. The roll motor produces a maximum of 0.677 Nm of torque in its high excitation mode of operation. The radial forces associated with the maximum torque are less than 1.56 N. The complete unit weighs 1 kg. Figure 2.6 and Table 2.2 show a description of the design used for the roll torque motor.

2.2.4 Vernier Latches

The five vernier latches are located on the baseplate of the vernier pointing assembly and are used to support the iron rotor during launch and recovery maneuvers. The latches locate and lock the rotor into the center position. Locking the rotor down with the vernier latches prevents damage to the magnetic bearing assemblies, proximity sensors, and data transfer electronics during maneuvering. In the event that the magnetic bearing assemblies fail, the vernier latches can be used to center the ring. With the latches locking the ring into the middle the system can still be used in coarse pointing mode by

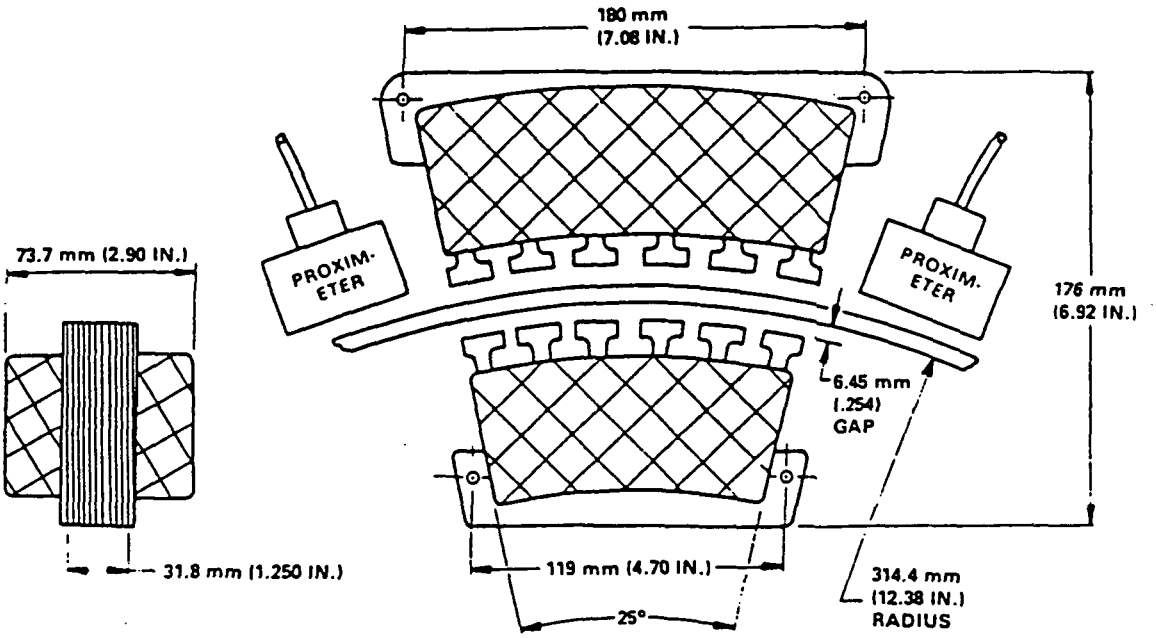

Figure 2.6 Roll Axis Torque Motor Design Description

PARAMETER	DESCRIPTION	
TYPE	AC INDUCTION MOTOR, SOLID IRON ROTOR WITH NICKEL AND COPPER PLATE	
CONFIGURATION	• TWO SEGMENTED STATORS • RADIAL MAGNETIC GAP OF 6.78 mm (0.267 IN.) • LOCATED FOR ZERO 1st ORDER RADIAL FORCE • PASSIVE ROTOR • INTEGRAL GAP SENSORS • RADIAL FORCES ELECTRONICALLY COMPENSATED • TWO LEVEL EXCITATION	
EXCITATION FREQUENCY	200 HERTZ	
POLES	48	
WEIGHT	9.1 Kg (20 LBS)	
	LOW EXCITATION	HIGH EXCITATION
PEAK TORQUE	0.027 NM (0.02 FT-LBS)	0.677 NM (.05 FT-LBS)
PEAK POWER	<4 WATTS	<100 WATTS
STANDBY POWER	<2 WATTS	<50 WATTS
COGGING AND RIPPLE TORQUE	<.03% 0 – PK	<.03% 0 – PK
HYSTERESIS	NEGLIGIBLE	NEGLIGIBLE
RADIAL FORCES (COMPENSATED)	< .089 N (.02 LBS)	< 1.56 N (.35 LBS)*
LEAKAGE FLUX (AT 12 INCHES)	<.02 GAUSS	<0.1 GAUSS

*UNCOMPENSATED: 3.5 POUNDS/SEGMENT

Table 2.2 Roll Motor Description

using the coarse gimbal assemblies. Detailed drawings of the vernier latching mechanism can be seen in Appendix C.

2.2.5 Roll Resolver and Rotary Transformer

The roll resolver and rotary transformer are located at the center of the vernier pointing assembly. Both designs use noncontacting methods to measure angular position and transfer power. The roll resolver is used to measure the angular rotation and position of the payload. The roll resolver uses motor-like components whose basic structure consists of a wound rotor and wound stator, concentrically arranged to provide a variable mutual coupling between the windings of the two members [1]. The resolver windings are spaced at 90 degrees phasing from each other. Reference 1 contains more information about the design of the roll resolver used on the ASPS. The rotary transformer is used to transfer power between the stationary base of the vernier pointing assembly and the payload. The power transfer is completed using a noncontacting method. The conceptual design of the rotary transformer for the ASPS is discussed in more detail in Reference 2.

2.3 Coarse Gimbal Assembly

The ASPS uses two coarse gimbal assemblies stacked one on top of the other. Each coarse gimbal assembly contains a permanent magnet, brushless two-phase DC torquer motor, a multi-speed wound rotor resolver for communication of the torquer drive signal, and a single-speed wound rotor resolver for position readout and control of the gimbal angle. Since both the elevation and lateral gimbals have limited rotational freedom the electrical connections are carried across the rotating gimbals through flex cables. Duplex gimbal bearing pairs are used in each gimbal assembly in a fixed/floating cartridge arrangement [1]. The Coarse Gimbal Assembly has been in use at the Marshall Spaceflight Center in Huntsville, Alabama [3].

2.4 Mounting and Jettison Assembly

The mounting and jettison assembly supports the coarse gimbal assembly and contains pyrotechnics to jettison the ASPS and payload in the event that the system should have multiple failures and stowage problems. The mounting assembly also contains a separate motor driven device mounted inside the assembly to mechanically disconnect the gimbal mechanical structure from the mast during the launch or the landing phase. This prevents loading of the gimbals when the payload is restrained by its launch locks.

2.5 Control Electronic Rack

The control electronic rack is a free standing rack that connects to the vernier pointing assembly through flexible cables. This assembly was for laboratory test purposes only. The electronic assembly contains the necessary hardware to drive the actuators, position sensors, and roll motor of the vernier pointing assembly. The control assembly is a system made up of analog circuits that use analog inputs made via the front panel of the control rack. Appendix D shows a the rack assembly layout. These inputs are used to change the system parameters that control the lateral and translational position of the iron rotor. Currently, this system is not working due to its outdated technology and lack of documentation. One of the goals of this research is to replace this system with up-to-date electronic systems. By replacing this system with off-the-shelf items the system can be designed in such a way that it will ensure its maintainability. The new control electronics rack will be discussed in more detail in Chapter 6.

2.6 Balance and Testing Fixture

The balance and testing fixture was used to simulate a zero-gravity environment. The apparatus consists of a counter-balancing system to unload the payload mounting plate and vernier pointing assembly in an attempt to simulate orbiter conditions. In the first stages of the testing there was difficulty in sorting out the dynamics of the test setup

and the hardware being tested. Significant advances were made in the zero-gravity suspension techniques employed, and after several modifications, the test fixture became sufficiently transparent in the data. Tests using the testing fixture were performed on servo dynamics, decoupling control, stability during cross-axis disturbances, and a variety of other parameters [4]. This system was loaned to Old Dominion University, but has not been recommissioned because inadequate space was available in the laboratory. Reference 3 contains more information on the balancing and testing fixture.

Chapter 3

Operating Philosophy

This chapter is written to give the reader a feel for the difference between analog controllers and digital controllers. The old controller used an analog computer to relate inputs and outputs in order to control the vernier pointing system. The new controller is a digital computer that changes analog inputs to digital format, and then processes the information while converting the final digital signal to an analog output. Digital computers have the advantage of being able to processing non-linear information more easily while analog computers need complex circuitry to complete non-linear calculations. Although this is true a non-linear controller will not be developed at this time.

3.1 Analog

In their day analog computers were very powerful machines and they are still used today in many control applications. Analog computers still play a part in the teaching of control system design. To this day, industry still uses analog computers to perform simulation and control of mechanical systems. An analog computer solves problems by solving analogous problems patched on electronic circuits. The term "patched" is used here to mean wires or connectors between the different circuit items that make up the analog computer. Two systems or problems can be analogous if all or certain elements that are measurable obey the same mathematical relationship [5]. Most general purpose analog computers use an active electrical circuit as the analogous system because it has no moving parts, good accuracy, a high speed of operation, and a high degree of versatility. The active electrical system consists of resistors, capacitors, and operational amplifiers.

When these circuits are connected together they are capable of simulating linear systems. This is because the voltage transfer characteristics of these electrical components are analogous to the basic linear mathematical operation encountered in a mechanical model. Analog computers can handle non-linear system with the use of diode function generators and special circuits which have non-linear voltage transfer characteristics.

The mathematical model of the physical system is functionally identical to the mathematical model of an analog computer that is used to simulate it. The voltage transfer characteristics of the electrical circuits are analogous to the desired mathematical operation. The corresponding mathematical variables of the problem are analogous to the input and output voltages to the computer. It is important to realize that the output of an analog computer is simply a voltage waveform whose time dependency is the same as that of the desired variable. The normal procedure for simulating a system starts with determining a mathematical model describing the physical system. Then an analogous block diagram of the electrical connections is made of the mechanical system. Once the electrical system is connected on the analog computer the computer is operated and the variables are recorded.

The analog controller originally used to control the vernier pointing system is now out of date by today standards. Digital computers are now fast enough to perform the mathematical calculations along with the analog conversion.

3.2 Digital

The speed and accuracy of digital computers over the last decade has increased dramatically. Now that digital computers are sufficiently fast it is no longer necessary to convert the mathematical equation to an analogous electrical system to perform calculations. The mathematical calculations performed by the digital processor allow non-linear systems to be implemented much more readily than with an analog processor, hence making the problem simpler to control. Since the digital computer cannot perform

calculations without analog inputs, the digital computer must first convert the analog signals sent from the experiment into usable digital signals. To do this an analog-to-digital converter must be installed into the digital computer in order for the analog signal to be converted to digital form. Once the analog signals are converted to digital signals they can be processed by the digital processor. Then a converter is necessary to convert the final digital output to a usable analog signal, thus eliminating the need to design complex analog circuitry to complete the task. Another advantage of digital processors is that they have the ability to implement adaptive control algorithms. The basic idea of adaptive control is to change the values of the gains or other parameters in the control law according to some on-line algorithm. In this way the controller can "learn" an appropriate set of parameters during the course of its operation [6]. Another advantage of a digital processor is that it has the ability to perform multiple input and multiple output control algorithms. Possibly the best advantage to using a digital process is its ability to be modified without painstaking hours of rewiring hardware. Once the programming language being used to program the digital controller is understood, modification can be made simply by modifying the controller algorithm. This is by far the greatest advantage of a digital processor.

Chapter 4

Previous Modifications

In 1992 when the ASPS was delivered to Old Dominion University, the status of the hardware was unbeknownst to the people who unpacked the system. Most of the systems described above were located, and organization of the sub-systems began. Several undergraduate design teams began work by trying to assemble the system components into their respective order. Documentation of how the ASPS was to be assembled was not easily found. The student groups searched through numerous old reports in order to gain an understanding of how the system operated.

4.1 Modifications to the Magnetic Bearing Assembly

Recommissioning the ASPS started with examining the vernier pointing assembly. The vernier pointing assembly was the main focus in early stages of study and still is today. Along with the ASPS system came an elaborate counter-balancing and test fixture used to simulate a zero-gravity environment. The system was not assembled due to a lack of available lab space. An alternative to this was to modify the vernier pointing assembly to operate in a one-g environment. To accomplish this the gap between the magnetic actuators and the iron rotor was reduced by 54.5% such that the magnetic actuators could suspend the rotor against gravity. This was a much simpler solution then to try and recommission the counter-balancing system at that time. The amount of current needed to suspend the rotor at the new gap was directly measured by supplying the magnetic bearing assembly actuators with the required power. Once it was determined that the new gap would not cause an over-heating problem of the magnetic coils the modification to the

magnetic actuators was made. The top plates as shown in Figure 4.1 were remanufactured with a thickness change from 6.35 mm to 9.53 mm. This new thickness would extend the core material of the magnetic bearing assembly, and reduce the air gap between the top plate and the iron rotor from 7.62 mm to 3.41 mm. The top plate attaches to the post with two fasteners. The post is also shown in Figure 4.1. The radial magnetic bearing assemblies were not modified. Appendix A contains more information on the various parts of the magnetic bearing assembly.

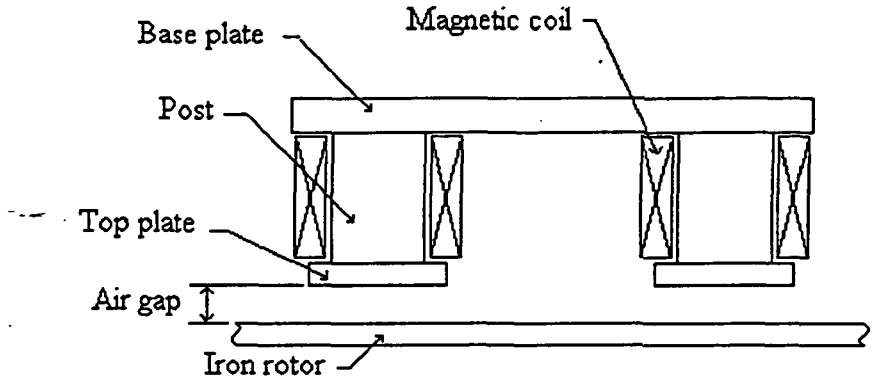

Figure 4.1 Magnetic Bearing Assembly.

4.2 Switching from Analog to Digital

Once the magnetic bearing assemblies were modified to work in a one-g environment it was time to look at recommissioning the control electronic rack. Once the necessary components of the electronic assembly rack were located, the system was powered up in an attempt to suspend the iron rotor at one magnetic bearing assembly. Several unsuccessful attempts were made to try and get the analog controller to work. It was then decided that only the necessary systems needed to power the magnetic bearing assemblies and the proximity sensors would be utilized from the controls electronic rack assembly. A digital computer was then used to run a control program. With the use of a programmable power supply and several other pieces of hardware the iron rotor was

successfully suspended at one magnetic bearing assembly using a Proportional plus Derivative (PD) controller implemented on a 486 PC.

Chapter 5

Analysis

This chapter will give a short introduction into the calculation of the force between the magnetic coils and the iron rotor. The method of Variation of Energy and Virtual Work was used to set up the force equation. Once the force to current relationship was calculated the relationship was used to determine the control law gains needed to control the iron rotor in five degrees-of-freedom.

5.1 Magnetic Circuit Analysis

To determine the force between the magnetic actuator and the rotor the method of Virtual Work was used. Calculation of the change in magnetic energy in a device in which there are moving parts is a simple method of calculating the forces on the moving parts in the device [7]. This method is based on the principle of virtual displacements. Simply stated the change in energy ΔW, is equal to the force F, multiplied by the displacement of the body Δd, ($\Delta W = F\Delta d$). Applying this to magnetic energy and taking the limit, gives $F=\frac{\partial W}{\partial d}$, where F and W are the force and the magnetic energy, respectively. Assuming the permeability of air remains constant as the body is displaced through a distance Δd, then the energy W of a magnetic bearing assembly is equal to

$$W = \frac{1}{2}\int_{v} \mu_o H^2 dv \tag{5.1}$$

where $\mu_o = 4\pi \times 10^{-7}$H/m, is the permeability of air, V is the total volume of the domain under study, and H is the field intensity in the air gap. Using Ampere's law for magnetic coils the field intensity can be found from

$$H2\ell = \mathrm{NI} \quad \therefore H = \frac{\mathrm{NI}}{2\ell} \tag{5.2}$$

where N is the number of turns in both the magnetic coil*, I is the current in the coil, and ℓ is the length of the air gap.

As stated before the magnetic force acting on the body is:

$$F = \frac{W_2 - W_1}{d} \tag{5.3}$$

$$d = \ell_2 - \ell_1 \tag{5.4}$$

where d is the distance the body has been displaced.

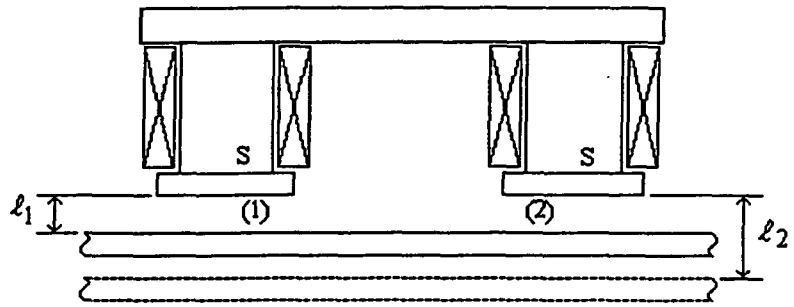

Figure 5.1 Magnetic Circuit of an MBA with movable Rotor.

The force exerted on the rotor, shown in Figure 5.1, can be calculated using Equation (5.3), and substituting for W_1 and W_2 as follows

$$W_1 = \frac{1}{2}\mu_o H_1^2 2S\ell_1 = \mu_o \left(\frac{\mathrm{NI}}{2\ell_1}\right)^2 \mathrm{S}\ell_1 \tag{5.5}$$

$$W_2 = \mu_o \left(\frac{\mathrm{NI}}{2\ell_2}\right)^2 \mathrm{S}\ell_2 \tag{5.6}$$

where S is equal to the cross-sectional area of the magnetic pole face. The surface area has a multiple of two because there are two air gaps in this circuit. The force between the rotor and the fixed part of the actuator can then be found by

*The magnetic circuit contains two coils each wound with 810 turns of No. 20 AWG wire.

$$F = \frac{(W_2 - W_1)}{(\ell_2 - \ell_1)} \tag{5.7}$$

$$F = \frac{\mu_o N^2 I^2 S}{4\ell_1 \ell_2} \tag{5.8}$$

Given that:

$\ell_1 = 3.41\ mm$; $\ell_2 = 3.41\ mm$; $S = 1.58 \times 10^{-3}\ m^2$; $N = 1620$; $\mu_o = 4\pi \times 10^{-7} H/m$.

$$F = 112 \cdot I^2 \text{ Newtons}$$

By rearranging the above equation and solving for current, I the following is found

$$I = \frac{2}{N}\sqrt{\frac{\ell_1 \ell_2 F}{\mu_o S}} \tag{5.9}$$

To generalize the above equation for a steady state operating point $\ell_1 \ell_2$ can be replaced with g^2. Upon substitution the current, I required to suspend the rotor at a prescribed air gap, g the current can now be calculated using

$$I = \frac{2}{N}\sqrt{\frac{g^2 F}{\mu_o S}} \tag{5.10}$$

given $F = \frac{1}{3}Mg$ or $F = 70.63$ Newtons, where M is equal to the mass of the rotor. Only a third of the mass is used in this calculation because each magnetic actuators supports a third of the rotor. The current needed to suspend the rotor at an air gap of $g = 3.41mm$ is

$$I = 0.794 \text{ Amps.}$$

To verify these calculations another method of calculating the magnetic field intensity was used. In the first set of calculations Ampere's Law was used and the permeability of Nickel Iron was assumed to be infinite. The relative permeability of Nickel Iron is not truly infinite but has finite value of approximately $\mu_{ni} = 4000$. This next method takes into account the permeability of the Nickel Iron core material used in the magnetic circuit. The magnetic bearing assembly was sectioned into areas where the cross section

of the material was constant. Figure 5.2 shows how the MBA was sectioned. After doing this, the reluctance of each section can be added together much like resistance in an electrical circuit.

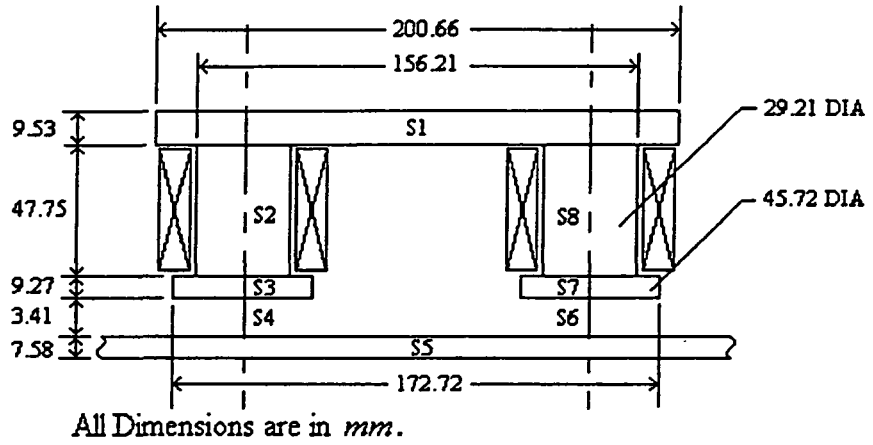

Figure 5.2 Magnetic circuit of a Magnetic Bearing Assembly.

The notation in Figure 5.2 is that the "S" indicate the cross sectional area of the material and the air gaps. The length of each section is given in *mm*. The closed loop circulation of magnetic field intensity, H is given by the following

$$h_1\ell_1+h_2\ell_2+h_3\ell_3+h_4\ell_4+h_5\ell_5+h_6\ell_6+h_7\ell_7+h_8\ell_8=2NI \qquad (5.11)$$

In order to solve equation (5.11) for the field intensities in the air gap the conservation of flux around the closed loop is given as

$$\Phi_1=\Phi_2 \quad \therefore \quad h_1S_1=h_2S_2$$

$$\Phi_2=\Phi_3 \quad \therefore \quad h_2S_2=h_3S_3$$

$$\Phi_3=\Phi_4 \quad \therefore \quad \mu_i h_3S_3=\mu_o h_4S_4$$

$$\vdots \qquad\qquad \vdots$$

$$\Phi_8=\Phi_1 \quad \therefore \quad h_8S_8=h_1S_1$$

where $\Phi=\frac{NI\mu S}{\ell}$ $\therefore h=\frac{\ell}{\mu S}$; where $\mu_o= 4\pi \times 10^{-7}$H/m, is the permeability of air. After

simplifying and solving for the magnetic field intensity in the air gap we get the following

$$h_4=\frac{\mu_i S_1}{\mu_o S_4}\left(2.499\times 10^{-7}NI\right)=\frac{B_4}{\mu_o} \tag{5.12}$$

where B_4 is the magnetic flux in the air gap. The force equation is as follows

$$F=\frac{\mu_o}{2}h^2 2S \tag{5.13}$$

The field intensity in the air gap can be calculated by substituting S_1=605.2 mm^2 and S_4=1641.7 mm^2 into Equation (5.12). The current can be found by substitute h_4 into equation (5.13), and rearranging equation (5.13) in terms of current, I.

$$I=\frac{3.411\times 10^{-3}}{N}\sqrt{\frac{F}{\mu_o S_4}} \tag{5.14}$$

I=0.779 Amps.

Given that the force, F is equal to $\frac{1}{3}$Mg where M is the mass of the rotor the current can be calculated as shown above.

5.1.1 Verification Using TOSCA

There is an acceptable agreement between these to calculated currents values, but these values are still found to be different from the measured values (see also Chapter 7). To develop an understanding of why there is a discrepancy between the calculated values and the measured values a finite element method of calculation of the field intensity in the air gap was used. The code used is TOSCA, by Vector Fields Incorporation. TOSCA is a three-dimensional, finite-element solution package for magnetostatic problems. Models are prepared for analysis and results presented using the companion pre- and post-processor OPERA, also by Vector Fields Incorporation. TOSCA can solve linear (constant permeability) or non-linear problems. A linear finite-element model of an axial MBA is shown in Figure 5.3. The magnetic flux in the air gap was found to be much less

uniform than had been anticipated, illustrated in Figures 5.4 and 5.5. Figure 5.4 is a plot of the magnetic flux on a line passing through the air gap between the rotor and the pole face. The Y-axis represents the magnitude of the flux and the X-axis represents the location in millimeters with the zero mark being centered between the two coils. The graph shows that the flux leaving the left pole face is equal in magnitude but opposite in sign of the of the right pole face, and that the flux is not uniform across the pole face. Figure 5.5 is a three dimensional plot of the flux in the air gap in a plane passing between the rotor and the pole face. Only one pole face is shown in Figure 5.5. With the air-gap set at 3.41mm, the flux at the center of the pole face is computed as $2385 \cdot I$ gauss. The "circuit model" (equations 5.12 and 5.13) gives a value of $2985 \cdot I$ gauss. The total flux passing into the suspended rotor is, however, slightly greater in the computed result, by about 12%. This is consistent with the flux fringing around the edges of the pole face, resulting in lower flux density. The lower flux density in turn causes lower reluctance and slightly increased total flux.

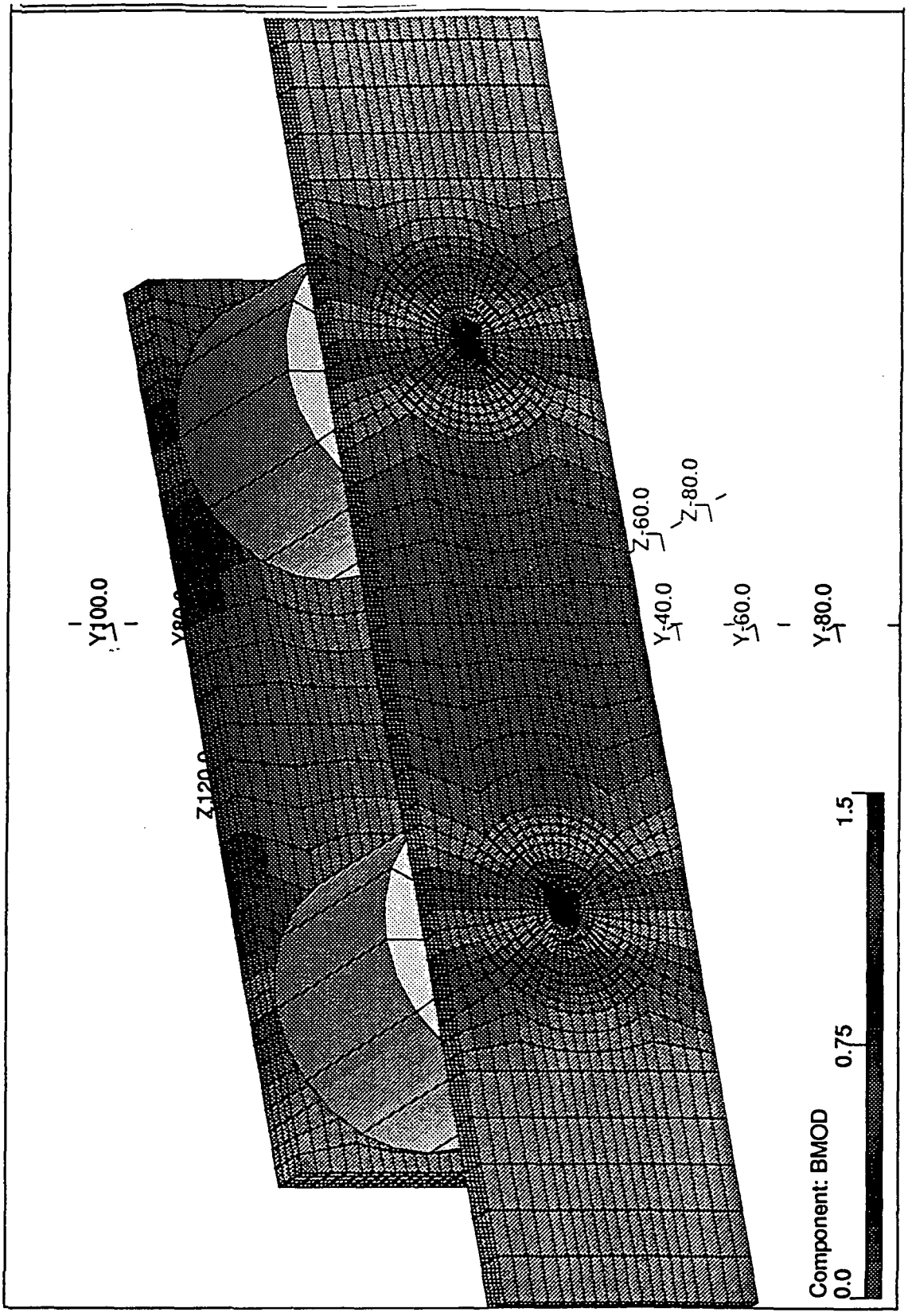

Figure 5.3 Finite Element Model of an Axial MBA

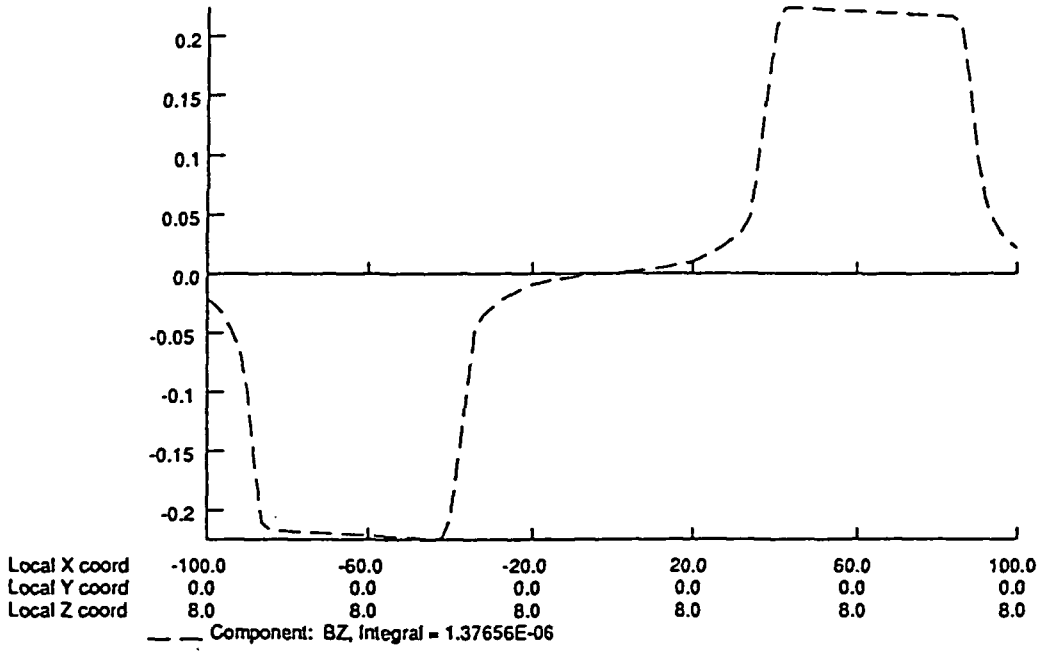

Figure 5.4 2-D Magnetic Flux in the Air Gap

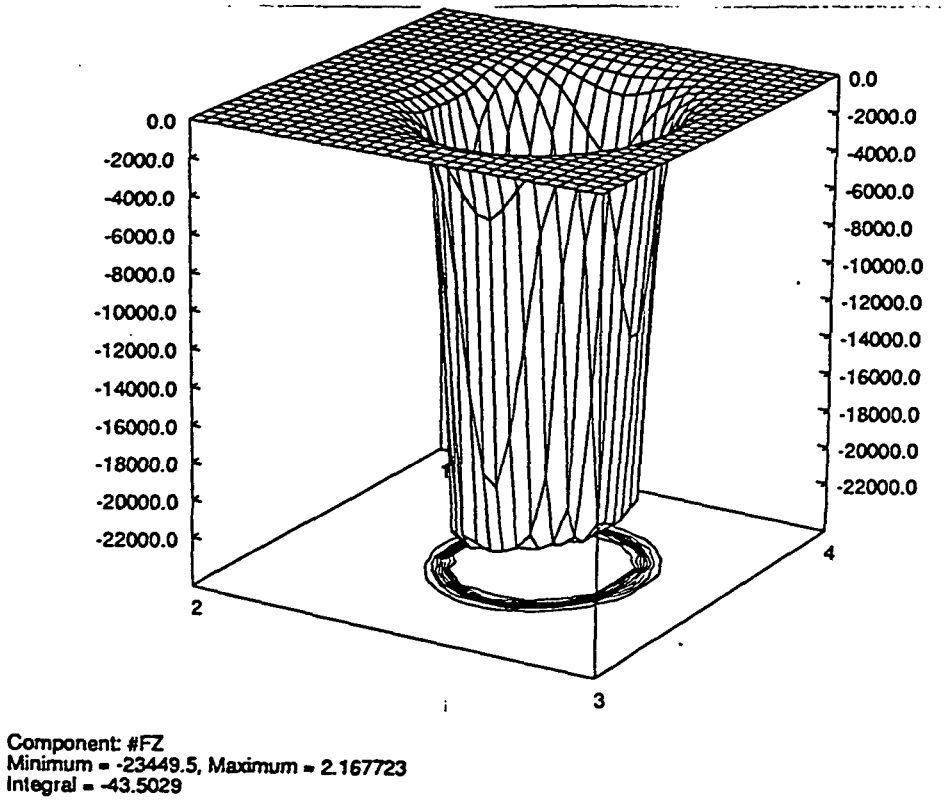

Component: #FZ
Minimum = -23449.5, Maximum = 2.167723
Integral = -43.5029

Figure 5.5 3-D Magnetic Flux in the Air Gap

5.2 Control Approach

The use of digital computers as a compensator device has grown in the past decade as the price and reliability of digital computers have improved dramatically [8]. Figure 5.3 illustrates a single-loop control system. The digital computer in the system

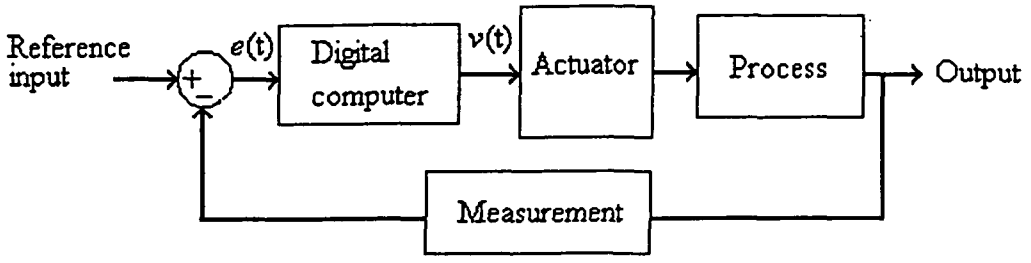

Figure 5.6 Block diagram of a computer control system.

loop receives an input of the system error, $e(t)$, and performs calculations to provide the output, $v(t)$. In Figure 5.6 the error is, $e(t)=X_D-X$, where X_D is the steady state air gap, and X is the air gap measured by the sensors. The output, $v(t)$ is the reference voltage to be supplied to the power amplifiers that drive the actuators. With this system, like many others, it is necessary to receive and manipulate several input variables, so a digital control system can often be a multivariable system. A more complete block diagram of a computer control system is shown in Figure 5.7. Figure 5.7 shows that a digital computer

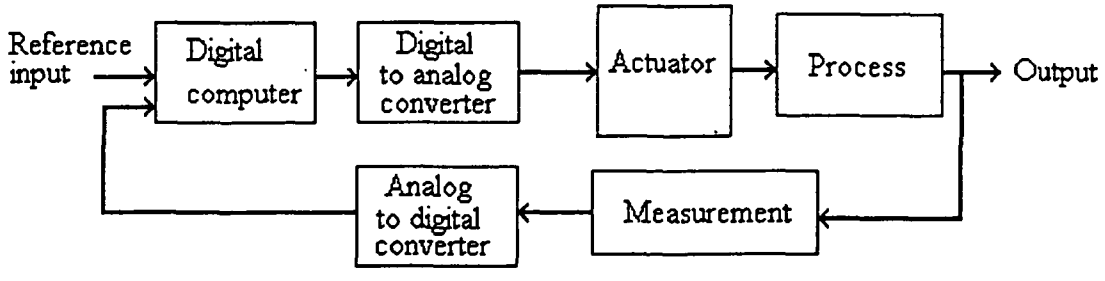

Figure 5.7 Block diagram of a computer control system, including the signal converters.

receives and operates on signals that are digital (numerical form), as contrasted to continuous signals [8]. The measured data is converted from analog form to digital form by a converter. After the digital computer has calculated the output, the output is converted to an analog signal by means of an digital-to-analog converter. If the time interval between samples used to perform the analog to digital function is small compared to the time constant of the actuator and process, the system essentially acts as a continuous system [8]. This allows the analog-to-digital and digital-to-analog converters to be transparent in the control system. Due to the high sampling rate available, the system being studied here can be considered as a continuous system. Figure 5.8 is a block diagram of the ASPS control system. The controller will be a proportional plus derivative also known as a PD controller. The system plant is made up of the power amplifiers, the actuators, and the suspended mass. Feedback in the control loop is a measure of

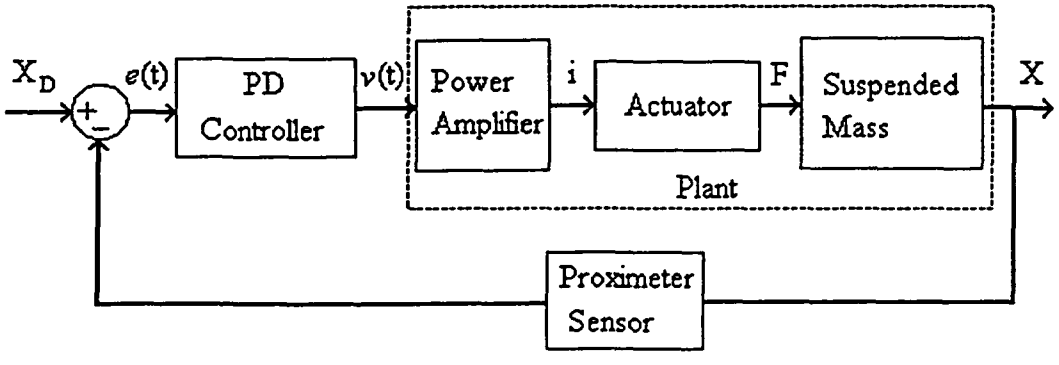

Figure 5.8 Block diagram of the ASPS control system.

suspended mass (rotor) displacement from steady-state conditions. In order to determine the proportional gain, K_p, and the derivative gain, K_D, the plant systems needed to be accurately represented by their transfer functions. In other words the better the transfer function represents the dynamics of the system the better the model will accurately

determine the controller gains. Figure 5.9 is a block diagram of the control system transfer function for each of the plant systems.

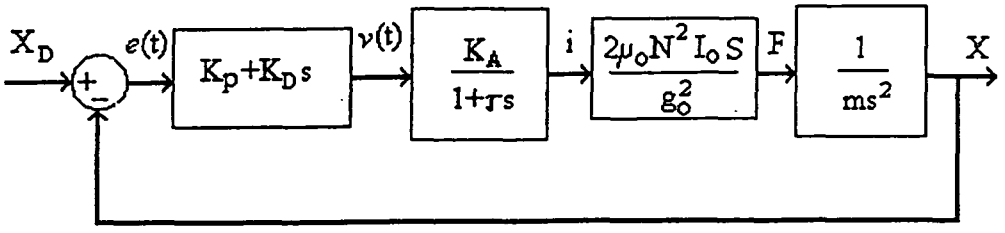

Figure 5.9 ASPS control system transfer functions.

Starting with the simplest part of the system, the transfer function representing the suspended mass is found from the equation

$$F=ma \quad \text{or} \quad F=m\frac{d^2x}{dt^2}$$

Taking the Laplace transform,

$$F=mxs^2$$

where s is the Laplace variable.

Therefore the transfer function of force, F to displacement, x is

$$\frac{x}{F}=\frac{1}{ms^2}$$

Next the transfer function representing the dynamics of the actuators comes from the force to current relationship calculated in section 5.1. The equation

$$F=\frac{\mu_o N^2 I^2 S}{g_o^2}$$

contains nonlinear terms, current, I, and air gap, g_o. The current, I can be linearized as follows. If the current is separated into a steady-state term plus a small perturbation $I=I_o+i$, then by squaring this equation and substituting it into the force equation the

nonlinear current relationship can be removed. The force equation becomes

$$F=\frac{\mu_o N^2 I_o^2 S}{g_o^2}+\frac{2\mu_o N^2 I_o S}{g_o^2} i$$

where

$$I^2=I_o^2+2I_o i+i^2$$

The i^2 term in the above equation is presumed to be small because it is the square of a small perturbation about the steady-state condition. Letting $F_o=\frac{\mu_o N^2 I_o^2 S}{g_o^2}$, then the change in force, $\delta F=F-F_o$ can be represented by

$$\delta F=\frac{2\mu_o N^2 I_o S}{g_o^2} i$$

This is the transfer function of the system actuators. Finally, the transfer function representing the power amplifiers was determined. Physical testing of the amplifier had to be carried out to determine the internal gain of the amplifier and current feedback gain. The gain K_A was determined by supplying a reference input signal to the amplifier an measuring the output current. The output at the amplifiers current monitor pin was recorded. The data was plotted and the relationship between the input and output was found as

Current measured=1.201 × Reference voltage supplied

Figure 5.10 shows the system representing the power amplifier connected to the actuator. The transfer function of the system in Figure 5.10 was found as follows.

$$V_o=KV_E=K(V_D-ki)$$

$$V_o=iR+L\frac{di}{dt}=iR+Lis$$

$$K(V_D-ki)=iR+Lis$$

$$KV_D=i[(R+Kk)+Ls]$$

$$\frac{i}{V_D} = \frac{K}{(R+Kk)+Ls}$$

$$\frac{i}{V_D} = \frac{K}{(R+Kk)} \times \frac{1}{1+\frac{L}{(R+Kk)}s}$$

where this final equation takes the form

$$\frac{i}{V_D} = K_A \times \frac{1}{1+\tau s}$$

where $\frac{K_A}{1+\tau s}$ is the transfer function of the amplifier system. The internal time constant, τ of the amplifier was determined by performing a frequency response analysis of the amplifier using an Hewlett Packard 3562A Dynamic Signal Analyzer. Several tests were performed in order to find the break frequency of the amplifier. The same test was performed on all three amplifiers that power MBA's A1, B1, and C1. With the analyzer a break frequency of approximately 35 Hz or τ=.00455 seconds was determined. Figure 5.11 shows the measured frequency response of the amplifier supplying power to MBA A1. Gain K_A was determined to be 1.201 and Appendix G has the results of the calculations for finding K_A. Table 5.1 summarizes all the gains and constants explained above.

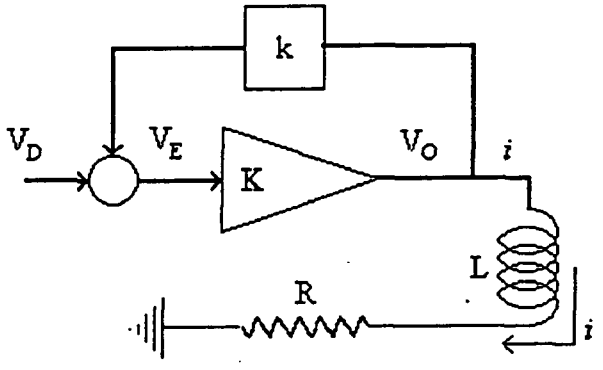

Figure 5.10 Diagram representing the power amplifier and actuator.

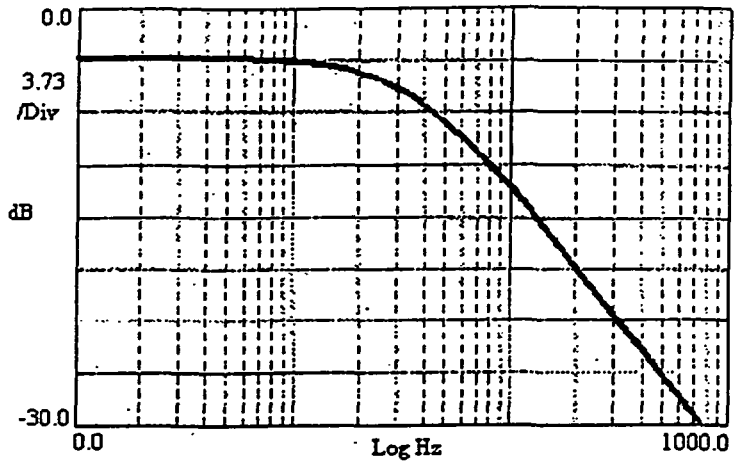

Figure 5.11 Frequency response of system power amplifier.

Table 5.1 Summary of constants used in transfer functions.

K_A	$1.201 \frac{\text{Amps}}{\text{volt}}$
τ	$.00455 \frac{\text{sec}}{\text{rad}}$
μ_o	$4\pi \times 10^{-7} \frac{\text{H}}{\text{m}}$
N	$810 \frac{\text{turns}}{\text{coil}}$
I_o	1.25 amps*
S	1641.7 mm^2
g_o	3.41 mm
m	7.19 kg

Now that the plant can be represented by the above transfer functions it is time to determine the proportional gain, K_p and the derivative gain, K_D. With a ratio of $\frac{K_D}{K_p}=0.1$ the closed-loop transfer function of the system shown in Figure5.9 is as follows

$$K_p \frac{34.949s+349.49}{.0327s^3+7.19s^2}$$

The root locus plot of this system shows that the closed-loop system is stable for a range of K from 0 to 10. An overall gain of 4.5 corresponding to a damping ratio of .7 can be determined graphically from Figure 5.12.

*Experimentally determined value.

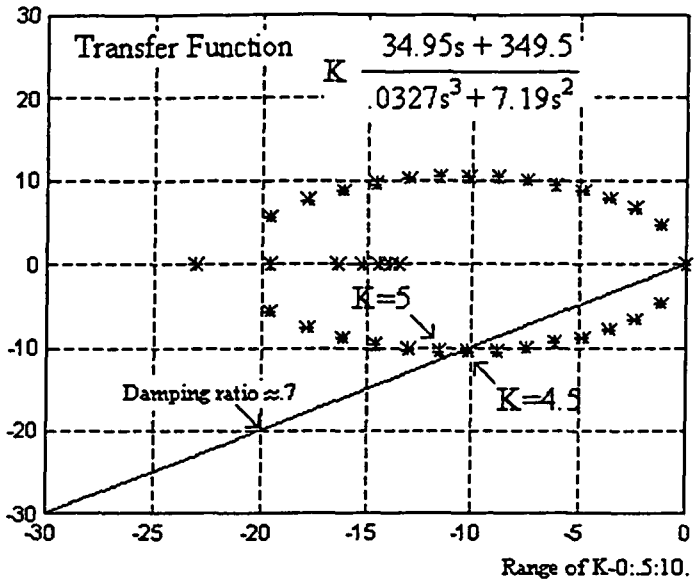

Figure 5.12 Root locus for a PD controller.

5.3 Implementation of Control Law

Using the proportional gain, K_p and derivative gain, K_D that were determined to be 45 and 4.5 respectively the controller program was constructed. The controller was written using Microsoft QuickC. When the program is executed it starts out by initializing the data acquisition hardware in order for it to accept values from the position sensors. The distance from equilibrium and velocity of the iron rotor are measured as functions of time. The change in position of the ring from steady-state is multiplied by the proportional gain and the velocity of the rotor is multiplied by the derivative gain. The velocity of the rotor is determined by taking the difference of two position readings and then dividing by the time interval between measurements. This method can be used because any very large velocity spikes will be quickly counteracted by a negative spike of equivalent magnitude. Also, the response of the system is slow compared to the time interval used to calculate the velocity. These values are then added to the steady state operating condition in order

to give a new force command to feedback to the power amplifiers supplying power to the magnetic actuators. A listing of this control program can be found in Appendix E.

Chapter 6

Recommissioning

This chapter will describe the design and components of the new control electronics hardware package. The development of the software used to communicate with the controller hardware and ultimately control the vernier pointing system in five degrees-of-freedom is also discussed.

6.1 Controller Hardware

The controller hardware is made up of a computer, several amplifiers, a data acquisition system, power supplies and miscellaneous wires and connectors. The computer selected to control the system is a Gateway 2000 4DX-33 personal computer with an Intel 33MHz 80486DX microprocessor, 4MB RAM, 64KB multisegmented cache 202 MB hard drive, and a Crystal Scan accelerated video with 1MB of memory. In order for the computer to be able to communicate with the ASPS control hardware a data acquisition system had to be installed. A Keithley Data Acquisition DAS-1402 board was installed in one of the expansion slots of the computer to read the information sent from the position sensors and amplifier current monitor outputs. The DAS-1402 is a multifunction, high-speed, analog-to-digital interface board for IBM and compatible computers. The DAS-1402 is designed in such a way as to minimize noise and crosstalk at high frequencies. The DAS-1402 offers 8 differential or 16 single-ended analog inputs with 12-bit resolution at 100 ksamples/sec. Inputs can be unipolar (0-10V) or bipolar (+/-10V), and the DAS-1402 offers gains of 1,2,4,and 8 [9]. The Keithley Data Acquisition DAS-1400 Series User's Guide contains more information about the DAS-1402 board

Appendix D contains a wiring schematic of the Fault Indicator Display Electronics design. The power supplies used to power the amplifiers are Copley Controls Series 661 unregulated DC power supplies designed especially for the Copley Controls servo amplifiers. To meet the needs of the six power amplifiers that are needed to control the six magnetic actuators. two Copley Controls Series 661 power supplies were required. Each 661 power supply produce 36 volts DC at a rating of 12 Amps maximum. Appendix D contains an outline and a functional diagram of the power supplies. The hardware designed to power the proximity sensors was mounted on the vernier pointing assembly and was utilized. The proximity sensor electronic system is made up of several components, an oscillator card, and two position sensor amplifier cards. The oscillator card produces a 10MHz signal with a 30V peak-to-peak output to drive the 14 proximity sensors. The oscillator card and position amplifier cards are driven by a $\pm$ 15 V power supply. The $\pm$ 15 V power supply is a Power-One International Series power supply capable of a maximum output current of $\pm$ 1.5 amps, Appendix D contains a data sheet on the power supply.

6.1.1 Integrating the Hardware

This section will describe the integration of all the hardware components described in the previous section. This section will cover the installation procedures, calibration procedures, and setup procedures necessary to integrate the hardware systems.

First, the computer had to be configured in order for the chosen compiler to operate properly. The installation procedures for installing Microsoft QuickC are outlined in the Up and Running manual supplied with the software package [12]. Additional programming procedures can be found in References 13 through 16. When the SETUP.EXE program is executed it creates two files NEW-VARS.BAT and NEW-CONF.SYS. The information created by the installation program was added to the

already existing AUTOEXEC.BAT and CONFIG.SYS files. The AUTOEXEC.BAT and CONFIG.SYS were modified as shown below:

```
*********AUTOEXEC.BAT*********
@ECHO OFF
PROMPT $P$G
LH C:\WINDOWS\SMARTDRV.EXE /X
set mouse=C:\msmouse
C:\msmouse\mouse.exe /Q
SET PATH=C:\MSMOUSE;C:\QC25\BIN;C:\;C:\DOS;C:\WINDOWS;C:\CIRRUS.V28;
SET LIB=C:\QC25\LIB
SET INCLUDE=C:\QC25\INCLUDE
SET TEMP=C:\TEMP
WIN

*********CONFIG.SYS**********
DEVICE=C:\WINDOWS\HIMEM.SYS
DEVICE=C:\WINDOWS\EMM386.EXE NOEMS I=E000-EFFF X=F000-F7FF
DEVICEHIGH=C:\DOS\SETVER.EXE
DEVICEHIGH=C:\WINDOWS\IFSHLP.SYS
DOS=HIGH,UMB
STACKS=9,256
FILES=10
BUFFERS=50
LASTDRIVE=K:
```

One thing to note in the AUTOEXEC.BAT file is the order of the SET PATH. If the order is changed the mouse may not work properly within the QuickC environment. These are not the most optimum settings for these files, but are the minimum requirements. The compiler was installed into the C:\QC25\BIN directory, and the libraries and include files are located in corresponding sub directories under the C:\QC25 directory. The QuickC Windows-Based Environment can be executed from within WINDOWS or from the DOS command line by typing in C:\QC25\BIN\QC. Information on how to edit, compile, link, debug, make, and get on line-help can be found in the Microsoft QuickC User's Guide [13]. Once the compiler was installed it was time to install the software drivers that were supplied with the data acquisition system. The distribution software for the DAS-1402 board was installed into the directory C:\DAS1600. Before the DAS-1402 board was installed into the computer the board configurations were made to the various switches on the board. The base address of the DAS-1402 board was set to 300 Hex. The program d1600cfg.exe located in the

C:\DAS1600 director was executed to create a file containing all the settings and configuration of the DAS-1402 board prior to installation. The file created was called my1402.cfg, and the contents of this file will be shown later in Table 6.1. The next step was to install the DDA-06 data acquisition board and to configure it for use. The base address of the DDA-06 board was set to 190 Hex. The output range of the board was set to ± 2.5 volts by selection the appropriate dipswitch settings. The board was then installed into an expansion slot at the back of the computer. The distribution software for the DDA-06 board was installed under the director C:\DDA06. The program DDA06.EXE is a calibration program, and the calibration was performed to determine the condition of the board. The ASO-1600/1400 is a collection of software that provides the capability of controlling the DAS-1600/1400 with DOS-based and WINDOWS-based programming languages. This collection of software was installed under the directory C:\ASO1600. The Pacer Timer board was installed according to the manual specifications and the distribution software was installed under the directory C:\PACER. The base address of the Pacer timer board was selected to be 230 Hex. With the computer, hardware, and software all configured and ready the wiring of the power supplies, power amplifiers, and necessary components could be started. An intricate wiring harness was constructed to connect all of the electronic hardware together in their corresponding order. A detailed drawing of the necessary connections to make one magnetic actuator operational is shown in Figure 6.2 and in Appendix D. This process was repeated for all six magnetic actuators used. It should be noted at this time that the two inner magnetic bearing assemblies were paired together, and were connected in parallel to the same power amplifier. This is only temporary, or until the additional power supplies are wired. Once all the wiring was complete it was time to develop a working knowledge of the software drivers installed for each of the digital hardware components. The next section goes into details of the software design.

6.2 Controller Software

The programming language used to control the hardware is Microsoft QuickC for Windows. The software drivers for the Keithley Data Acquisition system were supplied by the manufacturer and supported by Microsoft QuickC. Data Translation also supplied the necessary drivers to control the timer board, also supported by Microsoft QuickC. In order to gain an understanding of how the software supplied with the data acquisition and timer board communicated with the hardware several test programs were written. The program AD_DATES.C which stands for Analog to Digital and Digital to Analog test program, performs the necessary steps in order to initialize the Keithley Data Acquisition DAS-1402 and the DDA-06 for input and output respectively. AD_DATES.EXE was used to develop an understanding of how to read and write information using the Keithley Data Acquisition ASO-1600/1400 Driver software. When the program is executed a signal is supplied to amplifiers A1, B1, and C1 simultaneously. This reference signal supplied to the amplifiers allows the rotor to be suspended using aluminum shims placed between the magnetic pole and the rotor. These aluminum shims have a thickness of 3.41 mm (the designed air-gap). With the program running and the shims in place the minimum reference voltage can be determined by lowering the reference voltage until the rotor falls. The reference voltage can be increased or decreased .005 volts by using the UP and DOWN arrow key respectively. While the program is running the LEFT and RIGHT arrow keys will scroll through the input channels of the DAS-1402 data acquisition board. The DAS-1402 board is initialized with eight differential inputs. Channels 0-5 display the voltage signals measured by the proximity sensors. Channels 6 and 7 are not used at this time. To aid in configuring the DAS-1402, the distribution software that came with the hardware includes a program called D1600CFG.EXE. When this program is executed it creates a file that includes the board settings. This program was executed after the DAS-1402 board was installed into the computer. It created a file containing the settings used during this experiment. The file was called my1402.cfg, and Table 6.1 contains a listing of

the information contained within this file. Once the necessary programming to read and write using the DAS-1402 and DDA-06 was understood it was time to include the timer board into the program. In this application the timer board keeps track of time and controls input and output on a regular time interval by interrupting the program. This time

Table 6.1 Contents of file my1402.cfg

Board	0
Name	DAS1402
Address	&H300
ClockSel	10MHz
WaitState	NO
ADChanMode	Bipolar
ADChanConfig	Differential
DMAChannel	3
IntLevel	7
NumOfEXP16	0
NumOfEXPGP	0
NumOfSSH4A	0

schedule is needed in order to be able to calculate velocity of the rotor using the position measurements. The desired task of the timer board is performed in such a manner that the main body of the program will be interrupted at a given time interval throughout its execution. The idea behind this method is that it will allow the controller to perform keyboard interaction, screen updating, etc.. in the foreground whilst gain updating, reading, and writing can be performed in the background on a regular schedule. The program TIMER.C was written to try and implement this type of interrupt scheme using the software drivers that came with the Pacer timer board. To try and implement the above controls scheme program TIMER.C was written. The development of this method is incomplete at this time, but a copy of this program can be found in Appendix F. The method used is described as follows. In the above approach the main body of the program was interrupted on a regular time interval so that velocity calculations could be made.

With the new approach the velocity will still be calculated, but the method of keeping track of time is different. With this new method the main body of the program will be halted while a counter keeps track of how long before the program is resumed. The main body of the program will consist of an endless loop that will perform input and output to the data acquisition system. When the program reaches the bottom of the loop a counter will count to a terminal value before executing the next cycle of the loop. This way the timer board makes the program wait until the time interval has completed before proceeding. To test this method a program called TESTCOUN.C was written. This program will setup the internal frequency of the timer board to a given frequency. Then it will setup a counter to count once per clock tick. For demonstration proposes only this program will print "Hello World" to the screen once every second. In order to measure the frequency at which the loop is being executed an alternating value is written to channel 0 of the DDA-06 board. With the use of an oscilloscope the output can be measured, and the time of execution of the loop determined. As long as the calculations performed within the loop take less time than the time interval selected this method will work. With this it was now time to put the information found by writing AD_DATES.C, TESTCOUN.C, and the information developed in Chapter 5 about PD control together in order to design a program that will suspend the iron rotor. Program TESTABC.C was developed using the information given above. A copy of TESTABC.C in Appendix E.

Chapter 7
Results

7.1 MBA Fields and Currents

To verify the calculations made by the TOSCA program the field intensity in the air gap was measured using a Bell 640 Incremental Gaussmeter. The field intensity at a constant air gap of 3.41mm was measured at several different supply currents. Table 7.1 outlines the field strength at these different supply currents. These measured values compared with the calculated values supplied by the TOSCA program.

Table 7.1 Gauss Measurements in the Air Gap.

	Measured	Computer
Current (Amp.)	Field Strength (Gauss)	Field Strength (Gauss)
0.4	860	945
0.6	1200	1431
0.8	1620	1908
1.0	2010	2385
1.17	2310	2790

There is still a significant discrepancy between the measured and computed fluxes. Further study of the magnetic bearing assembly and further analysis with TOSCA will be required to resolve the discrepancy.

7.2 Verification of Levitation

In this section it will be shown that the system is really operational. The primary feedback to the controller is the displacement of the iron rotor from equilibrium. To demonstrate that the system works a time history of the displacements was plotted. These measurements were taken by saving the displacement measurements to an array while the rotor was being suspended. Figures 7.1-7.3 show the time history of the iron

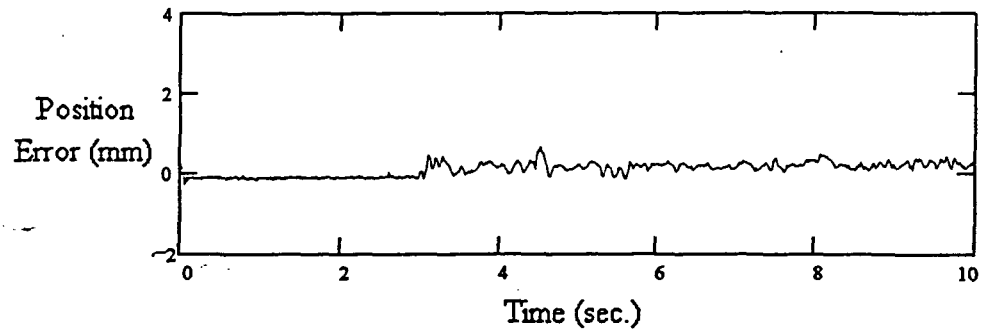

Figure 7.1 Time history of MBA A.

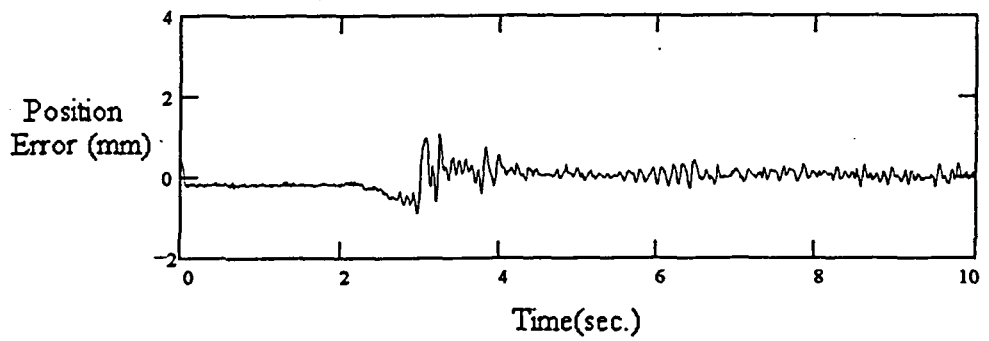

Figure 7.2 Time history of MBA B.

rotor in the vertical axis. By examining the position error as a function of time it can be seen that the Vernier latches closest to MBA B and C were released at about two seconds. The Vernier latch close to MBA A was then released at 3 seconds. At this time the iron rotor was fully suspended against gravity. Figure 7.4 is a plot of the position error, supply current, velocity and control variables at MBA A while the rotor is being suspended. This

plot is only for a time interval of one second to enhance the resolution. It can be seen from this plot that the position error and supply current follow approximately the same line but are separated by a constant. It can also be seen that some of the vibration in the position could be contributed by the large velocities calculated. The position tends to rise or dip depending on the mean average velocity over a particular time interval.

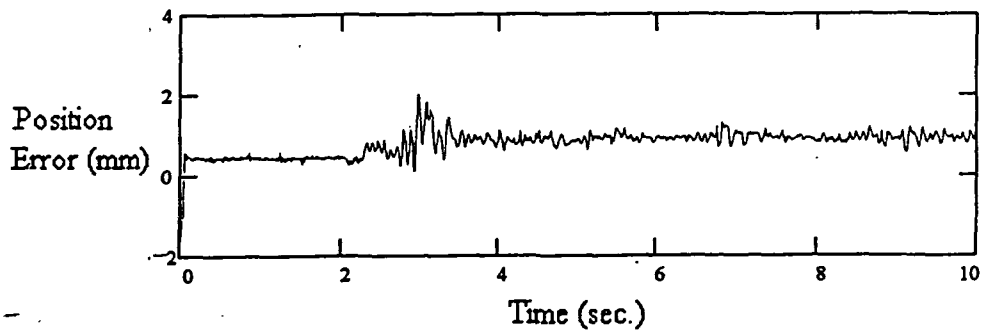

Figure 7.3 Time history of MBA C.

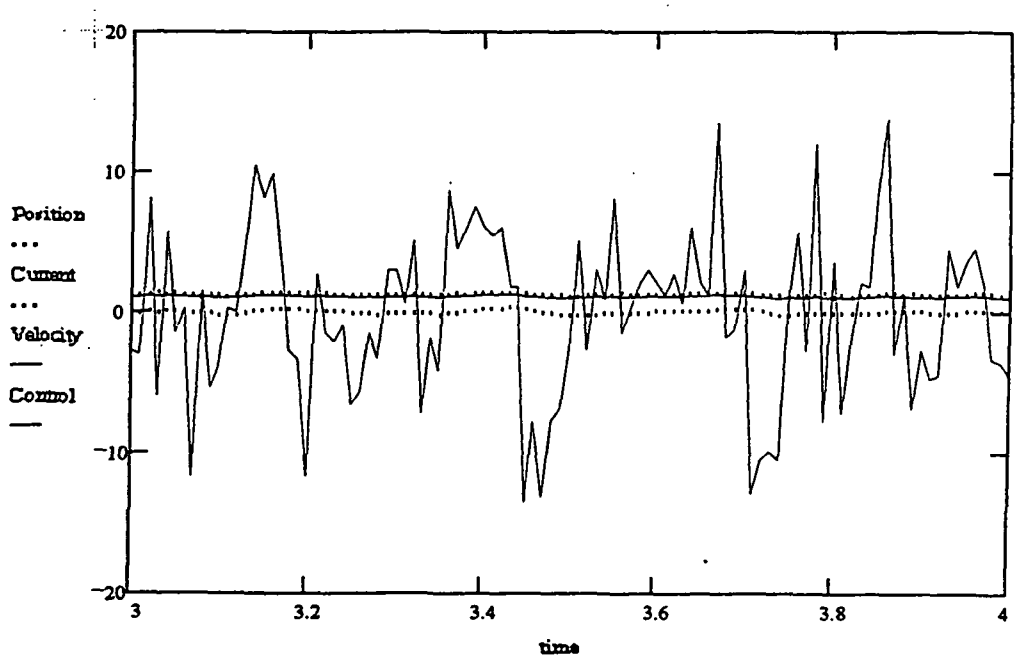

Figure 7.4 Plot of Input and Output Variables as a function of Time for MBA A.

After suspension was achieved the monitor pin supplied on the power amplifier, and the approximate air gap was measured using a dial indicator gage. These values can be seen in Table 7.2. At these measured air gaps the current was calculated using equation 5.10. Table 7.2 also contains these calculated values.

Table 7.2 Results of Current to Air Gap Measurements

MBA	Approximate Air Gap, mm	Approximate Current, Amp.	Calculated Current	Computed Current
A	4.42	1.52	1.03	1.28
B	3.45	1.30	0.80	0.84
C	3.77	1.42	0.88	0.98

The Control gains calculated in Chapter 5 were determined from the system model also developed in Chapter 5. In order to achieve magnetic suspension the magnitude of these gain had to be increased. The proportional gain and derivative gain calculated were 4.5 and .45 respectively. The actual proportional gain and derivative gain used were 330 and 45 respectively. The ratio of the new proportional gain and derivative gain is $\frac{K_D}{K_P}$=.136 These control gains provided the system with the necessary feedback to suspend the rotor. This PD controller is not in any way the most stable controller, but the results show that all the sub-systems are working together properly.

Chapter 8

Concluding Remarks

8.1 Conclusion

A description of the Annular Suspension and Pointing System was given at the beginning of this text. Even though the main focus of the research was on the Vernier Pointing Assembly, information was given about the other components that make up the ASPS. In order to achieve magnetic suspension in a one-g environment the magnetic actuators or magnetic bearing assemblies had to be modified. This modification to the core material of the magnetic actuator reduced the air gap and increased the force capability of the actuator. To give an understanding of the major change to the controls hardware Chapter 3 was included to give the reader an understanding of the two different design methods. An analytical analysis of the magnetic actuators was performed to develop a model of the system. These calculations showed the force to gap relationship is a non-linear function. The two different methods of calculating the field intensity in the air gap were used to verify the calculations. Given the force that each magnetic actuator has to support and the distance the rotor is to be suspended the current is calculated using the equations in Chapter 5. Even though the two methods produced a similar answer these two methods consistently produce a value that appears to be too low. To develop a better understanding of what was going on a finite element analysis was under-taken. The field strength in the air gap measured by a Gauss probe and calculated by the TOSCA program shows better agreement. The TOSCA program showed that the error between the

analytical model and the physical system might be because the analytical model does not take into account the fringing that occurs at the pole face. It was thought at first that this fringing would not be significant to be taken into account, but this is no longer the case. It appears that this fringing of the air gap is enough to change the force to gap relationship. Before this was discovered the analytical model was used to develop a PD controller for the system. The gain values calculated from this model were close, but adjustments were made in order to achieve suspension of the iron rotor. The ratio of derivative gain to proportional gain remained approximately the same.

Since it was decided not to use the existing analog controls hardware a new control hardware assembly had to be designed. The new components that make up the new controller were integrated together as discussed in Chapter 6. Even though the new controls hardware is working, further improvement in signal noise reduction will be necessary. The main contributor to this signal noise is grounding problems. It may be necessary the completely insulate all component from the controls electronic rack. By implementing this approach the individual components can be grounded to one common point. This will reduce the chance of a ground-loops occurring.

The software was written and the system enabled. Communication between the D/A, A/D, and timer boards is not an easy task. The steps developed to perform the task of communicating between the boards is shown though example. After some modification to the PD controller developed in Chapter 5 the iron rotor was successfully suspended. These modifications to the proportional and derivative gains may be due to the fact that the original system model was to simple and did not take into account the fringing effects of the magnetic actuator. The achievement of suspension confirmed that the controls hardware and software are working properly together. The PD controller used to suspend the iron rotor is not the most effective by any means, but it definitely shows that the system has great potential. Chapter 7 shows some results taken while the iron rotor was

being suspended. These results include a time history of the displacement measurements, a current to gap measurements, and the gains used in the PD controller.

8.2 Recommendation for Future Work

Now that the Vernier Pointing system is operational it is time to start focusing on future work. The most logical first step would be to update the controller hardware with the four additional power amplifiers necessary to power the three lower coil sets of the axial MBA's and the other inner coil set of the radial MBA. The next step might it to develop a controller that takes into account the non-linear characteristics of the magnetic actuators. This will allow the iron rotor to be displaced greater distances with better control. With the implementation of a non-linear controller to give better stability over a wide range of displacements the next step would be to perform a coordinate transformation of the system. This transformation would allow better control of payload position with fewer inputs. Recommisssioning of the Balance and Testing Fixture would be the next step. Test could be performed while simulating a zero-g environment. Once the testing in zero-g was completed it would now be time to start integrating the vernier pointing assembly with the rest of the ASPS components described in Chapter 2. There is a lot of work that needs to be performed in order for the ASPS to be flight ready for the Space Shuttle. With the above recommendations the system would be off to a good start.

References

[1] D. Cunningham, et al. Design of the Annular Suspension and Pointing System (ASPS) ; NASA CR-3343, October 1980.

[2] J. Kroeger, J. Drilling, and T. Gunderman, Final Report, "Conceptual Design of a Noncontacting Power Transfer Device for the ASPS Vernier System." NASA contractor Report 172238, April 1984.

[3] C.P. Britcher, N.J. Groom, "Current and Future Development of the Annular Suspension and Pointing System"; 4th International Symposium on Magnetic Bearings Zurick, August 1994.

[4] B.J. Hamiltion, "Final Report The Development of the ASPS Vernier System", Sperry Corporation Flight Systems Phonix, AZ ;Contract No.NAS1-15008, June 1983.

[5] Violet B. Haas, Analog and Digital Computer Handbook, Third Edition;1985

[6] Mark W. Spong and M. Vidyasagar, "Robot Dynamics and Control", Copyright 1989, by John Wiley & Sons, Inc.

[7] Nathan Ida and Joao P.A. Bastos, "Electromagnetics and Calculations of Fields", Copyright 1992, Springer-Verlag, New York, Inc.

[8] Richard C. Dorf, "Modern Control Systems", Sixth Edition, Addison-Wesley Publishing Company, 1992.

[9] Users Guide of the DAS-1400 Series Data Acquisition Boards, Keithley MetraByte Corporation; Copyright 1992.

[10] User Guide of the DDA-06 Data Acquisition Board, Keithley MetraByte Corporation, Copyright 1985.

[11] Pacer User Manual SP0170, Copyright 1989,1993 by Data Translation, Inc.

[12] Microsoft QuickC, Up and Running Version 2.0, Copyright Microsoft Corporation, 1988.

[13] Microsoft QuickAssembler, Programmer's Guide Version 2.51, Copyright Microsoft Corporation 1989,1990.

[14] Microsoft QuickC for Windows, Graphic Development Environment, C for Windows, Copyright 1991 Microsoft Corporation.

[15] Microsoft QuickC Compiler, C For Yourself Version 2.5, Copyright Microsoft Corporation 1988, 1990.

[16] Brian W. Kernighan and Dennis M. Ritchie, The C Programming Language Second Edition, Copyright 1988,1978 by Bell Telephone Laboratories, Inc.

Appendix A

Component Dimensions

The information presented in this Appendix was taken from blue prints that were delivered with the ASPS. These blue prints were reduced to fit in to an 8x11 page. The actual blue prints are kept with the system.

A.1 Vernier Pointing Assembly

Figure A.1 is a top view of the vernier pointing system. Figure A.2 is a sectional drawing of Figure A.1. Section A-A is a slice cutting through the MBA labeled A, a Vernier latch, the roll axis encoder, and the roll motor. These drawings are added here to aid in location parts of the vernier pointing system. Section B-B is a slice through the radial MBA. Section C-C shows the proximity sensors associated with the roll motor. Section D-D show a side view of a vernier latch and the cross-section of the rotor.

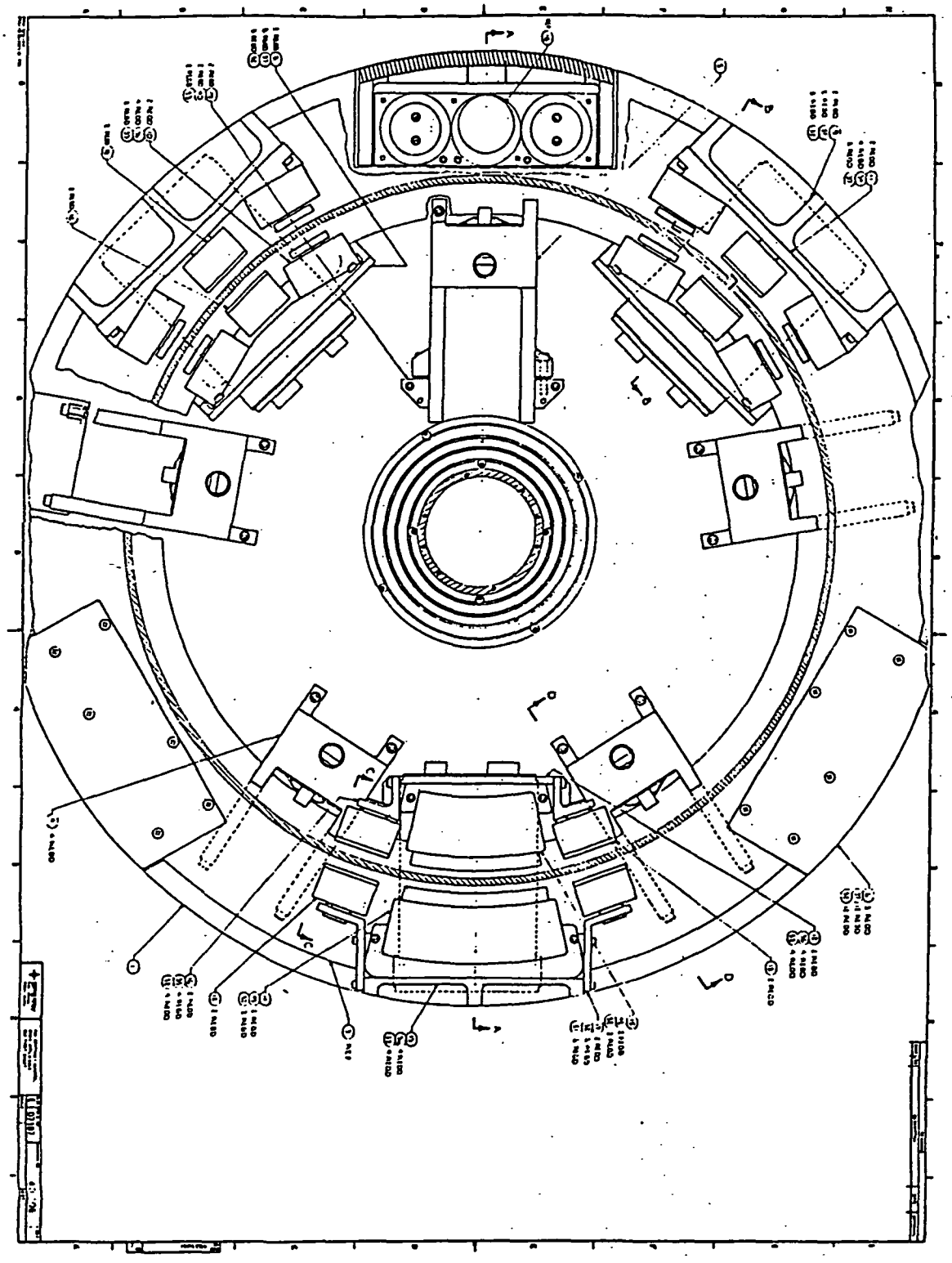

Figure A.1 Top View of the Vernier Pointing Assembly

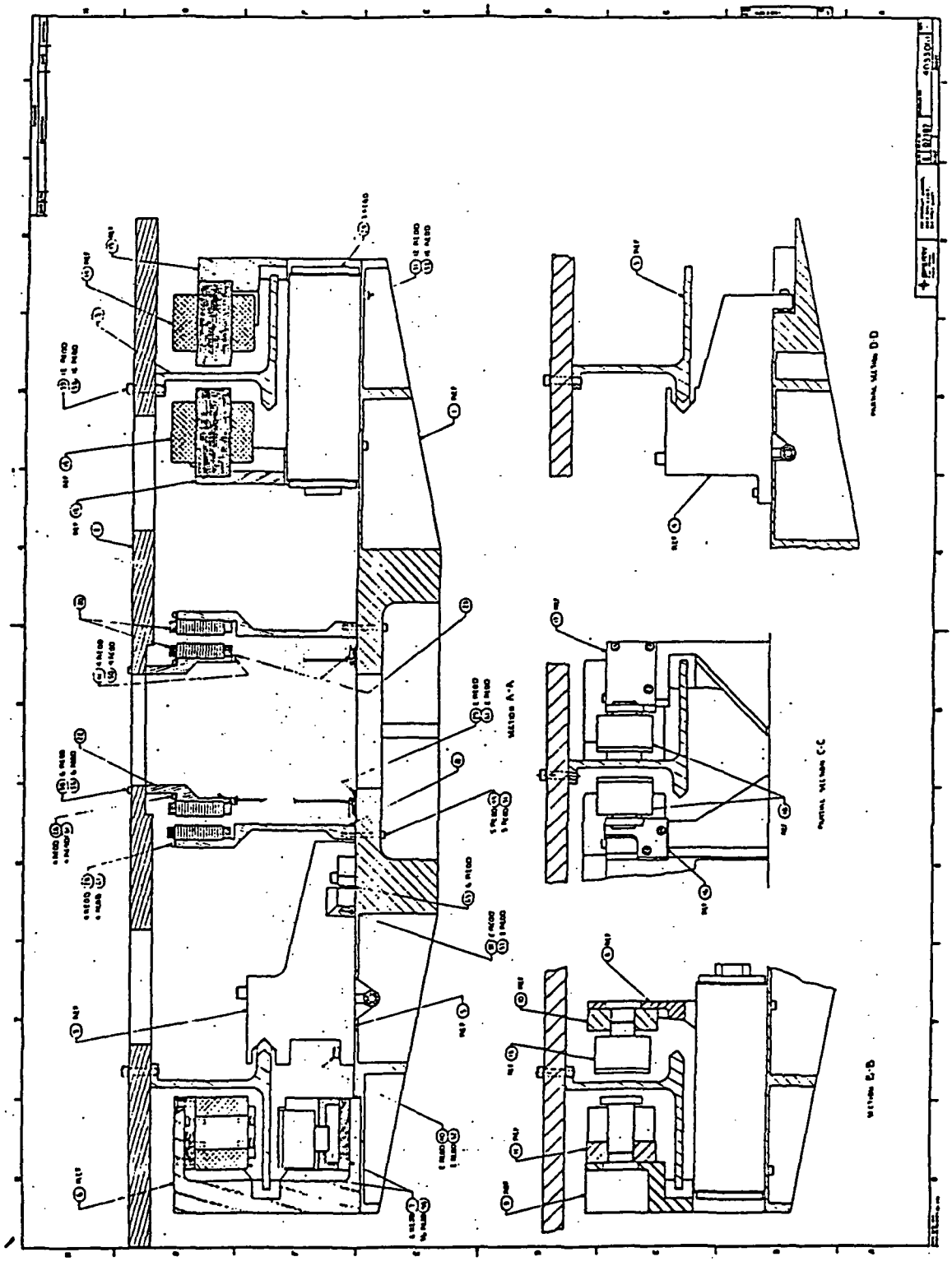

Figure A.2 Side Views and Section Drawings of the VPA

A.2 Axial Magnetic Bearing Assembly

The drawings shown in this section make-up the assembly drawings and individual component drawings of the axial MBA. Figure A.3 is a diagram of the axial MBA support bracket. Figure A.4 is an assembly drawing of the axial magnetic actuators of the MBA. Figure A.5 shows the dimensions of the base plate. Figure A.6 shows the dimensions of the top plate. This was the component of the axial MBA's that was modified. Figure A.7 is a drawing of the post, magnetic core. Figure A.8 shows the bracket that supports the proximity sensor.

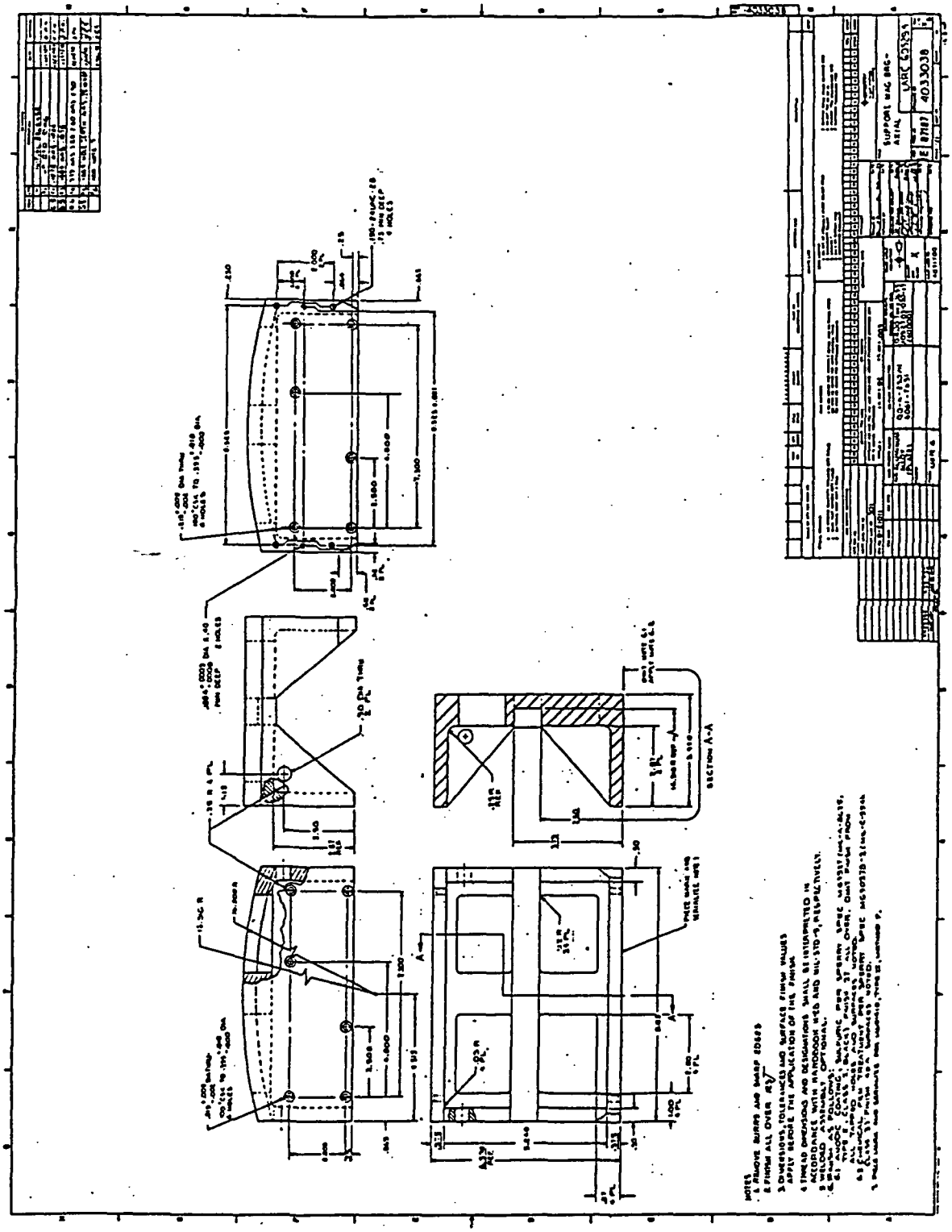

Figure A.3 Support Structure of Axial MBA

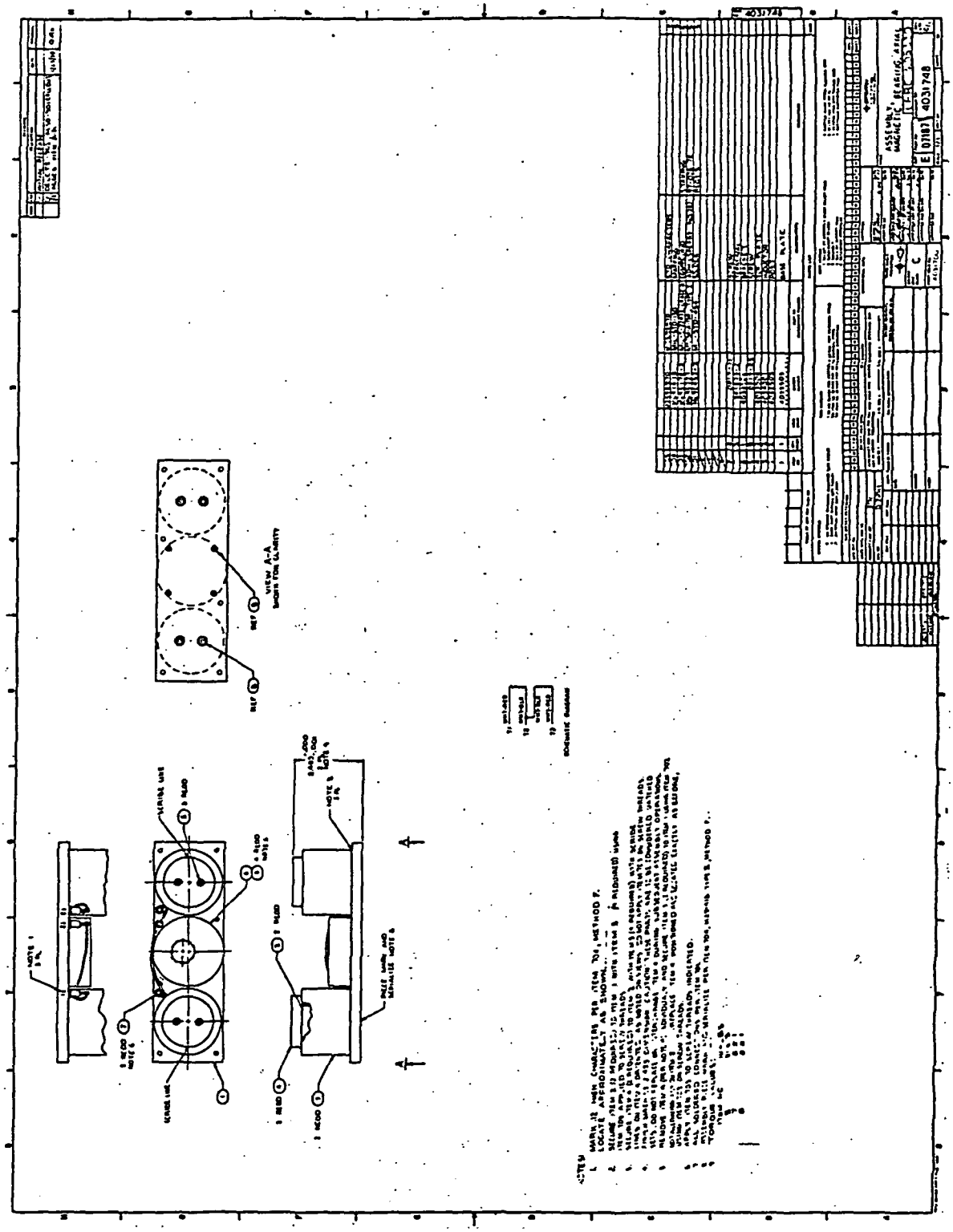

Figure A.4 Assembly of the Axial MBA

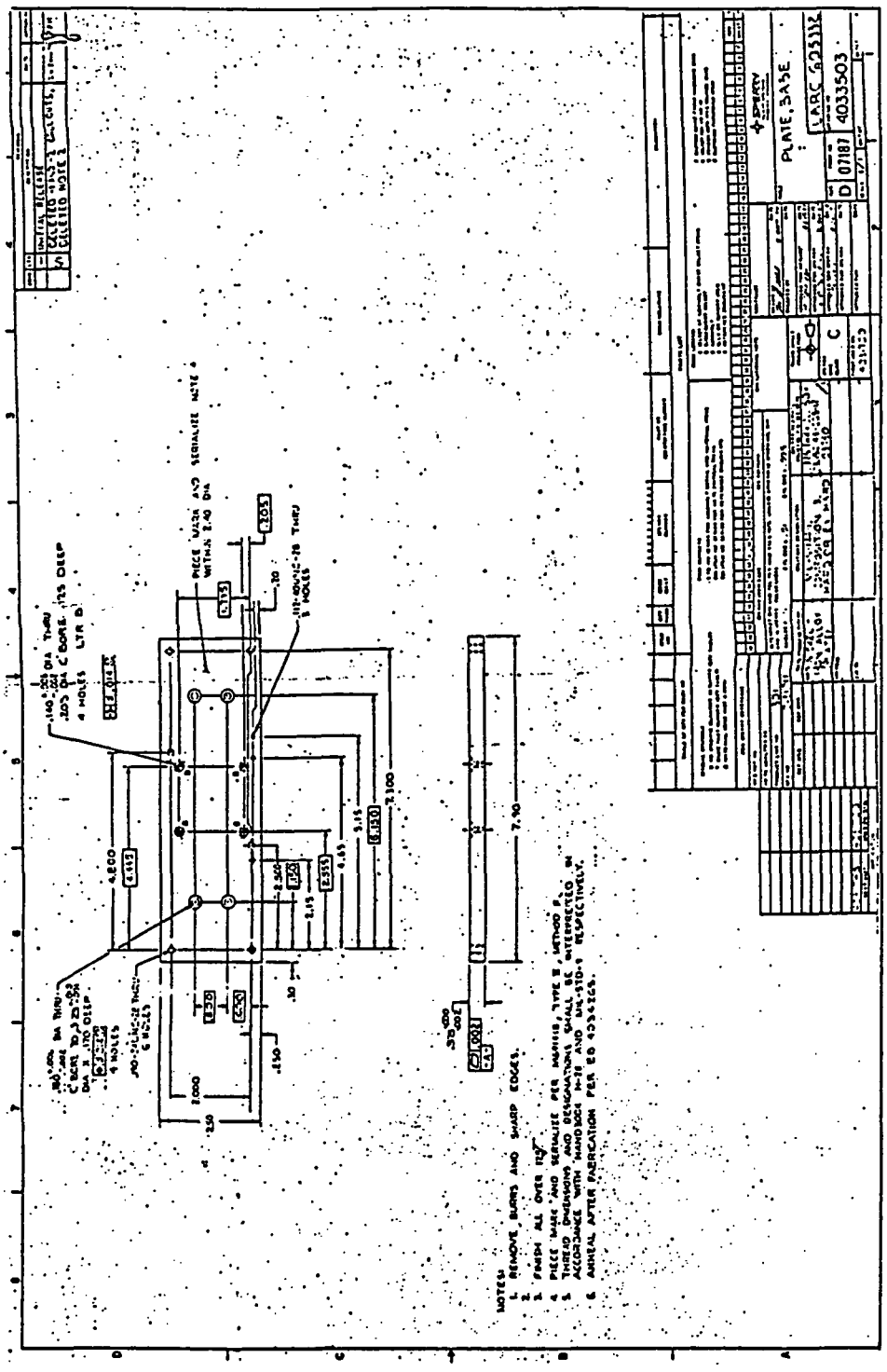

Figure A.5 Base Plate Dimensions of the Axial MBA

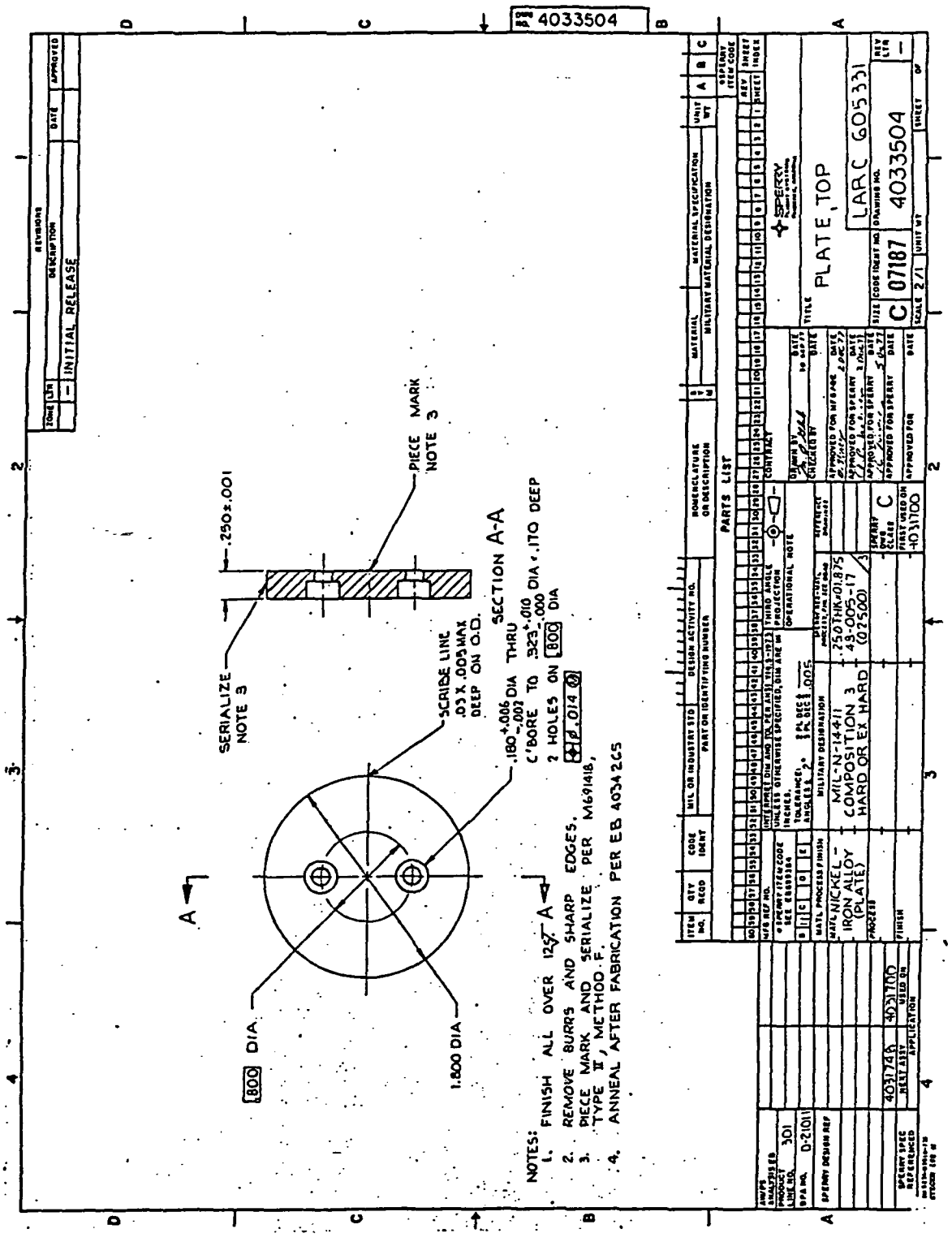

Figure A.6 Top Plate of the Axial MBA Core

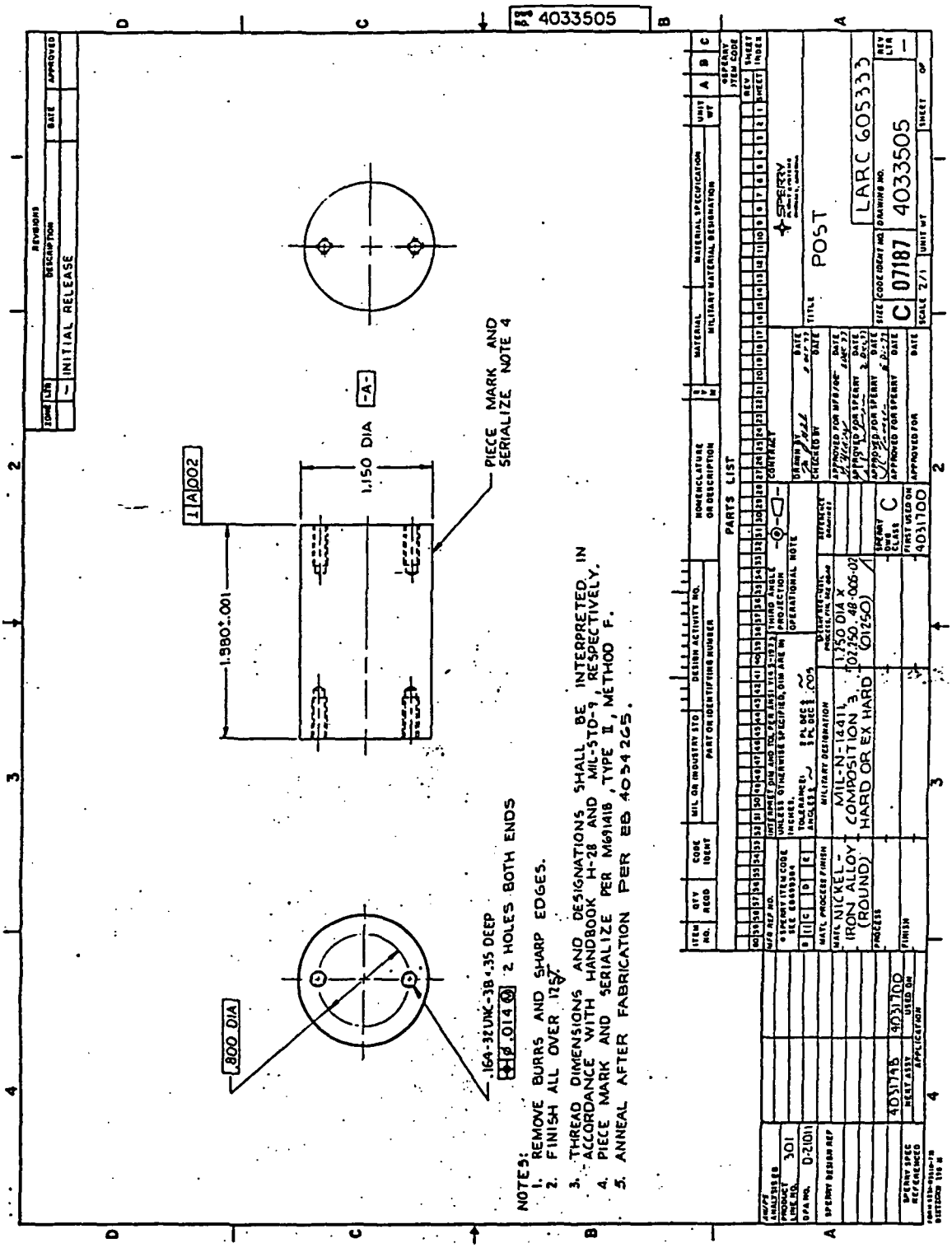

Figure A.7 Axial MBA Core Post

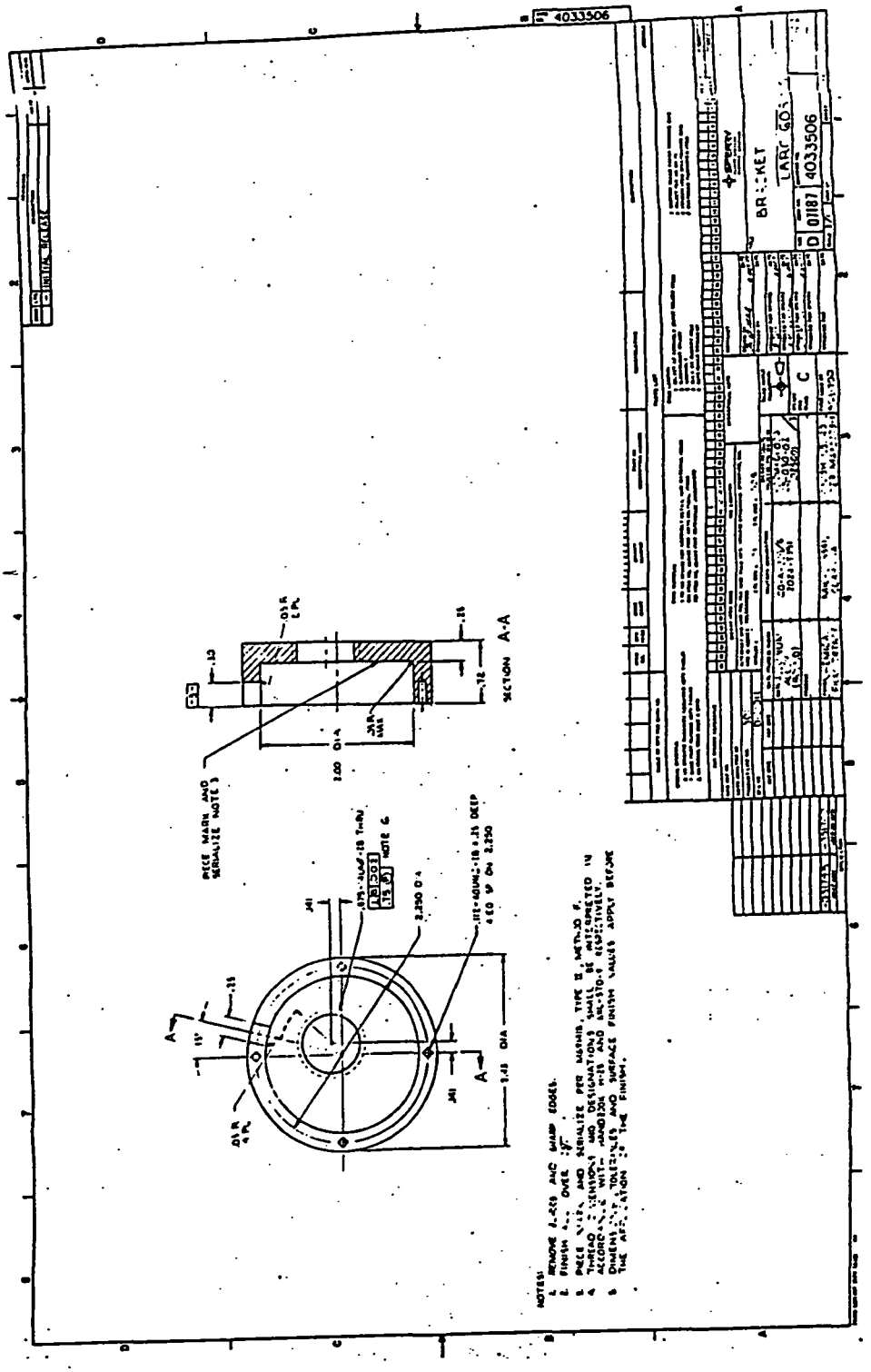

Figure A.8 Support Bracket for the Proximity Sensor.

A.3 Radial Magnetic Bearing Assembly

This section shows the individual drawings of the radial MBA's. Figures A.9 and A.10 show the dimensions of the inner and outer MBA support brackets respectively. Figure A.11 shows the assembly of the radial MBA's magnetic actuators. Figure A.12 shows the dimensions of the top plate. Figure A.13 shows the dimensions of the post. Figures A.14 and A.15 show the dimensions of the inner and outer radial base plates respectively.

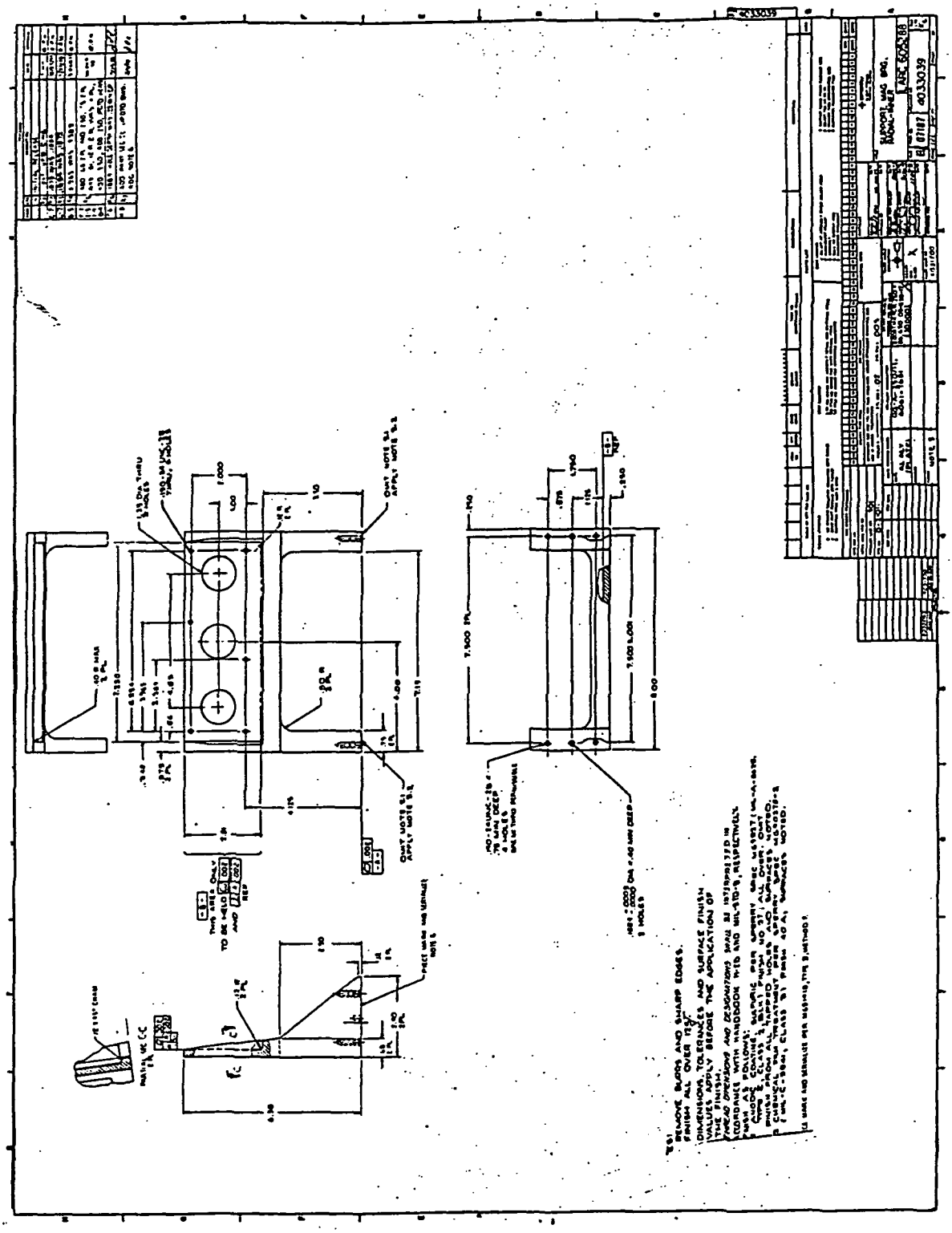

Figure A.9 Inner Support Bracket of the Radial MBA

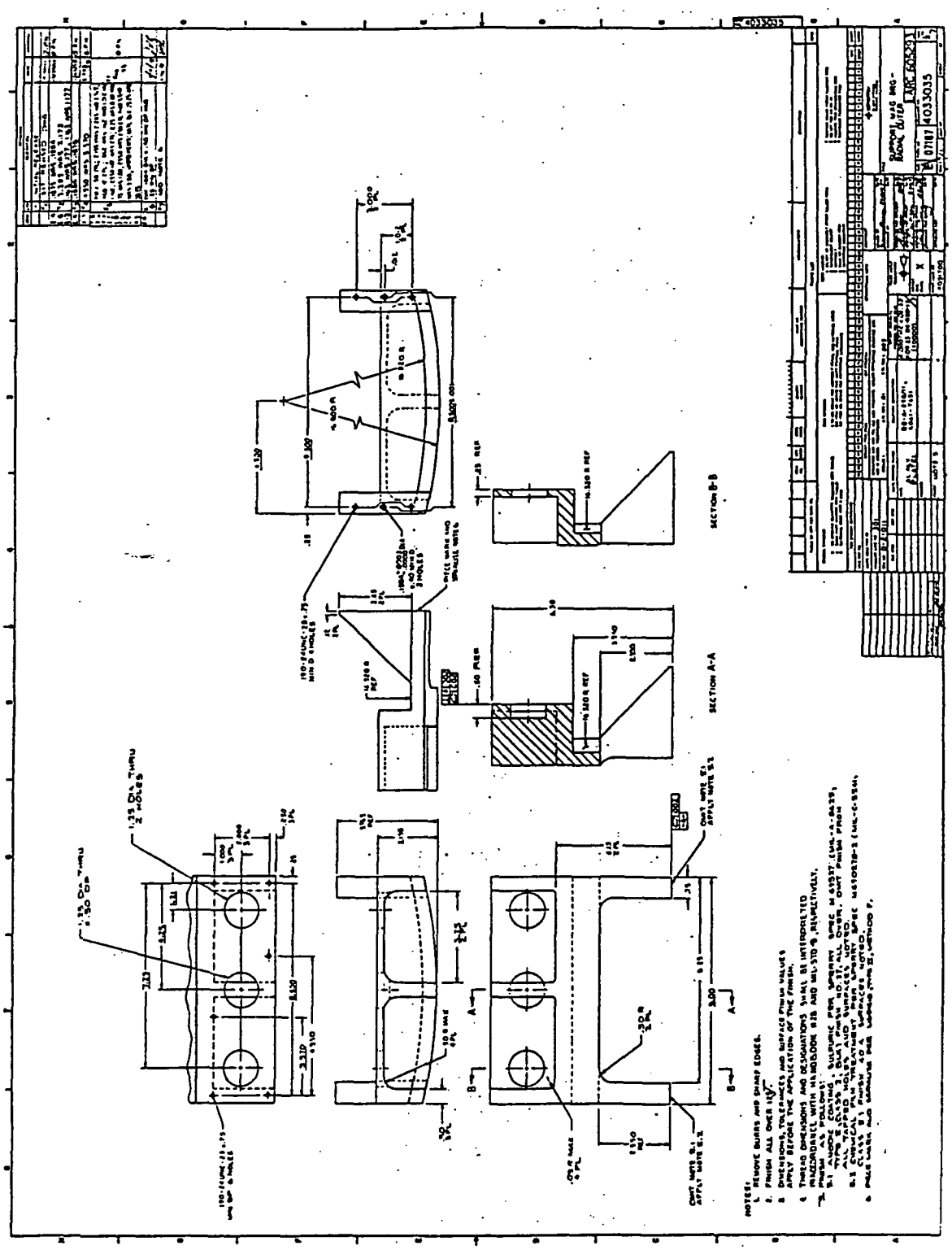

Figure A.10 Outer Support Bracket of the Radial MBA

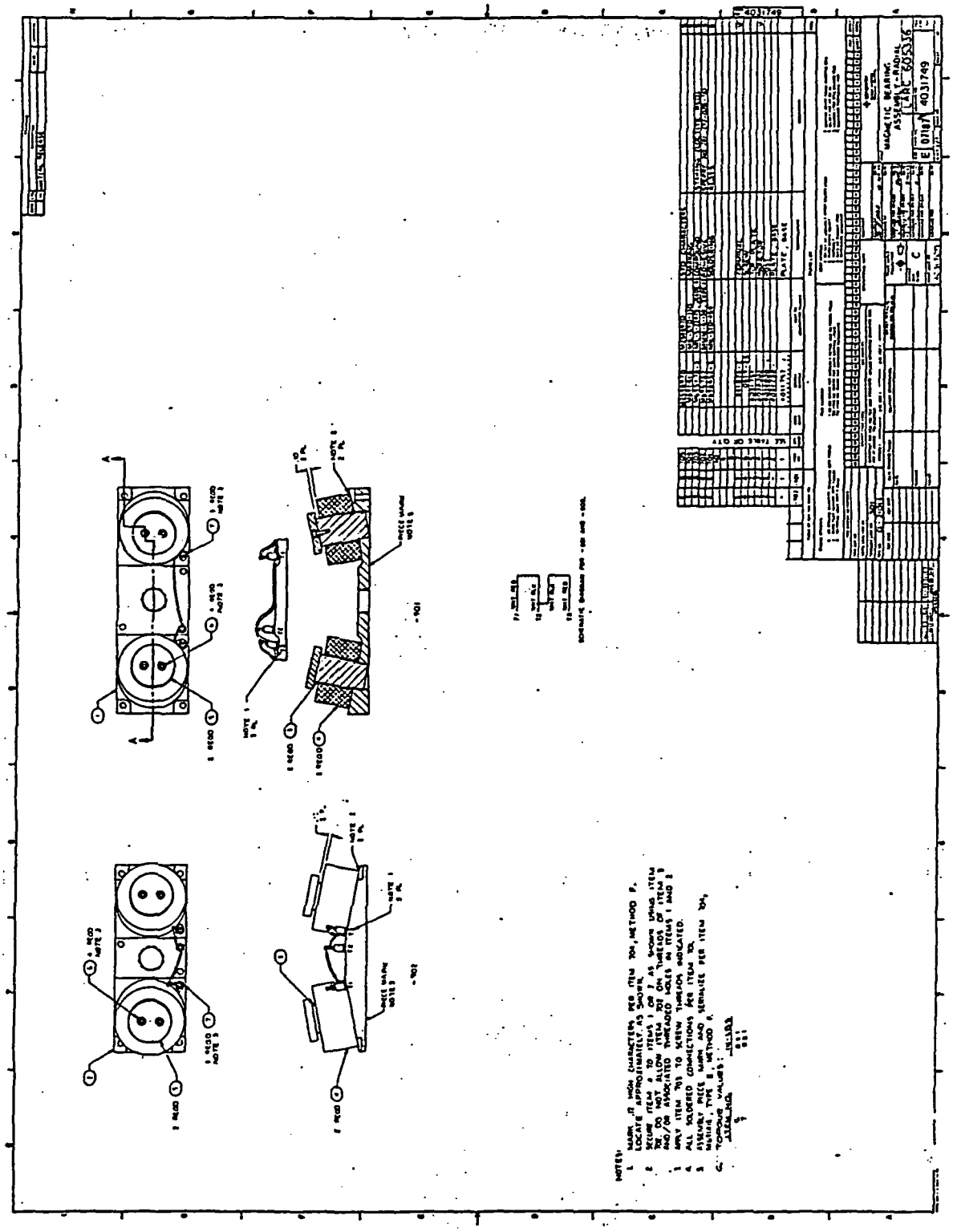

Figure A.11 Assembly of Radial MBA

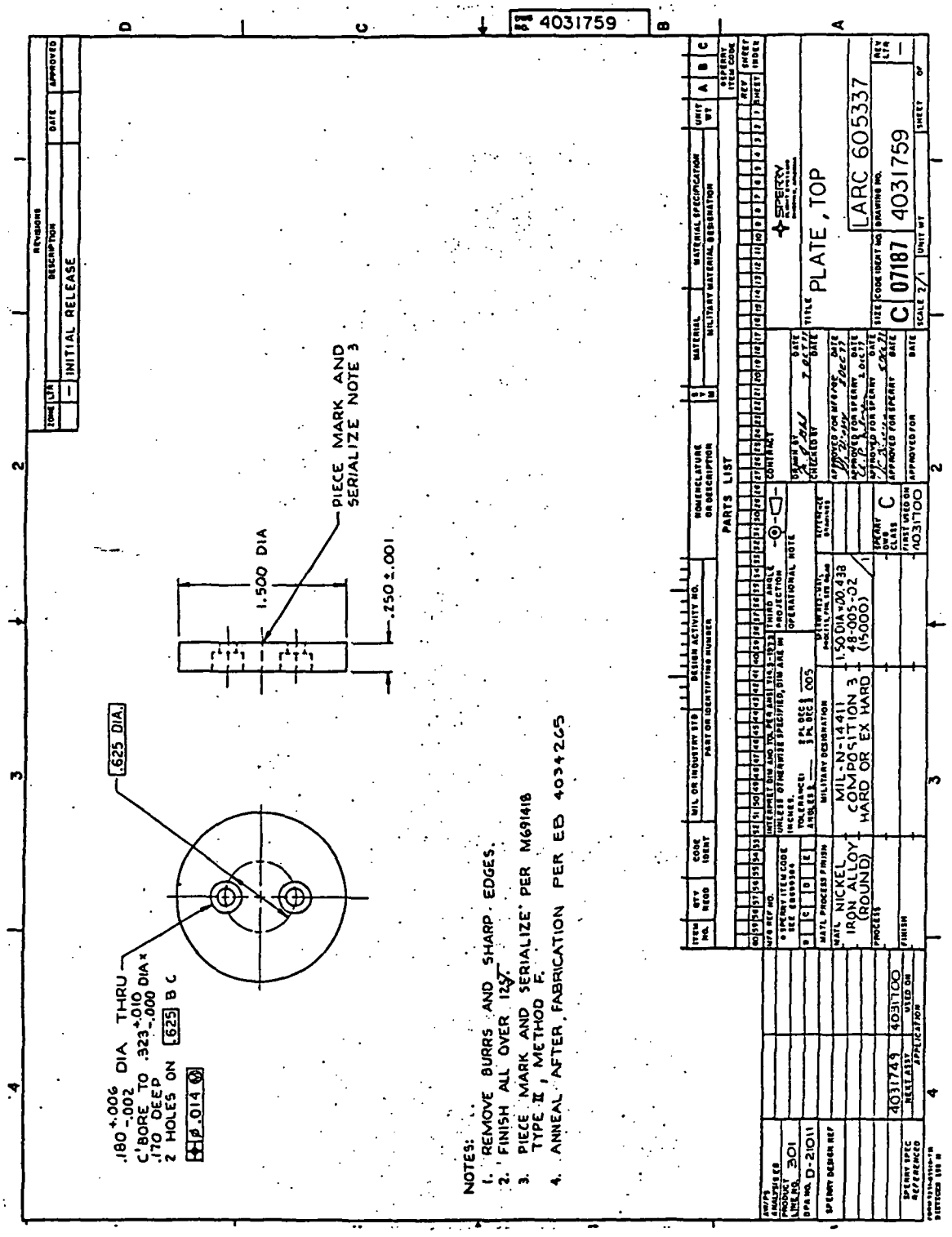

Figure A.12 Top Plate of the Radial MBA

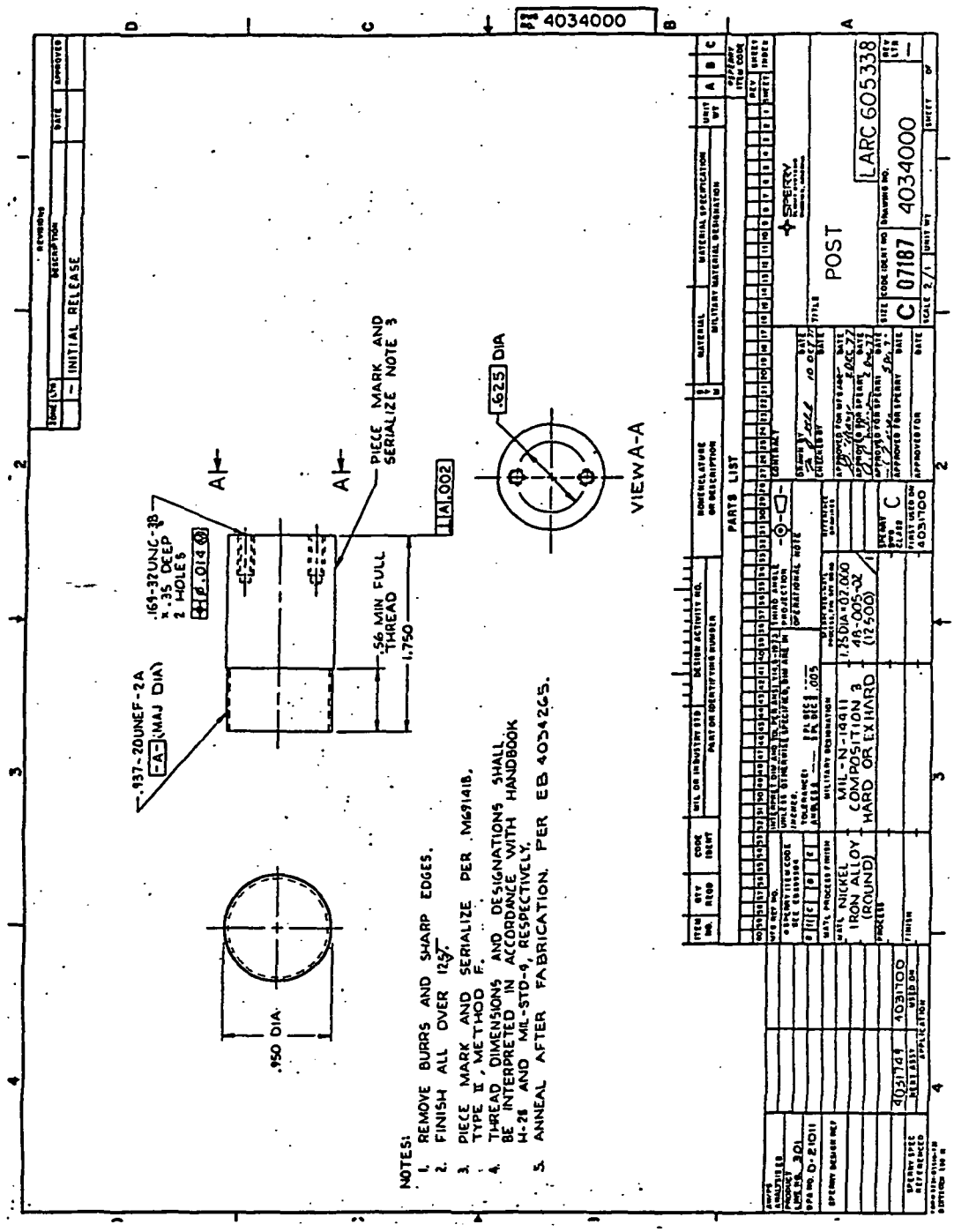

Figure A.13 Post of the Radial MBA

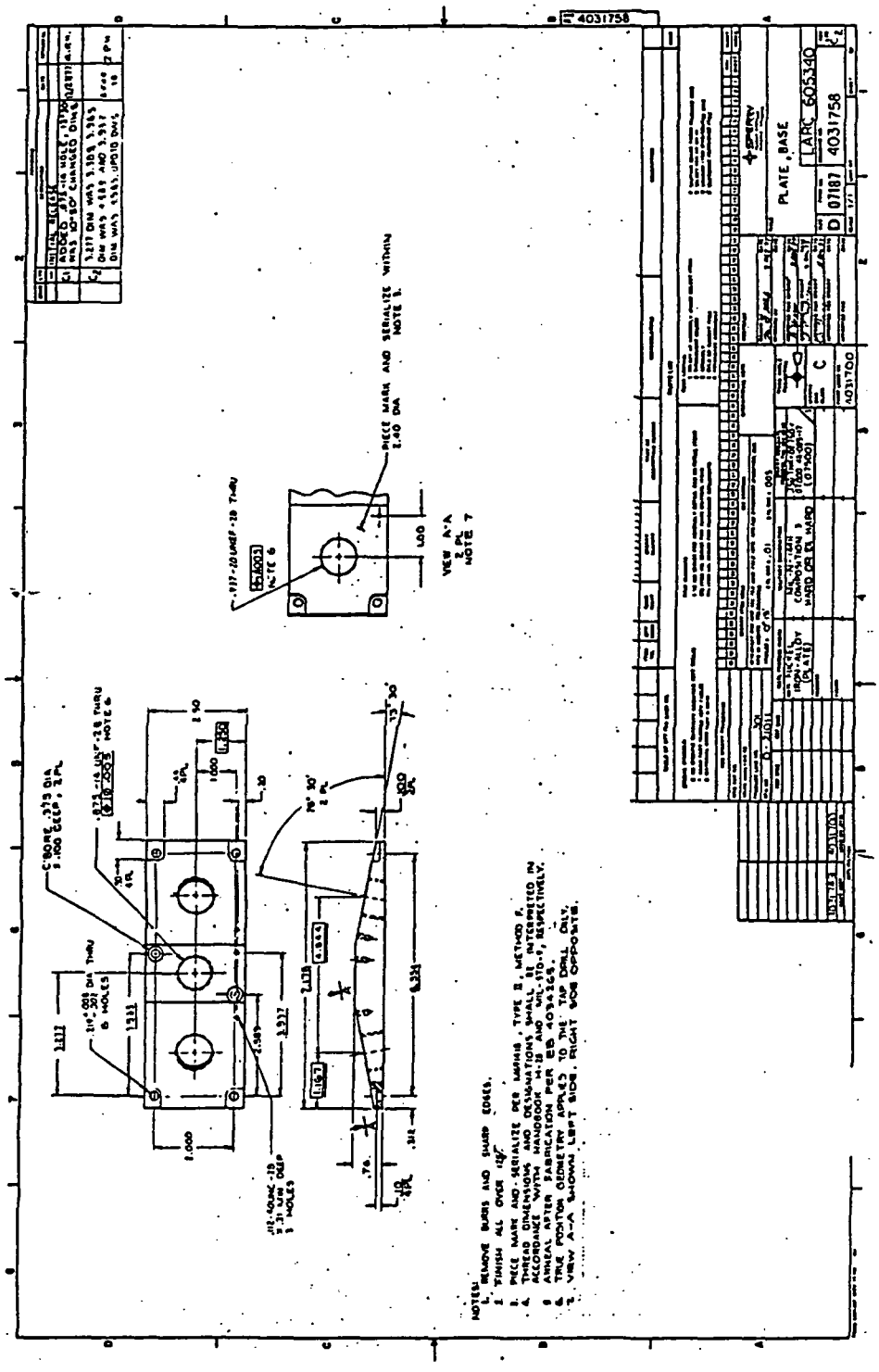

Figure A.14 Outer Base Plate of the Radial MBA

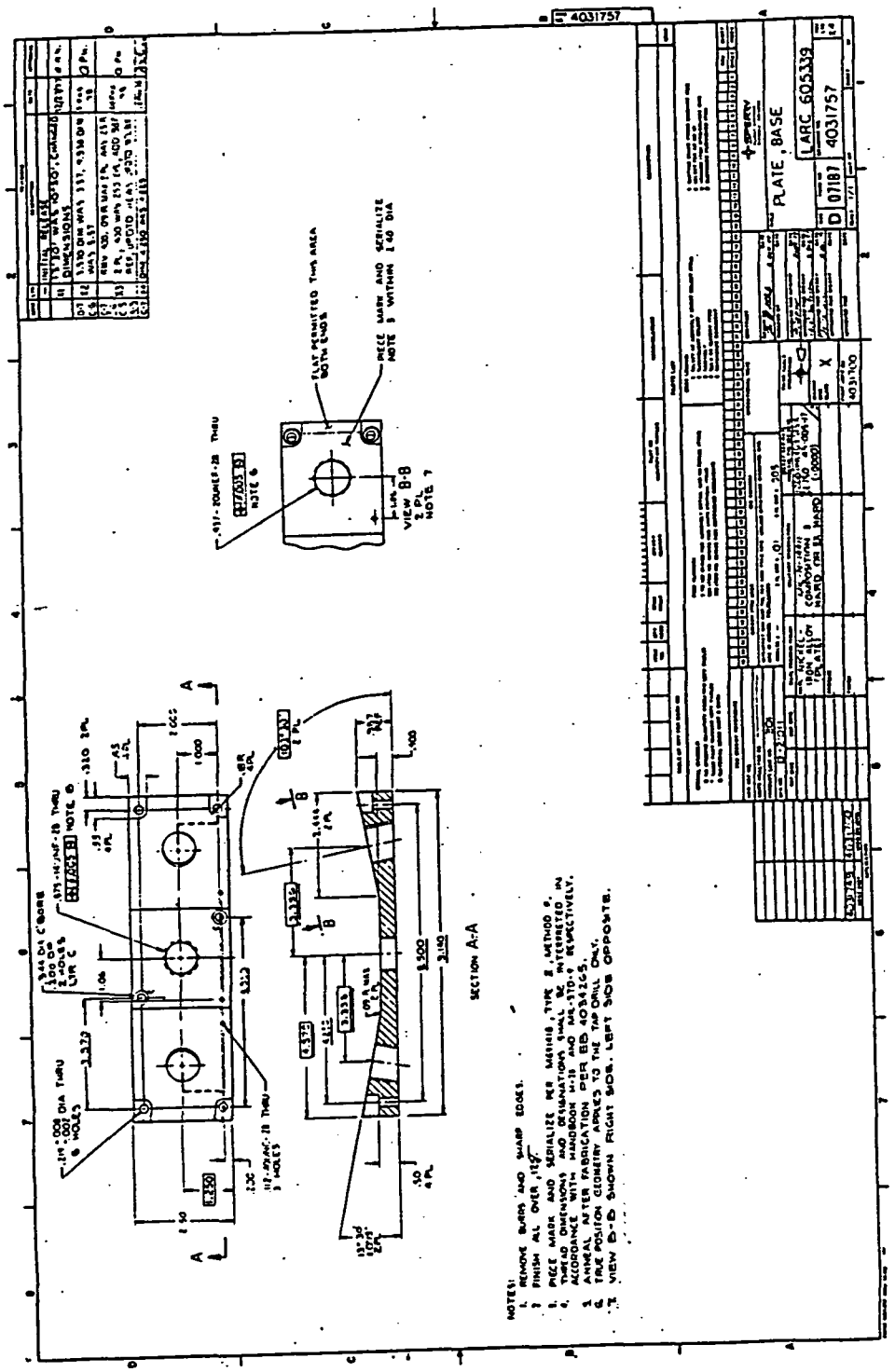

Figure A.15 Inner Base Plate of the Radial MBA

A.4 Annular Iron otor

This section shows the dimensions of the annular rotor.

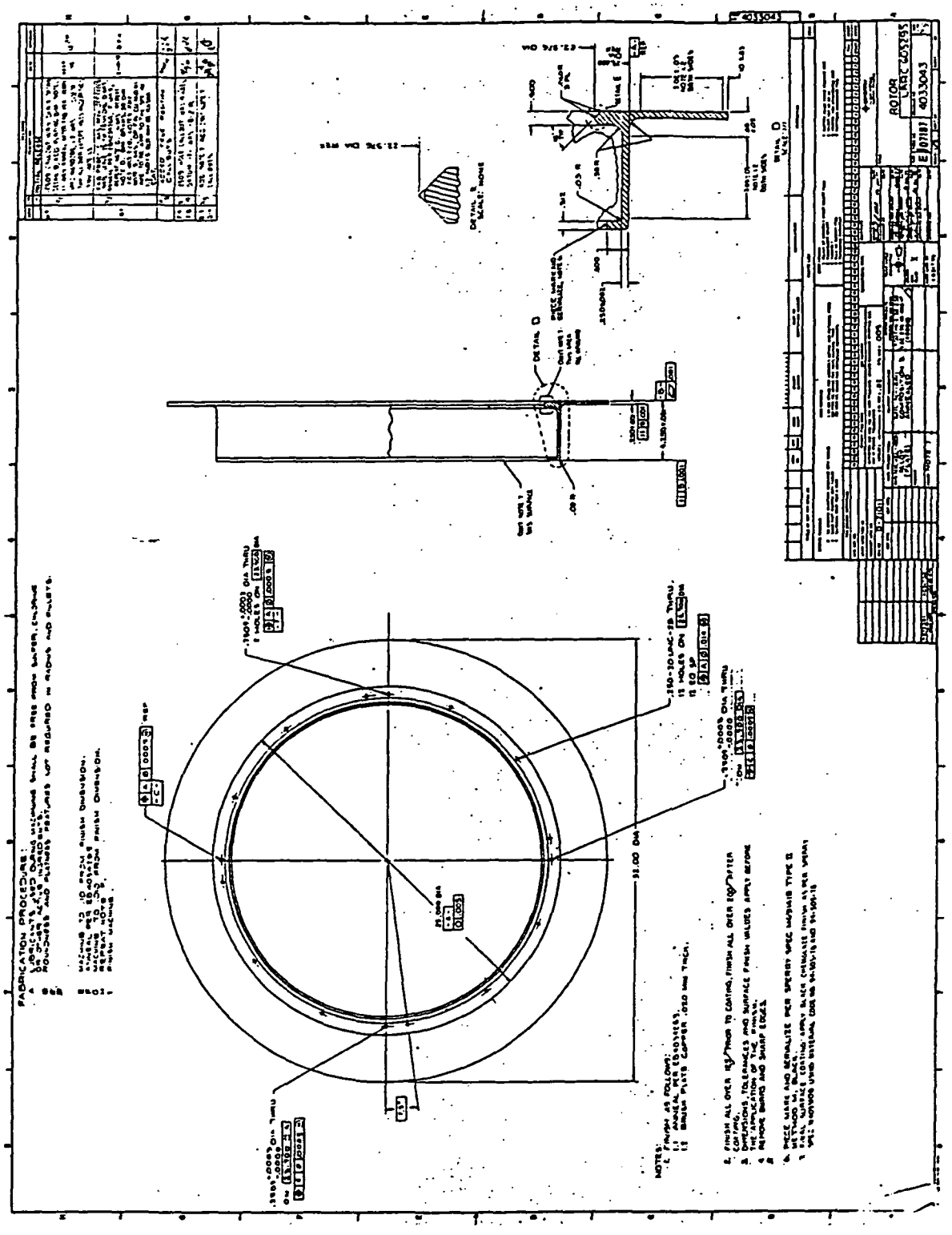

Figure A.16 Dimensions of the Annular Rotor

Appendix B

Proximity Sensor Electronics Assembly Design

The hardware layout along with the component schematic and component layout of the proximity sensor electronics is given here. These drawings are reduced copies of the blue prints supplied with the ASPS. Figure B.1 shows the layout of the proximity sensor electronics box. Figure B.2 is the design of the sensor amplifier card. Figure B.3 shows the component layout of the sensor amplifier card. Figure B.4 shows the design of the oscillator card, and Figure B.5 shows the component layout of the oscillator card.

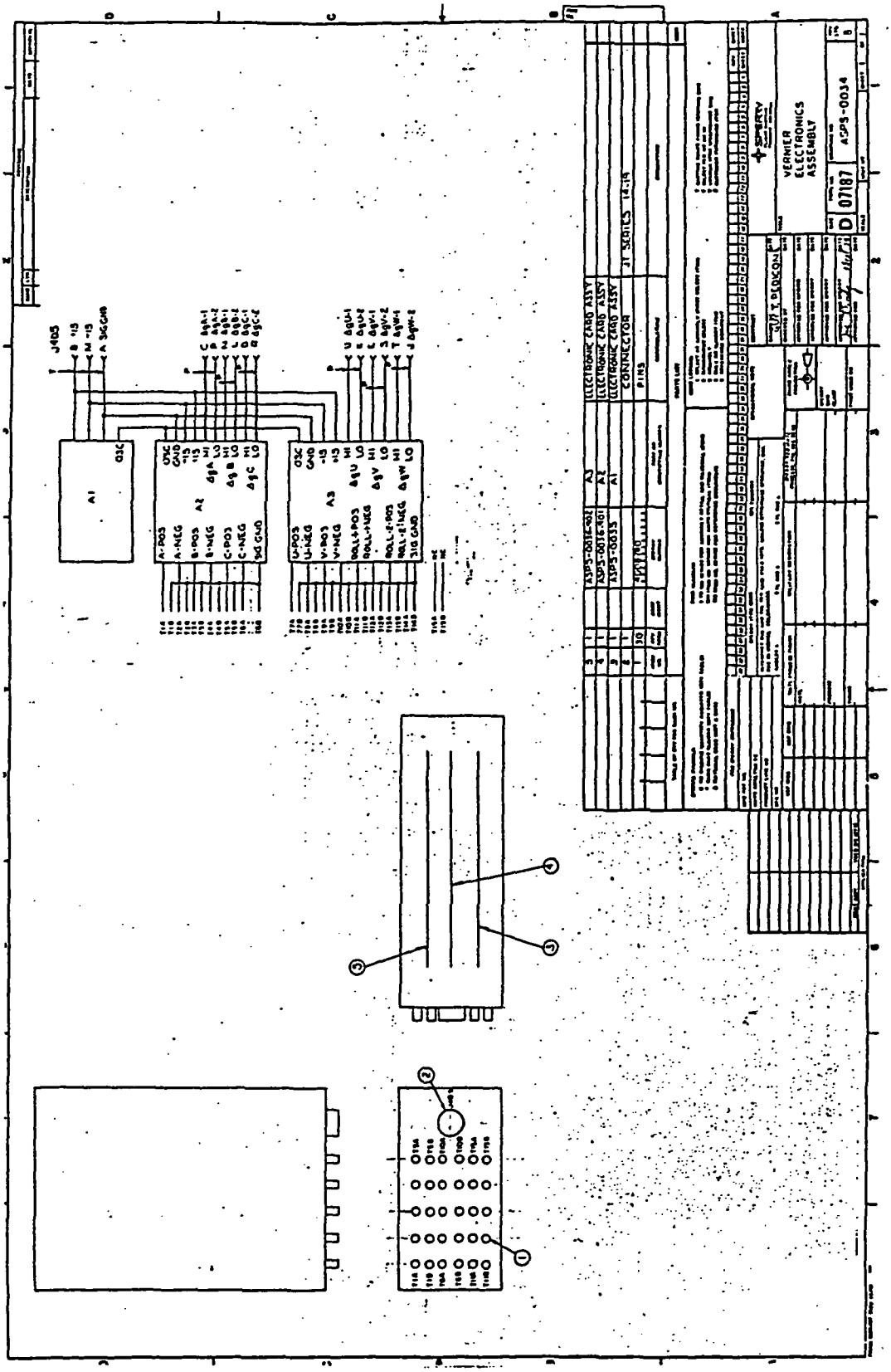

Figure B.1 Venier Electronics Assembly

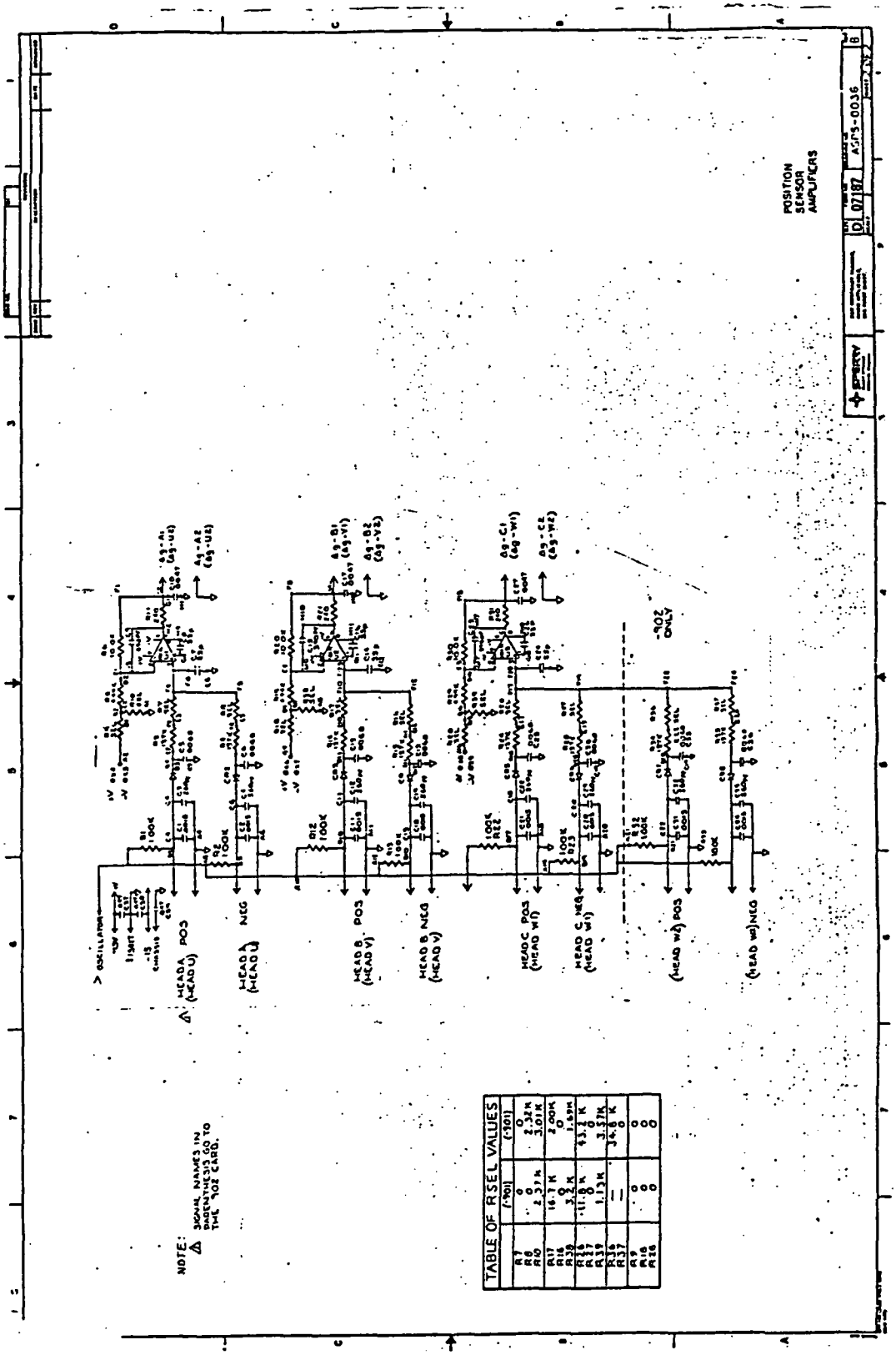

Figure B.2 Position Sensor Amplifier Design

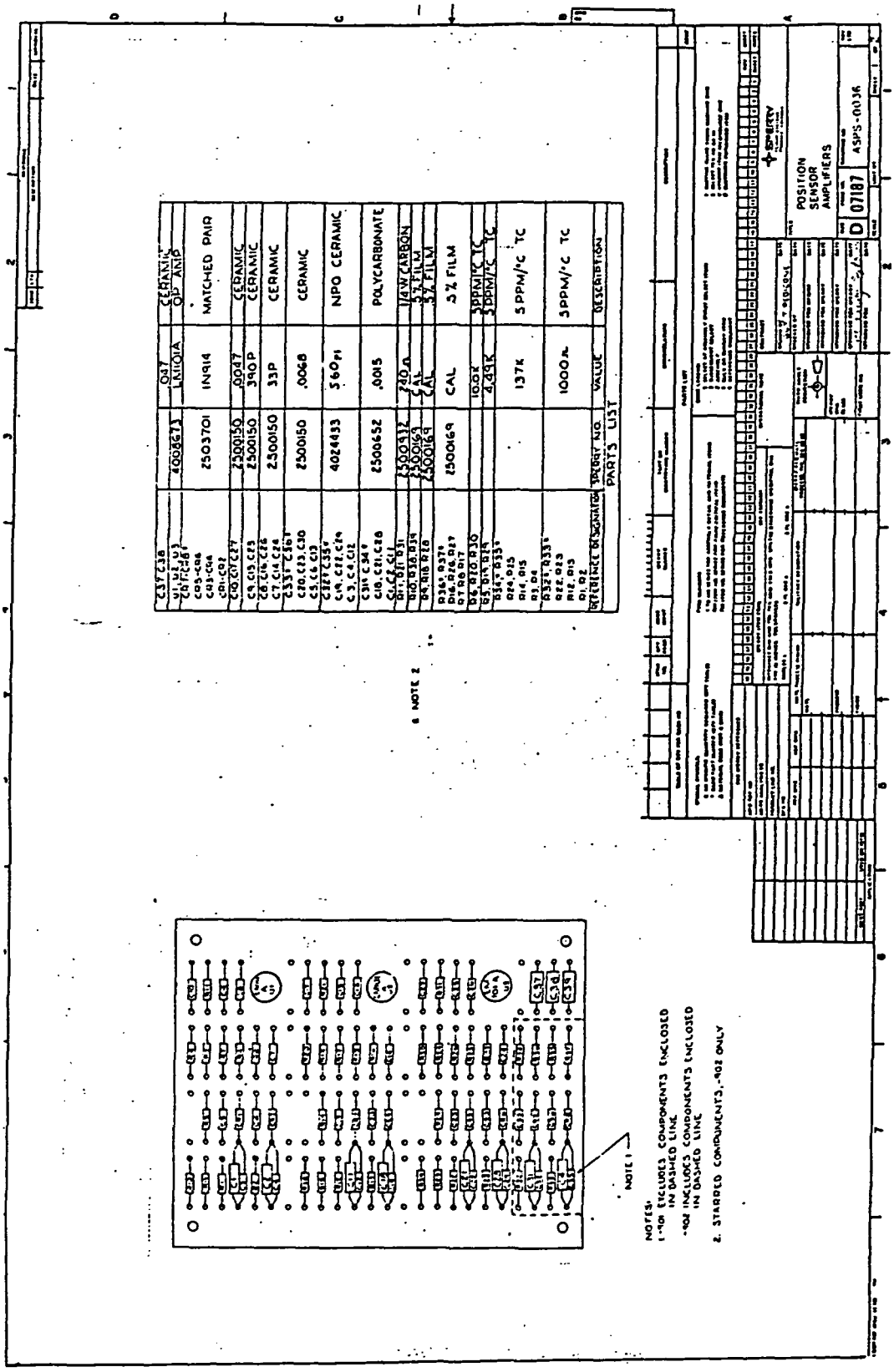

Figure B.3 Position Sensor Amplifier Card Layout

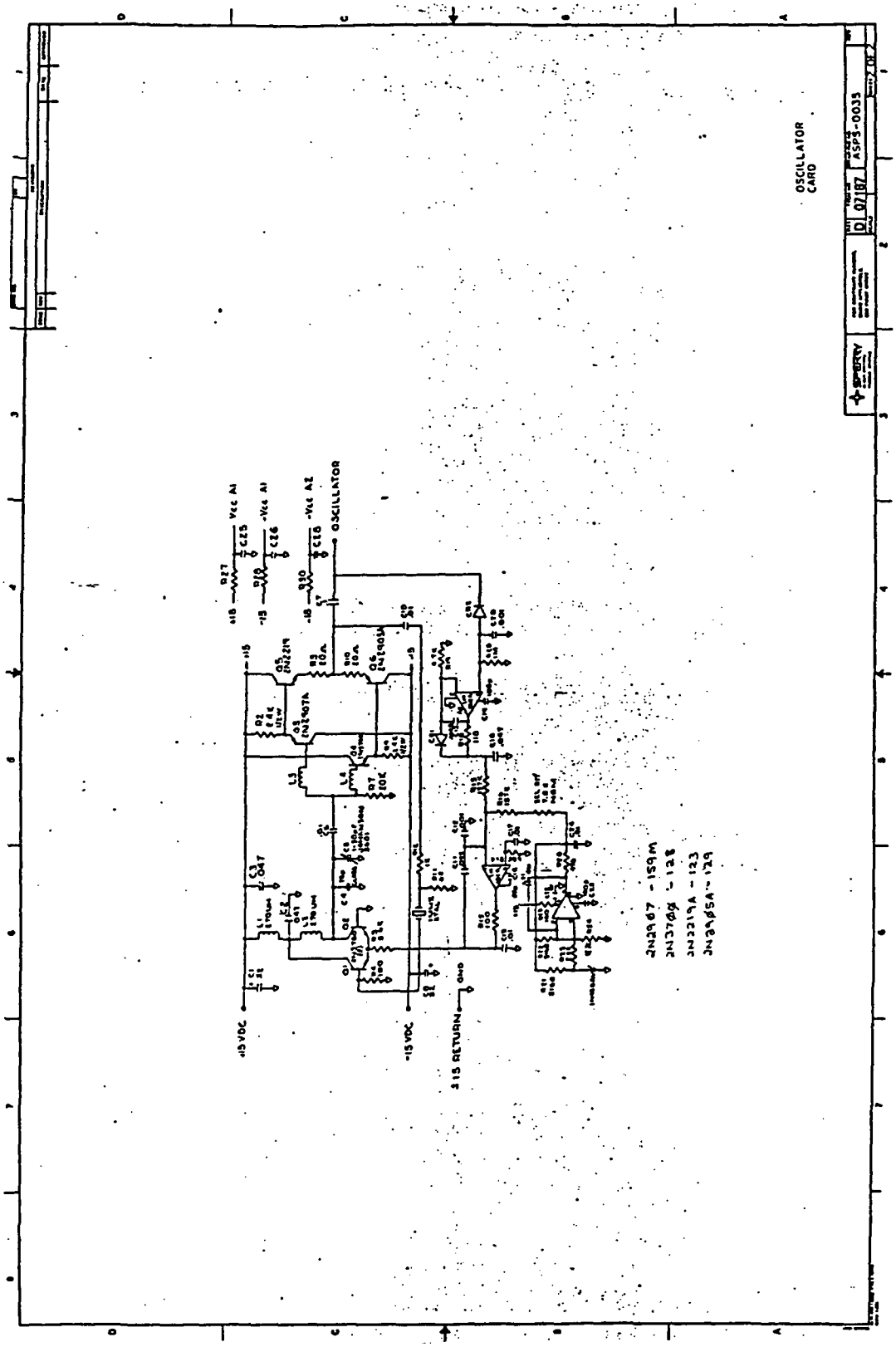

Figure B.4 Oscillator Card Design

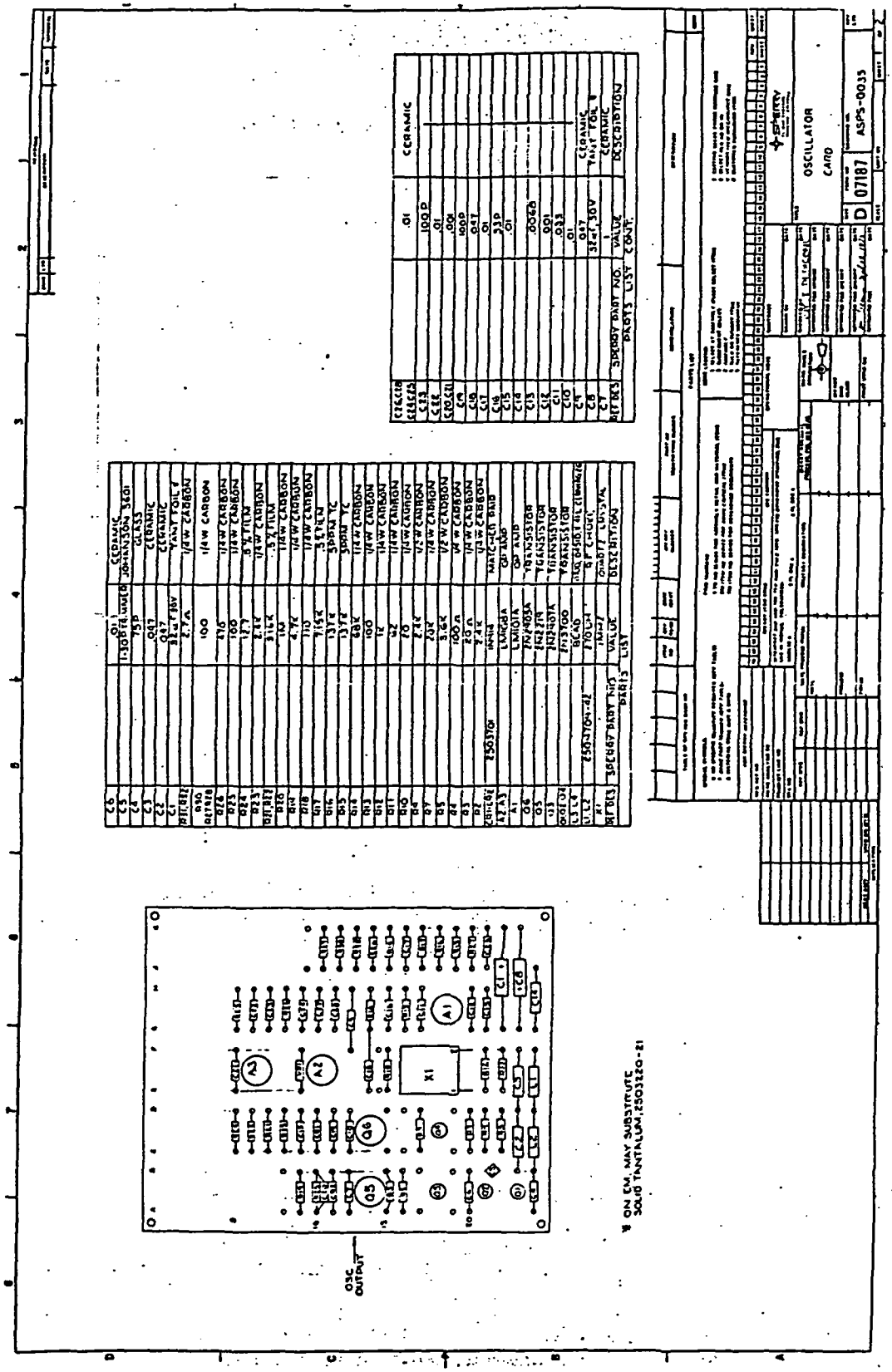

Figure B.5 Oscillator Card Layout

Appendix C
Vernier Latches, Rotary Transformer, and Roll Resolver Designs

These drawings are reduced copies of the blue prints supplied with the ASPS. This appendix is supplied here to give only a brief description of these systems. Figure C.1 shows the location of the vernier latches. Figures C.2 and C.3 show the design of the individual vernier latches. Figures C.4 and C.5 show the design of the roll axis resolver. Figure C.6 is a description of the rotary transformer.

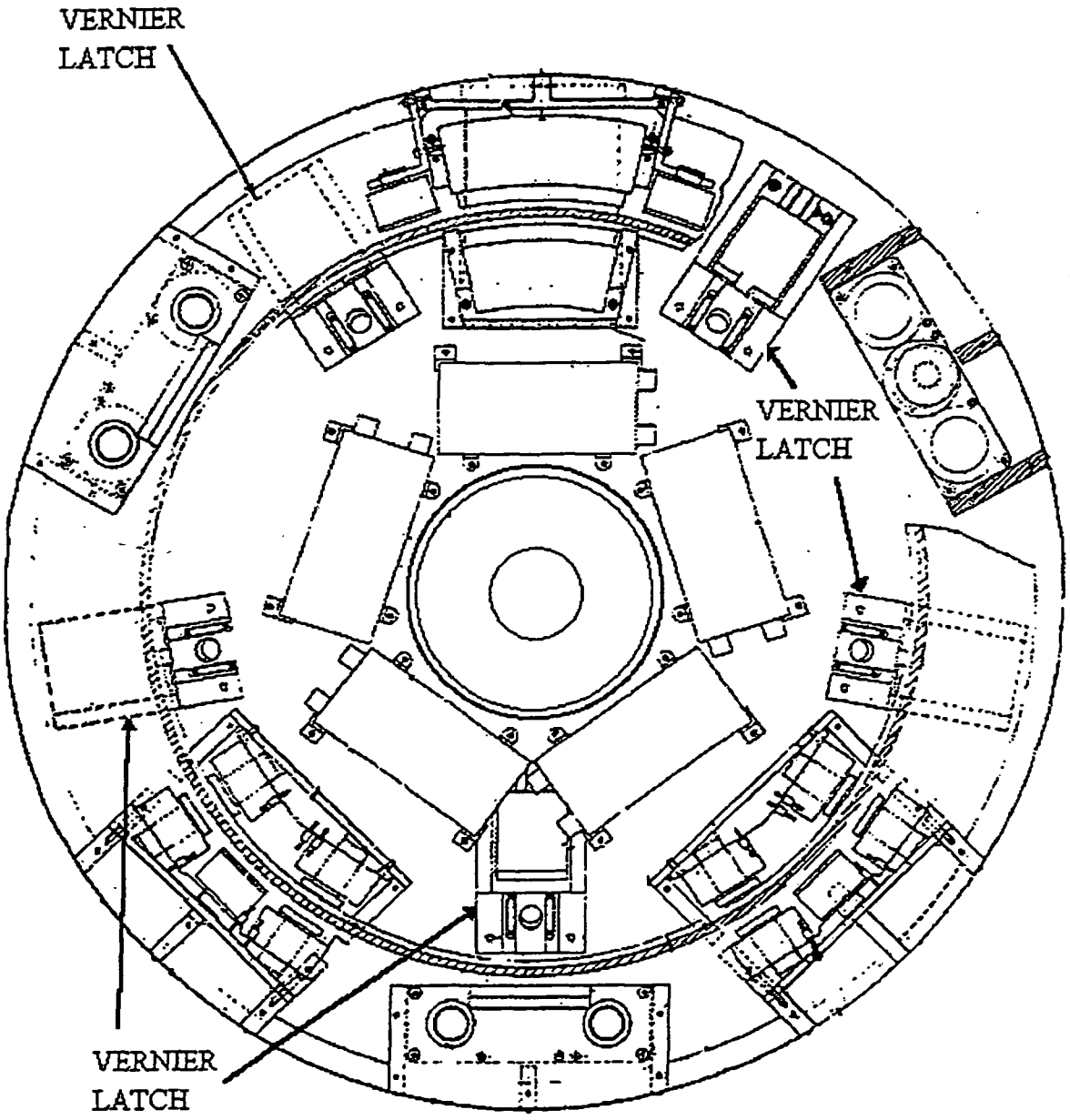

Figure C.1 Location of the Vernier Latches

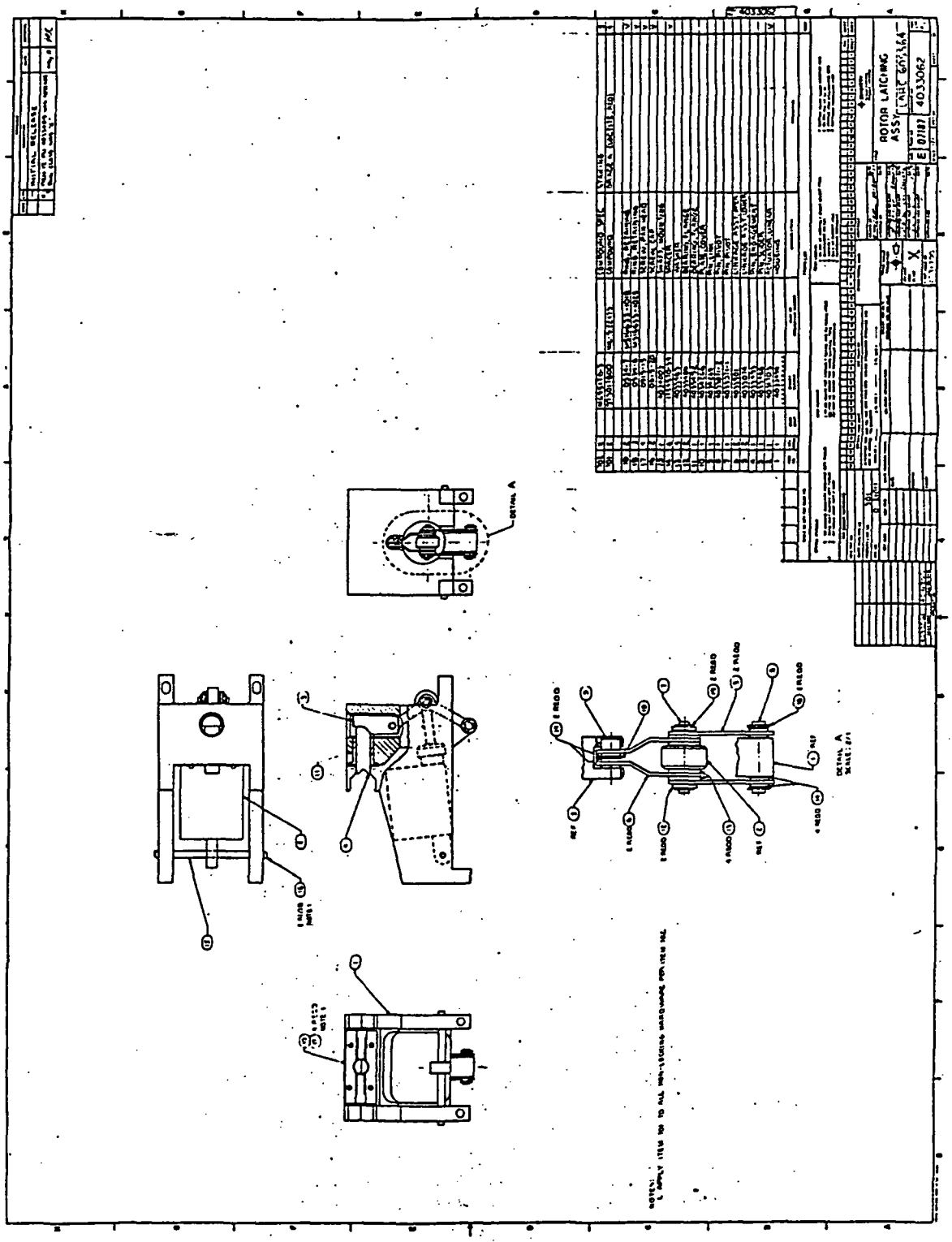

Figure C.2 Rotor Latching System

C-2

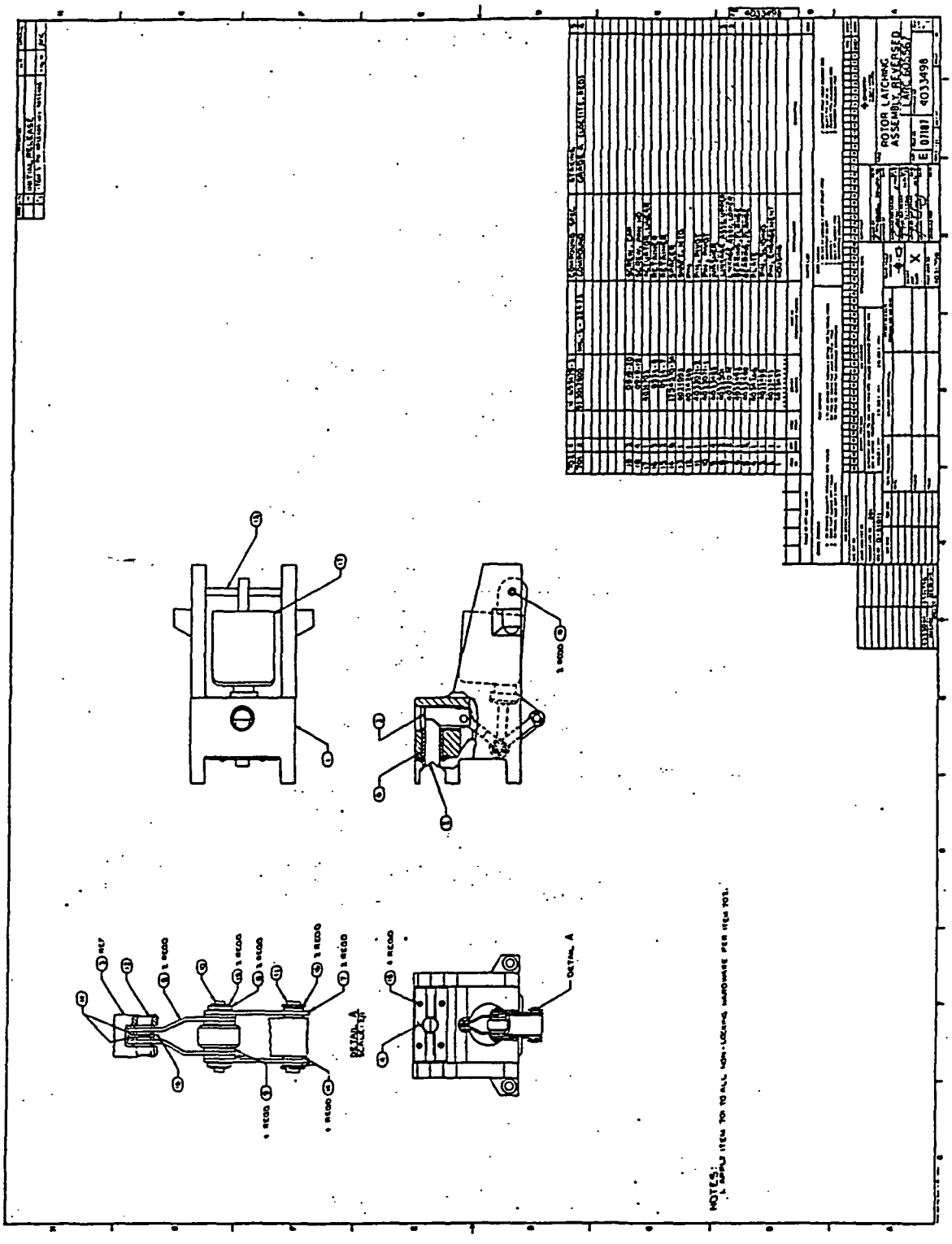

Figure C.3 Rotor Latching Sytem Reversed

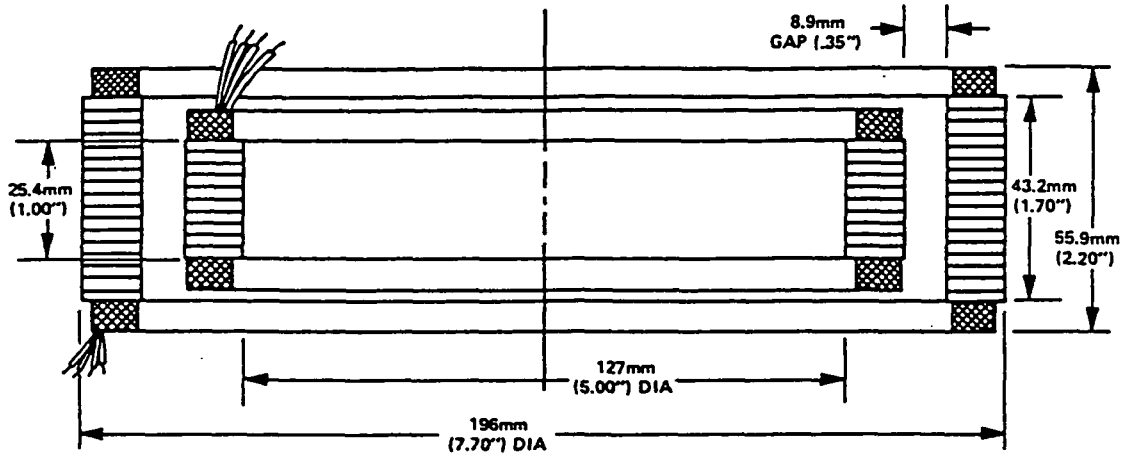

Figure C.4 Roll Resolver

Parameter	Requirements
Type	Single speed, sine-cosine resolver
Operating Clearance	
Radial	8.89 mm (.350 in.)
Rotor Motions	
Axial	±5.59 mm (.220 in.)
Radial	±5.08 mm (.200 in.)
Angular	±3/4 degree
Accuracy	
Resolver Transmitter(RX)	< 1 arc minute*
Resolver Control Transformer(RC)	< 1 arc minute* (Required only during ±.015 translational motions or angular motions to 3/4 degree)
Resolution	< 1 arc second
Weight	5.9 kg (13 LB)
Leakage Flux	< .1 gauss at .3 m (12 in.) from unit
Radial Forces	1.4×10^{-4} N m (10^{-4} FT-LB) > 65 cycles/revolutions
Rotational Forces	$< \frac{.0088}{N_c}$ N m ($\frac{.0065}{N_c}$ FT-LB) at Nc $\leq$ cycles/revolution

*Component accuracy goal.

Figure C.5 Roll Resolver Design Discription

PARAMETER	DESCRIPTION	
TYPE	NON-CONTACTING, LOW POWER	
WEIGHT	2.7 Kg (6 POUNDS)	
	STATOR EXCITED	ROTOR EXCITED
EXCITATION	10 VOLTS 400 HERTZ	10 VOLTS 400 HERTZ
INPUT IMPEDANCE	> 50 OHMS	> 100 OHMS
OUTPUT IMPEDANCE	< 10 OHMS	< 200 OHMS
TRANSFORMATION RATIO	.7	.7
PHASE SHIFT	5 DEGREES	5 DEGREES

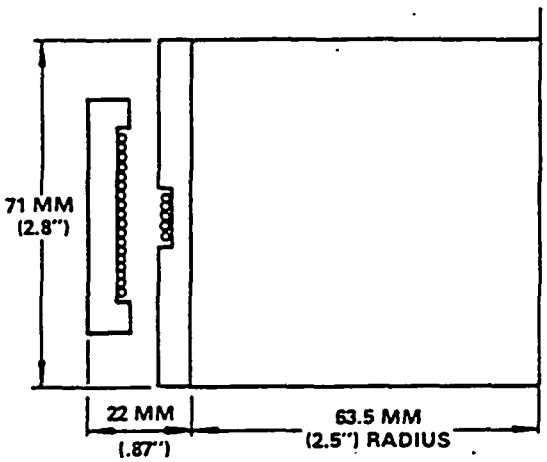

Figure C.6 Rotary Transformer Description

Appendix D
Controls Hardware Components

D.1 Old Controls Electronics Rack Layout

This section is not a detailed description of the old controls rack, but this section is only intended to give the reader an idea of the size of the old rack.

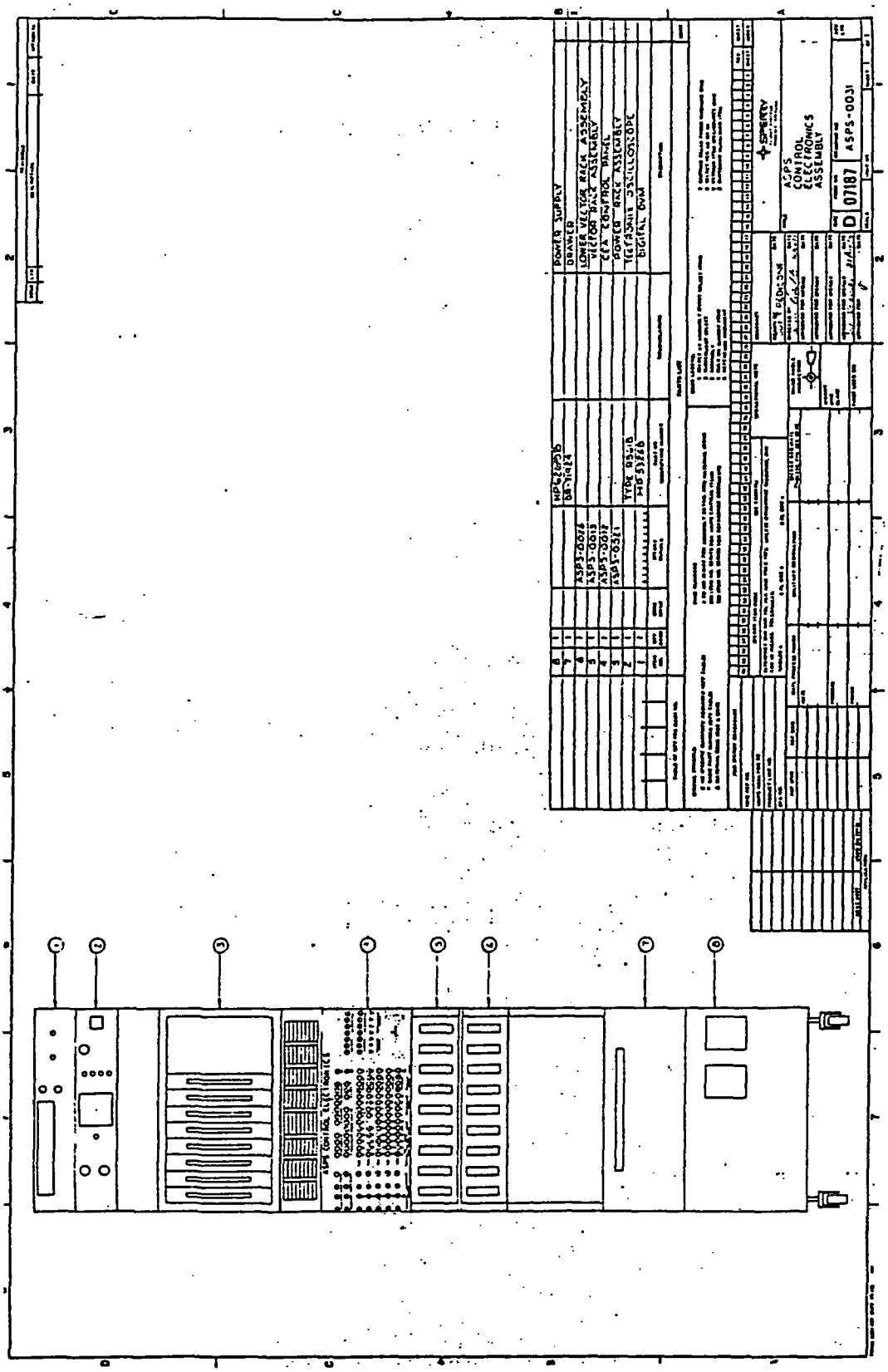

Figure D.1 Old Controls Electronics Rack

D.2 Functional Diagrams and Technical Specifications of the New Controls Hardware

Figure D.2 is a functional diagram of the power amplifier. Figure D.3 is a listing of the technical specifications of several of the amplifiers that Copley Controls Corp. manufacture. The one used to power the MBA's is the 303 series. Figure D.4 is a listing of the connectors, signals, and pinouts of the amplifier. Figure D.5 is a listing of the basic checklist for application. Figures D.6 and D.7 give a discription of the power supplies used to power the amplifiers.

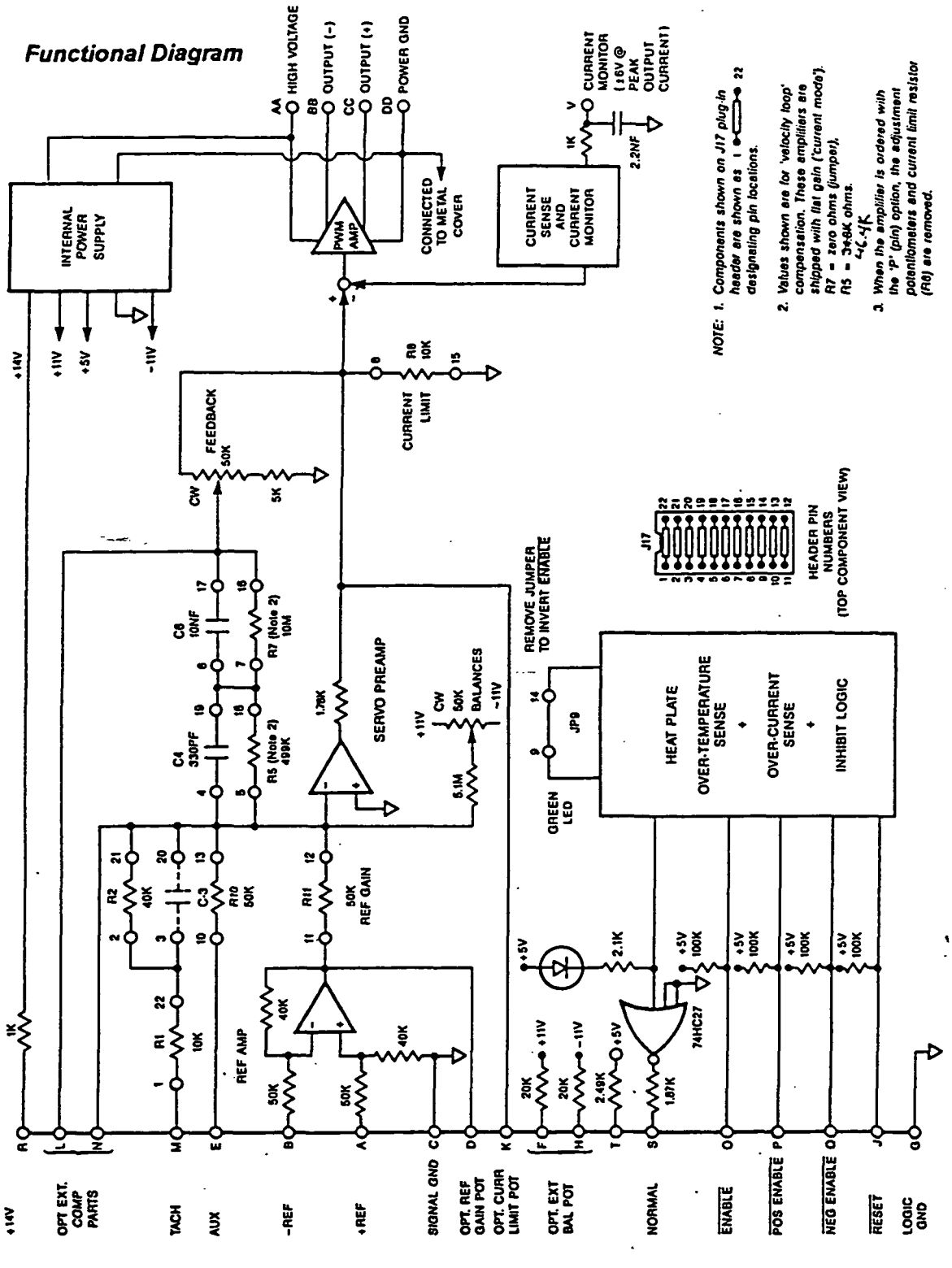

Figure D.2 Functional Diagram of the Power Amplifier

Technical Specifications

(B SERIES SPECIFICATIONS ARE SHOWN IN ( ) WHERE THEY DIFFER FROM SPECS SHOWN)

Typical specifications @ 25°C ambient. Load/Model 303: 2.5 ohms in series with 250µH at ±80 VDC.
Load/Model 306: 1.0 ohms in series with 125µH at ±80V. Load/Model 312: 14 ohms in series with 700µH at ± 160 VDC.

MODEL	303 (303B)	306 (306B)	306A (306AB)	312
PEAK POWER OUTPUT	±75V @ ±12A (±90V @ ±12A)	±75V @ ±25A (±90V @ ±25A)	±75V @ ±30A (±90V @ ±30A)	±150V @ ±9A
Unidirectional current change		1s		
Bidirectional current change		2s		
MAXIMUM CONTINUOUS CURRENT				
Heat sink mount @ 70°C	6A	10A	15A	4.5A
Forced air 400 cfm @ 50°C	6A	10A	15A	4.5A
With Heatsink (H)				
Ambient @ 40°C		10A	15A	4.5A
Forced air 400 cfm	6A @ 60°C	10A @ 60°C	15A @ 50°C	4.5A @ 60°C
OUTPUT VOLTAGE (V_{OUT})	V_h- (0.26) (I_o)	V_h- (0.13) (I_o)		V_h- (0.60) (I_o)
where: (V_{OUT}) = voltage to motor or load				
V_h = high voltage applied				
I_o = current into motor or load				
MINIMUM INDUCTANCE[1]				
@ 160 Volts	NA	NA		700µH
@ 80 Volts	250µH	125µH		350µH
@ 40 Volts	125µH	64µH		175µH
CURRENT LIMIT		*Adjustable from 0 to peak current*		
INPUT CHARACTERISTICS				
Reference		Differential, ± 10 VDC max; 98k ohms min		
Tachometer		Single-ended, 50k ohms (scale factor adjustable)		
BANDWIDTH				
Power stage, small signal		-3dB @ 3kHz		
Slew rate	80A/ms	167A/ms	200A/ms	60A/ms
SWITCHING FREQUENCY		22kHz		
REMOTE SHUTDOWN[3]				
ENABLE, switch closure, logic low		ENABLES output		
POSITIVE ENABLE, logic low		ENABLES pos output		
NEGATIVE ENABLE, logic low		ENABLES neg output		
AMPLIFIER PROTECTION				
Overload		Current limit		
Heatsink temp		Shutdown 83° C		
Latch Off		Until reapplication of power or reset 'low' [2]		
Overvoltage, temporary	>83 VDC (>99 VDC)	>83 VDC (>99 VDC)	>83 VDC (>99 VDC)	>166 VDC
Undervoltage	<16 VDC	<16 VDC	<16 VDC	<24 VDC
Shorts		Across outputs, or either output to GND		
INDICATORS				
Current monitor		± 6 VDC/I_{max}		
Status (HCMOS)		Logic high indicates normal operation		
		Logic low indicates amplifier fault or amplifier is disabled		
POWER REQUIREMENTS				
High voltage supply		+ 16 to + 80 VDC (+16 to + 90 VDC)		+24 to +160 VDC
Internal capacitance		200µF		20µF
THERMAL REQUIREMENTS				
Case temperature		0 to 70°C		
Power dissipation at continuous rating	19W	30W	48W	31W
Ambient		0 to 45°C		
Heat sink mount, flat surface		0 to 70°C		
Forced air, 400 cfm		0 to 50°C		
Heatsink option (H)				
Ambient		0 to 50°C		
Forced air, 400 cfm		0 to 60°C		
Storage		-30 to +85°C		
MOUNTING OPTIONS (See Ordering Guide)				
Standard model, connector mount		22-pin snap-on, screw terminal		
PCB mount		Option "P"		
Eurocard (3U)		Option "E"		
Adapter card MB4		Option "M"		

NOTES:

1. *For higher inductance, to maintain the bandwidth; Specify 303-1 for 4-18mH, 306-1 or 306A-1 for 2-9mH and 312-1 for 11-50mH.*
2. *If reset is low, the amplifier will attempt to reset every 25ms.*
3. *The logic sense of the 'enable' line can be reversed. See detailed description in this data sheet ("Logic inputs").*
4. *NA = not applicable*

Figure D.3 Technical Specifications

Basic Amplifier Connectors, Signals and Pinouts

If you are using the MB4 or Eurocard, the pinouts will be different (refer to the sections on the MB4 and Eurocard). Use this list when reading the following sections on hooking up the basic amplifier.

Types of signals are listed after the pin number or letter.

P	*Passive*	Power and ground
I	*Input*	Analog or digital signal inputs
O	*Output*	Signal, logic, and power-stage outputs

Note: See appendix for complete listing of connectors and part-numbers.

4 Pin power connector

	Type	Remarks
AA	P	+HV, the high-voltage DC power input
BB	O	Out- , or negative output
CC	O	Out+, or positive output
DD	P	Ground and +HV power return

22 Pin signal connector

Note that pins are referred to by letter and number. The letter refers to the functional schematic. The number is the actual connector-pin number on the cable header that connects to the amplifier.

-Pin-	Type	Signal	Remarks
1 (A)	I	+Ref	Differential (+) reference signal input
2 (B)	I	-Ref	(-)
3 (C)	P	Signal Gnd	Gnd for tachometer, signal gnd
4 (D)	O	Ref amp out	Output of differential input amplifier
5 (E)	I	Aux input	Auxiliary input
6 (F)	O	+11V	20K ohms in series with +11V
7 (G)	P	Logic gnd	Gnd for Enable inputs
8 (H)	O	-11V	20K ohms in series with -11V
9 (I)		N.C.	No connection to this pin
10 (J)	I	/Reset	LO or Gnd to reset fault condition
11 (K)	O	Preamp out	See schematic
12 (L)		Opt. ext. comp	See schematic
13 (M)	I	Tach input	Tachometer input
14 (N)		Opt. ext. comp	See schematic
15 (O)	I	/Enable	LO or Gnd to enable amplifier
16 (P)	I	/Pos Enable	LO or Gnd to enable positive output
17 (Q)	I	/Neg Enable	LO or Gnd to enable negative output
18 (R)	O	+14V	1K ohms in series with +14V
19 (S)	O	Normal	HI (+5V) when amplifier operating Normally
20 (T)	O	+5V	2.49K in series with internal +5V
21 (U)		N.C.	
22 (V)	O	Current monitor	Outputs +/-6V at amplifier peak current

Figure D.4 Amplifier Connectors, Signals, and Pinouts

Basic Amplifier: Current-Mode, NO Tachometer

Use this checklist for applications that don't employ a tachometer. These include microprocessor control systems that get position feedback from an encoder on the motor, as well as non-motor applications such as magnet-coil, solenoids, or other loads that require a set current from the amplifier in response to a control-voltage at the inputs. The components on the J17 header come from the factory preset for this operating mode. See functional diagram on page 2.

1. Connect DC power supply to amplifier +HV and GND. Check voltage to see that is is within the amplifiers' rating.
2. Ground amplifier to chassis at GND pin DD.
3. Connect motor or load between OUT+ and OUT-. *Do not ground load!*
4. Connect reference voltage source to REF+ and REF- inputs.
5. Ground ENABLE,POS ENABLE, NEG ENABLE to amplifier logic ground.
6. ~~Set REF GAIN pot to full CW.~~
7. Set FEEDBACK pot to full CW.
8. ~~Set CURRENT LIMIT pot to full CW.~~
9. Set V_{ref} to 0V
10. Turn power on
11. Check for green LED indicating Normal operation.
12. Adjust BALANCE trimpot for 0.0V between OUT+ and OUT-
13. Momentarily increase Reference voltage (±10V max).
14. Check motor direction: is it OK?
    YES: continue
    NO: remove power, reverse connections to Ref+ and Ref-.
15. Set Reference voltage to maximum value (+/-10V)
16. Check load current at CURRENT MONITOR output
17. Apply step or square-wave signal to Ref-inputs, adjust FEEDBACK CCW for best response with no oscillation.

Amplifier Connections

Numbered terminals are on the brown 22-pin connector. Double-letter terminals are on the orange 4-pin connector. See appendix for connector part numbers.

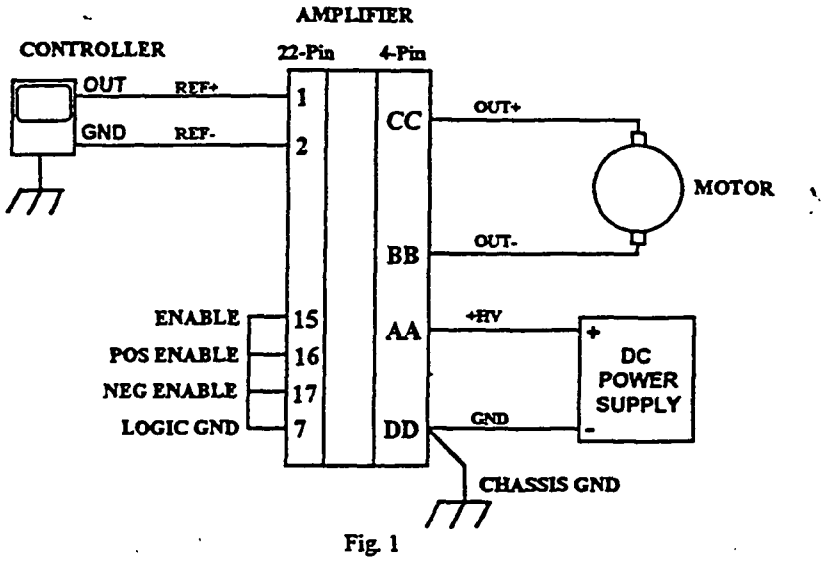

Fig. 1

Figure D.5 Basic Amplifier Connections

FEATURES

- Rugged L-bracket construction.
- Fused output.
- Simple — easy to use.
- Assembled with servo amps for multi-axis applications.
- Peak current rating 2.5 times nominal.

PRODUCT DESCRIPTION

The Series 600 power supplies have been designed to complement Copley Controls' servo amplifiers and to provide the user with a complete solution to single- and multi-axis DC drive applications. The Series 600 unregulated DC power source is an acceptable solution for most applications where output variations and AC ripple components can be tolerated. These unregulated power supplies are designed to provide the best cost-per-watt value. The output of these unregulated supplies varies with different loading conditions as well as changes in the AC line input. To minimize the effect of load variations a bleeder resistor has been added to keep a minimum load on the supply and thereby moving the operating point away from the zero load point. Copley Controls' unregulated power supplies have tapped primary windings to allow for 'fine tuning' the output voltage under actual application load. Ripple is a maximum of 3% of the output voltage at full rated load, and the output is fuse protected. Because of the requirement of peak load currents in most servo applications, the Series 600 power supplies have been designed to provide 1 second peak currents at 2.5 times nominal rating with a 20% duty cycle.

APPLICATIONS

The Series 600 power supplies have been used for a variety of applications. These include high voltage sources for DC and stepper servo motors. When combined with Copley Controls' family of PWM servo amplifiers the assembly can function as a complete high efficiency single- or multi-axis drive.

The Series 600 has also been used in other non-motion applications such as lamp loads or as inputs to onboard 3-terminal regulators.

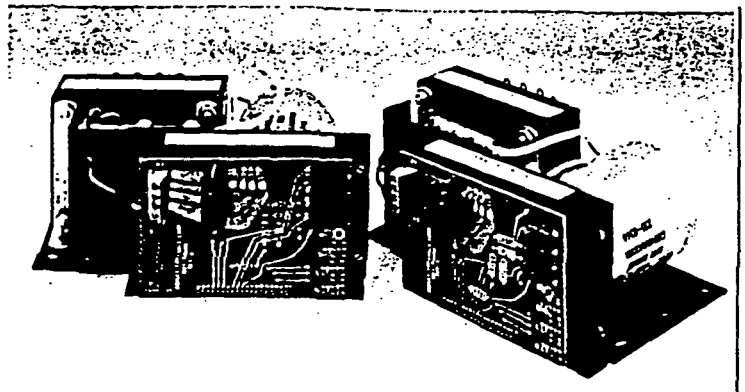

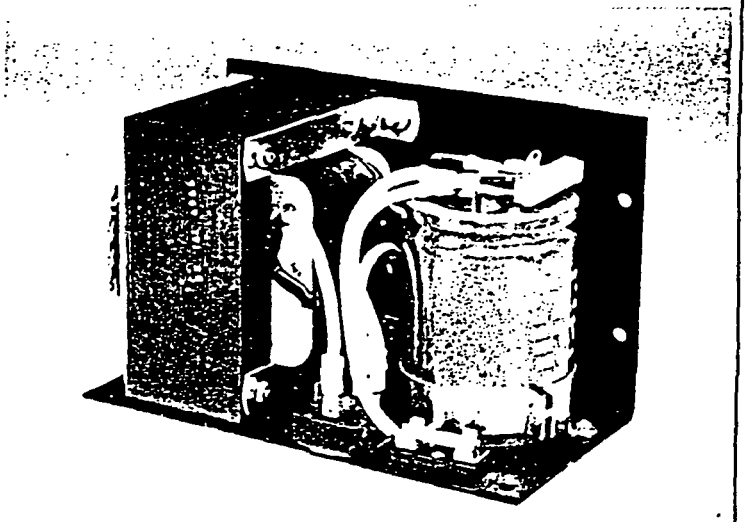

Figure D.6 Power Supply Description

KEY SPECIFICATIONS

Typical specifications @ +25°C ambient.

INPUT VOLTAGE[1]	115 VAC, 50/60 Hz
OUTPUT	Floating fixed output at full load rating (see Table 1).
	Transformer taps provide ±10% or ±5% output adjustment.
Ripple	3% rms maximum at full load output.
Peak Current	2.5 times nominal, 1 sec, 20% duty cycle.
OPERATING TEMPERATURE	0°C to +50°C
Derating	2% per °C from 50°C to 71°C
OUTPUT PROTECTION	Fuse

[1]Optional input: 115/230 VAC available, consult factory.

TABLE 1. Typical Full Load Output Voltage/Current Ratings

MODEL NO.	RATING VOLTAGE	RATING CURRENT	ADJUSTMENT TAPS	CASE	WEIGHT (LBS)
620	25V	3.5A	±10%	A	6.3
621	28V	5A	±10%	B	12.3
661 (33V)	33V	12A	±10%	C	20.5
662 (33V)	33V	8A	±10%	C	20.5
664 (33V)	33V	15A	±10%	D	28.5
640	48V	1.8A	±10%	B	12.3
641	48V	4A	±10%	C	20.5
645	48V	15A	±5%	C	20.5
660	65V	4A	±5%	B	12.3
661	65V	6A	±5%	C	20.5
662	65V	8A	±5%	C	20.5
663	75V	8A	±10%	C	20.5
664	65V	15A	±5%	D	28.5
666	75V	15A	±10%	D	28.5
668	120V	5A	±5%	C	20.5

FIGURE 1. Typical Load Regulation

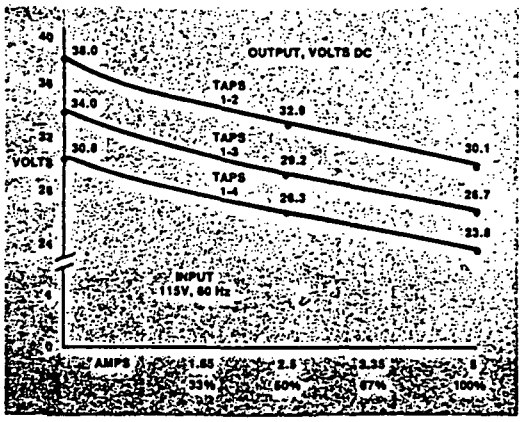

OUTLINE DIMENSIONS

CASE A

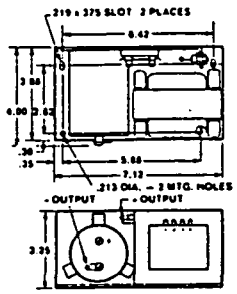

CASE B

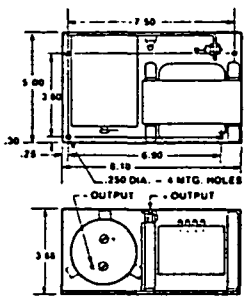

CASE C

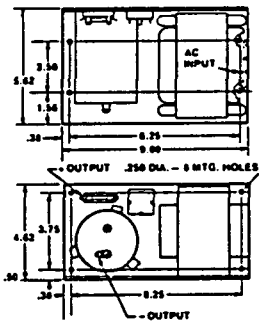

CASE D

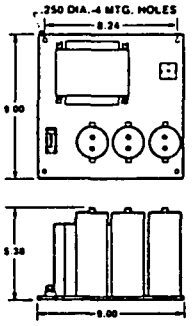

FUNCTIONAL DIAGRAM

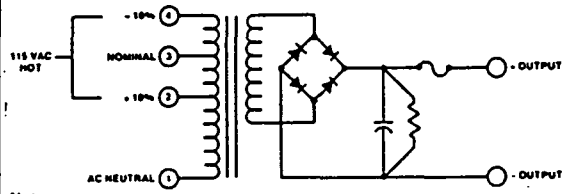

Notes:
1. Full wave bridge shown above for Models 660-668.
2. Half-wave bridge used for Models 620-645.

ORDERING INFORMATION

SERIES PART NUMBER
NUMBER OF ASSEMBLED AMPLIFIERS
AMPLIFIER TYPE[2]

620 – X X

0	NONE
1	ONE (1)
2	TWO (2)
3	THREE (3)
4	FOUR (4)

1	MODEL 201
2	MODEL 210
3	MODEL 215
4	MODEL 220[3]
5	MODEL 230[3]
6	MODEL 211
7	MODEL 215A
8	MODEL 218

Notes:
1. Model 690, bias supply (± 15V) must be ordered with this assembly.
2. For mixed combinations of amplifiers, consult factory for part number.
3. Amplifiers and mounting cards (MB1, MB2 or MB3) must be ordered separately.
4. Some amplifier combinations will not fit mechanically. Contact factory if this is questioned

Figure D.7 Power Supply Specifications

D.3 Wiring Schematic for the Fault Indicator Display Electronics

The Fault Indicator Display Electronics package was developed to aid the remote normal operation LED of the power amplifiers. It was discovered that the current delivered by the normal operation lead was insufficient to operate the indicator lamps purchased. These lamps were mounted on the front panel of the controls electronics rack. These lamps indicate the normal operation of the power amplifiers. The signal supplied by the power amplifier is a CMOS logic output. In order to be able to supply enough current

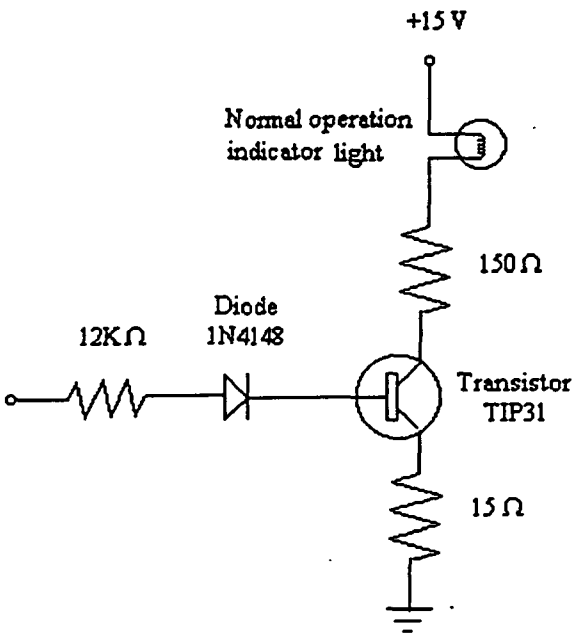

Figure D.8 Circuit Diagram for one Fault Indicator Display

to the normal operation lamps mounted on the front panel the circuit in Figure D.8 was designed. This circuit uses a transistor as a switch. The transistor is operated by the

CMOS output of the amplifier, and the normal indicator lamp is supplied with 15 Volts through the transistor. The resistor limit the current through the transistor and lamp. With this circuit the green lamp at the front panel of the controls electronics rack indicates the normal operation of the amplifier.

The Fault indicator display electronics hardware has two connectors running to it. One connector is a 25-pin connector and the other is a 9-pin connector. The 25-pin connector receives the signal from the power amplifiers to indicate the amplifiers is operating normally. The signal is then processed by the electronics and the corresponding green indicator lamp is turned on. The 9-pin connector supplies the indicator lamps with the +15 volts from the $\pm$ 15 volt power supply that also supplies power to the proximity sensor electronics. The connectors are wired as follows.

25-pin connector located on one end of the fault indicator display electronics hardware box.

PIN		
1	yellow	To indicator lamp A2.
14	green	Normal +5V, twisted w/pin 1
2	orange	To indicator lamp B2.
15	green	Normal +5V, twisted w/pin 2
3	white	To indicator lamp C2.
16	blue	Normal +5V, twisted w/pin 3
4	white	To indicator lamp U2.
17	black	Normal +5V, twisted w/pin 4
5	orange	To indicator lamp V2.
18	black	Normal +5V, twisted w/pin 5
6	black	+15 V to lamps U1,V1
7	not connected	
8	green	+15 V to lamps U2,V2 twisted w/pin 6
19	black	+15V to lamps A2,B2,C2
20	red	+15V to lamps A1,B1,C2 twisted w/pin 19
9	white	To indicator lamp V1.
21	green	Normal +5V, twist w/pin 9
10	yellow	To indicator lamp U1.
22	black	Normal +5V, twisted w/pin 10
11	orange	To indicator lamp C1.
23	red	Normal +5V, twisted w/pin 11
12	blue	To indicator lamp B1.

24	red	Normal +5V, twisted w/pin 12
13	blue	To indicator lamp A1.
25	black	Normal =5V, twisted w/pin 13

9-pin connector is located on the opposite end of the fault indicator display electronics hardware box.

PIN	
1	+15 Volts
2	+15 Volts
3	+15 Volts
4	+15 Volts
5	not connected
6	ground

D.4 Wiring Schematic for the New Controls Electronics Rack

This section contains a list of connectors and corresponding connections made on each. A brief description of the location is given along with the label name given to each connector. This section is meant as an aid in locating and trouble shooting connections between the various parts of the ASPS system. It is very difficult to make a very accurate representation of the method used in constructing the hardware of the system, so this will not be done. This description used closely with the physical system should be adequate to trouble shoot most problems that may occur and to reproduce the system if necessary.

PROX is a cannon 50-pin connector located on lower back panel of the controls electronic rack, and carries the wires for the proximity sensor measurements. These signals are carried via the PROX cable connected to the Vernier Pointing Assembly and the back of the controls electronics rack labeled PROX.

PIN	
1	DELTA G A HI
2	DELTA G B HI
3	DELTA G C HI
4	DELTA G U HI
5	DELTA G V HI
6	DELTA G W HI
8	Roll Resolver Rotor HI
9	Roll Resolver Stator Sine HI
10	Roll Resolver Stator Cosine HI
17	PEA Telemetry HI
18	DELTA G A Low
19	DELTA G B Low
20	DELTA G C Low
21	DELTA G U Low
22	DELTA G V Low
23	DELTA G W Low
25	Roll Resolver Rotor Low
26	Roll Resolver Stator Sine Low
27	Roll Resolver Stator Cosine Low

33	PEA Telemetry S
34	+15
35	Signal Ground
36	-15
39	Chassis Ground
50	PEA Telemetry Low

MBA is a cannon 50-pin connector located on the lower back panel of the controls electronics rack, and this connector carries the signal sent to the magnetic actuators from the power amplifiers. Signals are carried from the vernier pointing assembly via the MBA cable to the back of the controls electronics rack. The A and B at the end of each code number correspond to a twisted pairs. The 1 or 2 corresponds to upper/outer and lower/inner respectively. Example: MBA A 1 A and MBA A 1 A at pins 1 and 3 respectively are a twisted pair and correspond to the upper magnetic coils of MBA A.

PIN	
1	MBA A 1 A
2	MBA A 1 B
3	MBA A 1 A
4	MBA A 1 B
5	MBA A 2 A
6	MBA A 2 B
7	MBA A 2 A
8	MBA A 2 B
9	MBA B 1 A
10	MBA B 1 B
11	MBA B 1 A
12	MBA B 1 B
13	MBA B 2 A
14	MBA B 2 B
18	MBA B 2 A
19	MBA B 2 B
20	MBA C 1 A
21	MBA C 1 B
22	MBA C 1 A
23	MBA C 1 B
24	MBA C 2 A
25	MBA C 2 B
26	MBA C 2 A
27	MBA C 2 B
28	MBA U 1 A
29	MBA U 1 B
34	MBA U 1 A
35	MBA U 1 B
36	MBA U 2 A
37	MBA U 2 B

38	MBA U 2 A
39	MBA U 2 B
40	MBA V 1 A
41	MBA V 1 B
42	MBA V 1 A
43	MBA V 1 B
44	MBA V 2 A
45	MBA V 2 B
46	MBA V 2 A
47	MBA V 2 B

DAS-1400 37-pin connector located on the back panel of the controls electronics rack. This connector/ribbon cable carry the proximity sensor readings from the controls electronic rack to the computer. These signals are analog inputs to the computer.

PIN	
13	DELTA G W ch5 Low in
14	DELTA G V ch4 Low in
15	DELTA G U ch3 Low in
16	DELTA G C ch2 Low in
17	DELTA G B ch1 Low in
18	DELTA G A ch0 Low in
32	DELTA G W ch5 HI in
33	DELTA G V ch4 HI in
34	DELTA G U ch3 HI in
35	DELTA G C ch2 HI in
36	DELTA G B ch1 HI in
37	DELTA G A ch0 HI in

DDA-06 37-pin connector located on the back panel of the controls electronics rack. This connector and ribbon cable carry the signals from the computer to the back of the controls electronics rack. These are analog signals sent to the reference inputs of the power amplifiers.

PIN	
1	Amp A1 +Ref ch5 out
2	Amp B1 +Ref ch4 out
12	Amp C1 +Ref ch3 out
13	Amp C1 -Ref ch3 L.L.GND.
14	Amp U1 +Ref ch2 out
15	Amp U1 -Ref ch2 L.L.GND.
16	Amp V1 +Ref ch1 out
17	Amp V1 -Ref ch1 L.L.GND.
18	Amp U2 +Ref ch0 out
19	Amp U2 -Ref ch0 L.L.GND.

20	Amp A1 -Ref ch5 L.L.GND.
21	Amp B1 -Ref ch4 L.L.GND.

Each power amplifier has two connectors a 22-pin and a 4-pin. Each is labeled with the letter and number corresponding to the amplifier it belongs to. The following is a listing of the types of connections made to each amplifier.

22-Pin Connector

PIN	
1	+Ref
2	-Ref
3	Signal Ground
7	Logic Ground
10	/Reset
15	/Enable
16	/Pos Enable
17	/Neg Enable
19	Normal
22	Current Monitor

4-Pin Connector

PIN	
AA	+High Voltage DC Power input, Enable switch indicator light front panel
BB	Negative Output
CC	Positive Output
DD	Ground, GND for light.

The above connectors above can be located on Figure D.9. Figure D.9 is a wiring schematic showing the wiring required for one magnetic bearing assembly, one power amplifier, a power supply, computer, and miscellaneous other connections. Table D.1 is a list of the components shown in Figure D.9. Figure D.9 is meant to used in trouble shooting and reproducing the system. Currently there are six power amplifiers being used A1, B1, C1, U1, V1, and U2. Four additional amplifiers are necessary to make the system complete. Power amplifiers for the lower magnetic coils of MBA's A, B, and C and the inner magnetic coils of MBA V need to be added to make the system complete. That is amplifiers V2, A2, B2, and C2 will need to be wired according to Figure D.9. Figure D.10 shows the AC connections made to the DC power supplies.

Table D.1 Listing of Components on Figure D.9

1	Reset switch for overtemp, or output short-circuit fault condition.
2	Enable Amplifier switch. In for enable.
3	Side view of switches 1 and 2.
4	4-Pin power connector.
5	22-Pin signal connector.
6	Normal operation LED.
7	Magnetic Bearing Assembly
8	Copley Controls Corp. 303 series amplifier.
9	MBA Connection cable.
10	PROX Connection cable
11	Fault indicator display electronics.
12	Proximity sensor electronics assembly.
13	DDA-06 Ribbon Cable and connector to Digital to analog output from computer.
14	DAS-1400 Ribbon cable and connector to analog to digital signals sent to computer.
15	Ground and DC power strip.
16	DC power switch to supply power to axial top, axial bottom, and radial amplifiers.
16a	Power indicator light , Red.
17	33 volt DC power supply.
18	Computer/Digital Controller
19	$\pm$ 15 volt DC power supply for proximity sensor electronics.

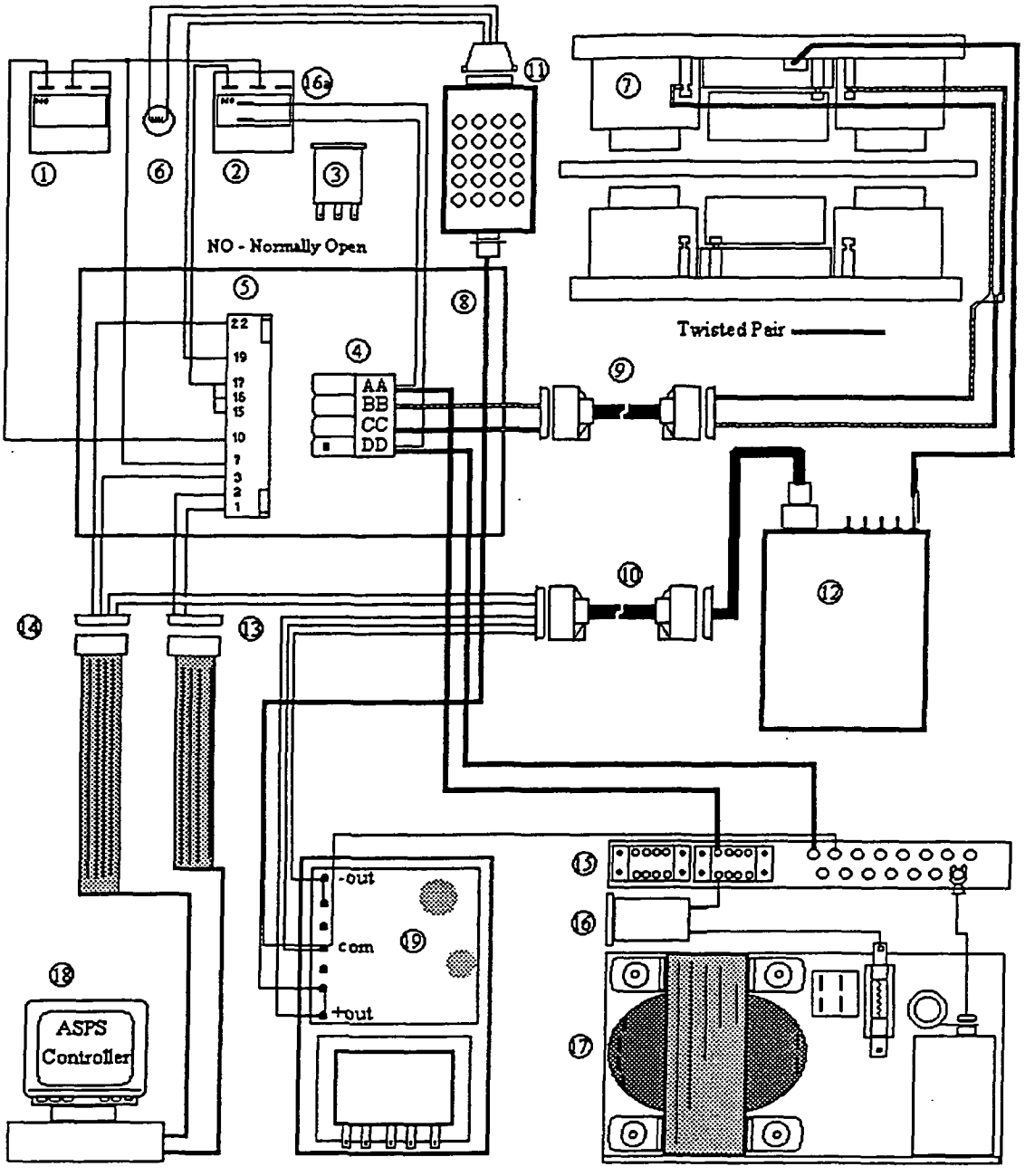

Figure D.9 Wiring Schematic containing one Amplifier and one MBA.

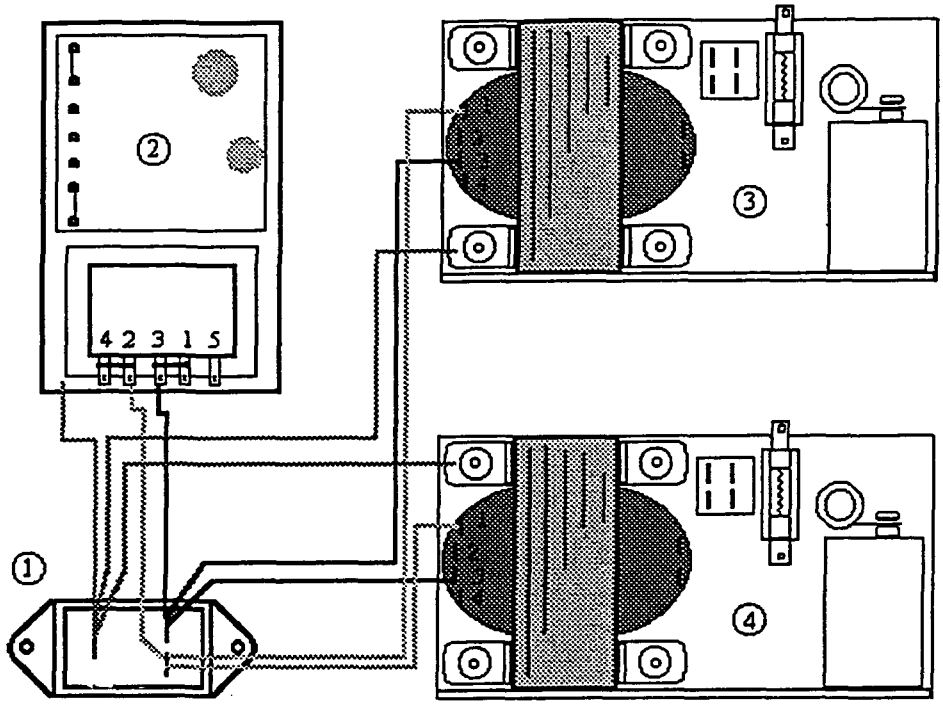

Figure D.10 Wiring schematic of AC power supplies.

Figure D.11 is a block diagram representing the component cost and connection.

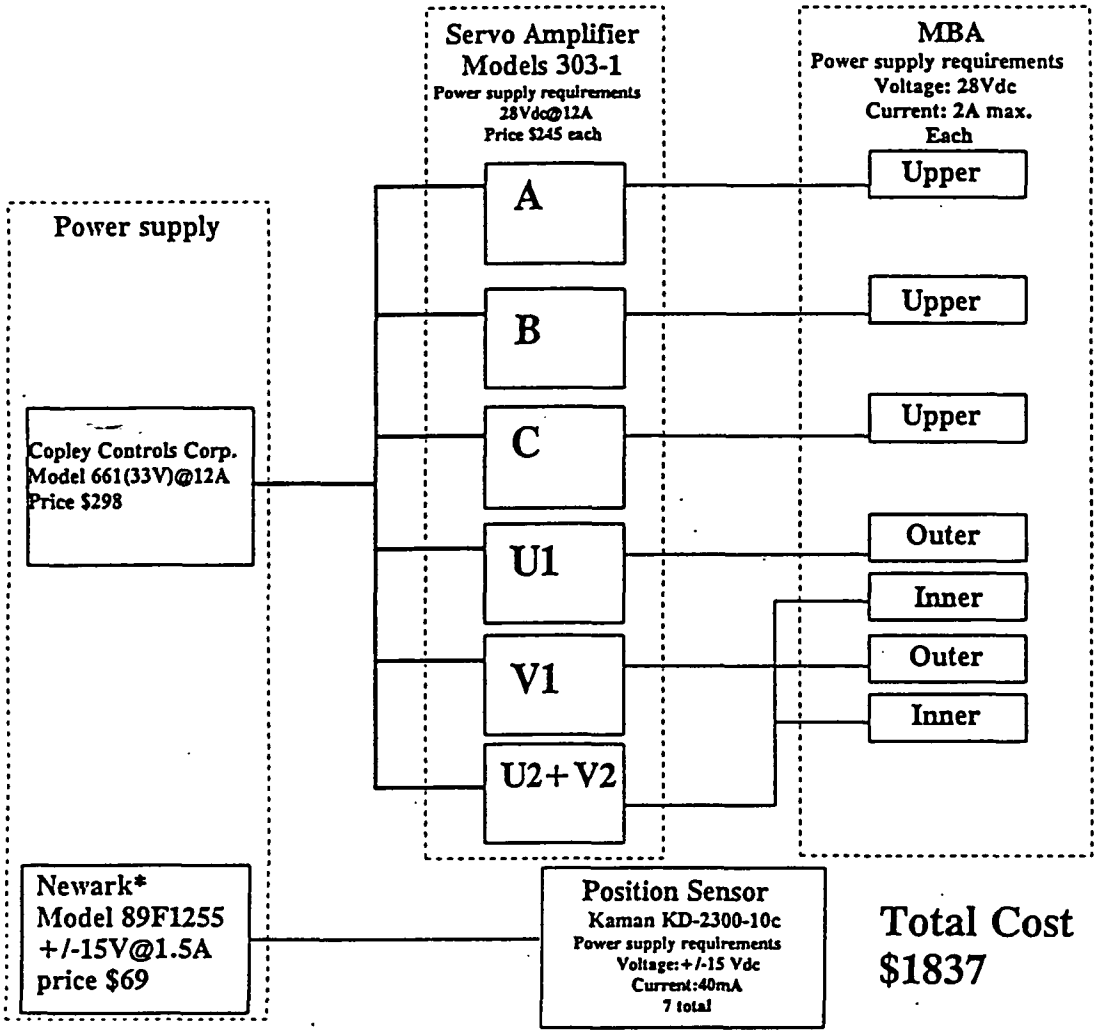

Figure D.11 Cost and Connection of Components of Controller.

Appendix E

Software

E.1 File my1402.cfg

This file contains the DAS-1402 board configuration, and this file is nesessary for initalizing the board. The contents of the file are listed below. The following file was created by using the program D1600CFG.EXE. This program was supplied with the Keithley Data Acquisition DAS-1400 Series board.

```
Board          0
Name           DAS1402
Address        &H300
ClockSel       10MHz
WaitState      NO
ADChanMode     Bipolar
ADChanConfig   Single-ended
DMAChannel     3
IntLevel       7
NumOfEXP16     0
NumOfEXPGP     0
NumOfSSH4A     0
```

E.2 Program AD_DATES.C

```
/*              Program A/D AND D/A TEST
   This program was used to develope an understanding of how to read
   and wrtie information using the Keithley Data Acquisition ASO-1600/
   1400 Driver software.  The porpose of this program was to determine
   the minumum Reference voltage necessary to suspend the rotor using
   the aluminum gap shims (3.41 mm).
   This program will supply a reference signal to the amplifiers
   that drive the MBA's, therfore it will supply the same reference
   voltage to chanels 3, 4, and 5 of the D/A board, MBA's A, B, and C
   respectively.
   The UP arrow will increase the reference voltage .005 volts per
   key strike.  The DOWN arrow will decrease the reference voltage
   .005 volts per key strike. The ESC key will end the program.
   The Left and RIGHT arrow keys will scroll throw chanel 0-7.

   In order for this program to work properly the ASPS hardware system
   must be powered up and conected to the VPA.  The connections from the
   hardware to the back of the computer must be made.  This program will
   not suspend the rotor without the aluminum gap shims placed between
   the rotor and MBA poll.
   Channels 0-5 will display the voltage read from the proximity sensors.
   Channels 6 & 7 are not used at this time.

   To compile this program it must be linked with DAS1600.LIB and
   DASRFACE.LIB.  The file my1402.cfg must be in the BIN directory.

                        Writen by Daniel Neff
                           2-28-95                    */
#include <stdio.h>
#include <stdlib.h>
#include "dos.h"
#include "graph.h"
#include "userprot.h"     /* Include file for Keithley DAS-1402 D/A Board */

#define ESC 27
#define UP 72
#define DOWN 80
```

```
#define RIGHT 77
#define LEFT 75
#define base 400   /* Base Address of DDA-06 D/A Board */

        DDH    DAS1402;  /* DevHandle contains base address of DAS1402*/
        FRAMEH frameHandle;
        long far clkTicks;
        char   NumberOfBoards, M, NN;
        int    Err, count, i;
        float  involts;
        float  outvolt;
        long   ADvalue, D;
        char   ch, chin;
        int    N, high, low, c;

void keyboard(void);
main()
{               /* Sets the initial value in order to supply      */
        D=2892;         /* a small positive reference voltage to the Amp's.*/
        NN=0;           /* Initial channel                          */
        high=(D/256);
        low =D-high*256;
/*  Initiali e board, Reads my1402.cfg and returns Number of Boards */
        if (( Err = DAS1600_DevOpen ("my1402.cfg", &NumberOfBoards )) !=0)
          {
          putch (7);
          printf("Error %d during GetDevOpen ",Err );
          exit(Err);
          }
/*  Get Device Handle to locate devices associated with card. */
        if (( Err = DAS1600_GetDevHandle( 0, &DAS1402)) !=0 )
          {
          putch (7);
          printf("Error %d during GetDevHandle ",Err );
          exit(Err);
          }
printf("\n\n\n\t\t\tProgram A/D and D/A Test\n\n");
printf("\t\tAnnular Suspension and Pointing System\n");
printf("\t\t\tWritten by: Daniel Neff\n");
printf("\t\t\tOld Dominion University\n");
printf("\t\tDepartment of Aerospace Engineering\n");
printf("\t\t\t    March 5, 1995\n\n\n");
printf("UP arrow will increase Reference voltage to Amplifiers by .005 volts.\n");
printf("DOWN arrow will decrease Ref. voltage by .005 volts.\n");
printf("RIGHT and LEFT arrow keys will scroll between channels 0-13.\n");
```

```
printf("ESC will end program.\n\n");
printf("Read program listing for more information on this program\n\n");
printf("Hit any key to continue\n\n\n\n\n");
getch();
while(ch != ESC)            /* Test to end program              */
{
keyboard();
        high=(D/256);       /* Calculation of high and low byte  */
        low =D-high*256;    /* to supply to the DDA-06 board     */
        for(N=3;N<=5;++N)
        {
        outp(base + 2*N, low);      /* Writes to channels 3-5    */
        outp(base + 1 + 2*N, high); /* on the DDA-06 board       */
        }
/* Read channel NN on the A/D Board. */
        K_ADRead(DAS1402,NN,2,&ADvalue);
        involts=(((ADvalue>>4)-2047)*20)/4096.0; /* converts count to voltage*/
        printf ("Volts read on ch(%d)=%d",NN,ADvalue>>4);
        outvolt=((D-2047)*5)/4096.0;        /* converts count to voltage */
        printf (" Ref V. supplied to Amp's:%2.2f;Count %ld\n",outvolt,D);
}
        D=2048;                 /* Resets channels 0-5 on the    */
        for(N=0;N<=5;++N)       /* D/A board to  ero.            */
        {
        high=(D/256);
        low =D-high*256;
        outp(base + 2*N, low);
        outp(base + 1 + 2*N, high); /* End reset section */
        }
        printf("End of Program.");exit(0);
}
void keyboard(void)             /* This is the nessesary part to  */
{                       /* use the keyboard interface.    */
if (kbhit() !=0)
        {
        chin=getch();
                switch(chin)
                {
                case ESC:ch=ESC;    /* End program               */
                        break;
                case UP: D = D +1;  /* Increase Reference voltage. */
                        break;
                case DOWN: D = D - 1; /* Decrease Reference voltage. */
                        break;
                case RIGHT: NN=NN+1;  /* Increase Chanel.          */
```

```
                break;
            case LEFT: NN=NN-1;     /* Decrease Chanel.          */
                break;
            }
        }
    }
```

E.3 Program TESTCOUN.C

```
/*                  TESTCOUN.C

        This program was developed to use the Pacer Timer Board to
        perform a controled loop within a program.  This program will
        set up a frequence and counter so that a program loop will be
        exicuted on a constant time schedule.
        FOUT pin must be connected to sourse 1 in order for this
        program to work properly.

                        Written By: Daniel J. Neff
                              March 5, 1995
                        Annular Suspension and Pointing System
                              Old Dominion University
                        Department of Aerospace Engineering          */


#include <stdio.h>
#include <conio.h>
#include <math.h>
#include <dos.h>
#include "pacerdef.h"

#define ESC 27
#define base 400
        char ch, chin;
        double freq=10000;    /* Frequence to be set at the FOUT pin */
        int count=100;        /* number of counts before program continues */
        int  flip, dhigh, dlow, dumout, MM;
void keyboard(void);

main()
{

        WORD result;
                              /*  freq/count=time for one loop exicution */

        PA_INITIALIZE(0x230); /* Initializes Pacer Timer Board at base */
```

```
                        /* address 230                  */
        PA_RESET();         /* set board to start up conditions */
        PA_SET_FOUT(freq);   /* Set frequence at FOUT pin to freq */
        /*Set up counter 1 with Source 1  */

PA_RATE_GENERATOR(1,SOURCE_SRC1,GATE_NONE,MODE_OUTPUT_LOW|
MODE_COUNT_UP,0);

        PA_WRITE_COMMAND(armCounters,0x1);  /*Arm counter 1 */
        PA_READ_FOUT(&freq);

        printf("\n\n\n\t\t\tProgam TESTCOUN.C \n\n");
        printf("\t\tAnnular Suspension and Pointing System\n");
        printf("\t\t\tWritten by: Daniel Neff\n");
        printf("\t\t\tOld Dominion University\n");
        printf("\t\tDepartment of Aerospace Engineering\n");
        printf("\t\t\t    March 5, 1995\n\n\n");
        printf("\tThis program will print \"Hello World\" to the screen at a rate\n");
        printf("\tof Frequence/Count\n\n");
        printf("\t\tConnect the FOUT pin the Source 1\n\n");
        printf("\t\tFrequence set at FOUT pin %.2f\n",freq);
        printf("\t\tNumber of counts set is %d\n",count);
        printf("\t\tTime to print \"Hello World\" %.1f second.\n\n",freq/count);
        printf("\tHit ESC after program has started to end the program.\n\n");
        printf("\t\t\tHit any ket to continue\n\n");
        getch();
        flip=400;
         MM=0;

while(ch != ESC)
 {
 keyboard();
        printf("Hello world\n");
        flip=-flip;
        dumout=2048+flip;
        dhigh=dumout/256;
        dlow=dumout-dhigh*256;
        outp(base+2*MM,dlow);
        outp(base+1+2*MM,dhigh);

        while (result<count)     /*  Waits until Counter counts to result*/
         {
         keyboard();
         PA_WRITE_COMMAND(saveCounters,0x1);
        /*  PA_READ_COUNTERS(1,1,&result);  */
```

```
            PA_READ_AM9513(cntr1Hold,&result);
            printf(" %d",result);
            }

            result=0;
            PA_WRITE_COMMAND(loadCounters,0x1);

    }

    PA_RESET();             /* Resets timer to start up conditions*/
    printf("BOARD RESET");
}
void keyboard(void)
{
if(kbhit() !=0)
        {
        chin=getch();
                switch(chin)
                {
                case ESC:ch=ESC;
                        break;
                }
        }
}
```

E.4 Program TESTABC.C

```
/*                TESTADC.C

This program was developed to use the Pacer Timer Board to
perform a controled loop within a program. This program will
set up a frequence and counter so that a program loop will be
exicuted on a constant time schedule.
FOUT pin must be connected to sourse 1 in order for this
program to work properly.
This program will read six channels from the DAS-1401 A/D
Data acquisition board. The inputed values will be used
to calculate the distance and velocity of the iron ring.
Once the distances and velocities are calculated the controller
multiplies the proportional gain and the derivative gain to the
distance and velocity respectively. Once the output of the
controller is calculated the program writes six values using the
DDA-06 D/A data acquisition board.
Ultimately this program will also suspend the annular ring in
five degrees of freedom.
This program can be compliled within the Quick C editor program,
but can only be executed from the DOS command line.
To compile this program correctly it must be linked with several
libraries which are: DAS1600.LIB, DASRFACE.LIB, and PACER.LIB.
The file my1402.cfg must be in the C:\qc25\bin directory defore
compiling this program. This file contains the information about
the DAS-1402 configuration.
Create a MAKE file that includes these three libraries and TESTABC.C
before compiling this program from the Quick C editor. After the
MAKE file has been created if not already from the Make menu select
Build Program. This will recompile the program if any changes
have been made to the programs .C file.

Note: This porgram will not run properly if run from within
      windows. This program must be run from the DOS command
      line.

                Written By: Daniel J. Neff
                    April 12, 1995
            Annular Suspension and Pointing System
```

```
                    Old Dominion University
                Department of Aerospace Engineering          */

#include <stdio.h>
#include <conio.h>
#include <math.h>
#include <dos.h>
#include "userprot.h"    /*Include file for Keithley DAS-1402 D/A Board*/
#include "pacerdef.h"    /*Include file for Pacer Timer Board */
                         /* Note the order of above Include Files */


#define ESC 27
#define UP 72
#define DOWN 80
#define RIGHT 77
#define LEFT 75
#define base 400         /*Base address of DDA-06 D/A Board*/

        char ch, chin, NumberOfBoards;
        double freq, freq1=1000;    /* Frequence to be set at the FOUT pin */
        int pacercount=10;      /* number of counts before program continues */
        DDH DAS1402;        /*DevHandle contains base address of DAS1402*/
        FRAMEH frameHandle;
        long far clkTicks;
        int  high, low, i, counter;
        unsigned result, MODE;
        FILE *data;
        float timer[1000];

        char  A, AA;
        long  ADvalueA, RefVoltsA, XdemandA, XoldA, ControlA;
        int   highA, lowA;
        float VelocityA, XoffsetA, ControlVoltsA, InVoltsA, CurrentVolts;
        float dXA[1000], current[1000], control[1000], Velocity[1000];
                        /* used only to collect displacement data,  */
                        /* Simular variable for each displacement   */
                        /* measured.*/
        float GainControlDA, GainControlPA;
        long  CurrentA;

        char  B, BB;
        long  ADvalueB, RefVoltsB, XdemandB, XoldB, ControlB;
        int   highB, lowB;
```

```
        float VelocityB, XoffsetB, ControlVoltsB, InVoltsB;
        float dXB[1000];
        float GainControlDB, GainControlPB;

        char  C, CC;
        long  ADvalueC, RefVoltsC, XdemandC, XoldC, ControlC;
        int   highC, lowC;
        float VelocityC, XoffsetC, ControlVoltsC, InVoltsC;
        float dXC[1000];
        float GainControlDC, GainControlPC;

        char  U, UU;
        long  ADvalueU, RefVoltsU, XdemandU, XoldU, ControlU;
        int   highU, lowU;
        float VelocityU, XoffsetU, ControlVoltsU, InVoltsU, CurrentsVolts;
        float GainControlDU, GainControlPU;

        char  V, VV;
        long  ADvalueV, RefVoltsV, XdemandV, XoldV, ControlV;
        int   highV, lowV;
        float VelocityV, XoffsetV, ControlVoltsV, InVoltsV;
        float GainControlDV, GainControlPV;

        char  W, WW;
        long  ADvalueW, ControlW;
        int   highW, lowW;


void keyboard(void);

main()
{           /* Note order of initiali ing boards, Pacer before Keithly*/

        WORD result;
                                /*  freq/count=time for one loop exicution */

        PA_INITIALIZE(0x230); /* Initiali es Pacer Timer Board at base */
                              /* address 230                          */
        PA_RESET();          /* set board to start up conditions */
        PA_SET_FOUT(freq1);   /* Set frequence at FOUT pin to freq */
        /*Set up counter 1 with Source 1  */

PA_RATE_GENERATOR(1,SOURCE_SRC1,GATE_NONE,MODE_OUTPUT_LOW|
MODE_COUNT_UP,0);
```

```
    PA_WRITE_COMMAND(armCounters,0x1);  /*Arm counter 1 */
    PA_READ_FOUT(&freq);

/*Initali e DAS-1402 board and reads my1402.cfg and returns Number of Boards*/
    DAS1600_DevOpen("my1402.cfg",&NumberOfBoards);
    /*Get Device Handle*/
    DAS1600_GetDevHandle(0,&DAS1402);

    printf("\n\n\n\t\t\tProgram TESTABC.C \n\n");
    printf("\t\tAnnular Suspension and Pointing System\n");
    printf("\t\t\tWritten by: Daniel Neff\n");
    printf("\t\t\tOld Dominion University\n");
    printf("\t\tDepartment of Aerospace Engineering\n");
    printf("\t\t\t    April 12, 1995\n\n");
    printf("WARNING This program will not run within WINDOWS");
    printf(" only from the DOS command line.\n");
    printf("\tYou must exit WINDOWS before running this program.\n\n\n");
    printf("\tConnect the FOUT pin to Source 1 on the Timer board.\n\n");
    printf("\t\tFrequence set at FOUT pin %.2f\n",freq);
    printf("\t\tNumber of counts set is %d\n",pacercount);
    printf("\t\tTime to exicute loop is %1.5f H .\n\n",freq/pacercount);
    printf("\t\t\tHit any key to continue\n\n");
    printf("\t\t    Then Hit ESC to end the program.\n");
    getch();

                /* Initial values of variables */
    XdemandA=2027;
    XoldA=XdemandA;
    RefVoltsA=2931;       /* Minumum count value to suspend ring at A*/
    GainControlPA=330;
    GainControlDA=40;
    AA=0;                 /*Input Channel for MBA A*/
    A=5;                  /*Output Channel for MBA A*/

    XdemandB=2002;
    XoldB=XdemandB;
    RefVoltsB=2892;       /* Minumum count value to suspend ring at B*/
    GainControlPB=330;
    GainControlDB=45;
    BB=1;                 /*Input Channel for MBA B*/
    B=4;                  /*Output Channel for MBA B*/

    XdemandC=2260;
    XoldC=XdemandC;
    RefVoltsC=2811;       /* Minumum count value to suspend ring at C*/
```

```
        GainControlPC=330;
        GainControlDC=45;
        CC=2;              /*Input Channel for MBA C*/
        C=3;               /*Output Channel for MBA C*/

        XdemandU=1717;
        XoldU=XdemandU;
        RefVoltsU=2277;      /* Minumum count value to suspend ring at U*/
        GainControlPU=330;
        GainControlDU=45;
        UU=3;              /*Input Channel for MBA U*/
        U=2;               /*Output Channel for MBA U*/

        XdemandV=1742;
        XoldV=XdemandV;
        RefVoltsV=2411;      /* Minumum count value to suspend ring at V*/
        GainControlPV=330;
        GainControlDV=45;
        VV=4;              /*Input Channel for MBA V*/
        V=1;               /*Output Channel for MBA V*/

        ControlW=2848;       /*Count used to suppliy Small current to */
                             /*inner MBA's at U & V.  */
        WW=5;              /*Input Channel for MBA U&V inner*/
        W=0;               /*Output Channel for MBA U&V inner*/
        i=0;

while(ch != ESC)
 {
        i=i+1;
        counter=i;
        timer[i]=i/100.0; /* used to collect displacement data. */

        keyboard();

        K_ADRead(DAS1402,AA,2,&ADvalueA); /* Reads proximity sensor signals*/
        K_ADRead(DAS1402,BB,2,&ADvalueB);
        K_ADRead(DAS1402,CC,2,&ADvalueC);
        K_ADRead(DAS1402,UU,2,&ADvalueU);
        K_ADRead(DAS1402,VV,2,&ADvalueV);
        K_ADRead(DAS1402,WW,2,&ADvalueW);
        K_ADRead(DAS1402,6,2,&CurrentA);

        /* Calculates distance and velocities, Calculates control using P and D
          gains.  Calculates Control volts and In volts for printing purposes
```

```
only. Same calculations performed for all inputs above.        */

        XoffsetA=-(XdemandA*.003-2.045)+((ADvalueA>>4)*.003-2.045);
        VelocityA=(((ADvalueA>>4)*.003-2.045)-(XoldA*.003-
2.045))/(pacercount/freq);
 ControlA=(GainControlPA*XoffsetA+GainControlDA*.1*VelocityA+RefVoltsA);
        ControlVoltsA=(ControlA-2047)*5/4096.0;
        InVoltsA=((ADvalueA>>4)-2047)*20/4096.0;
        CurrentVolts=((CurrentA>>4)-2047)*10/4096.0;

        XoffsetB=-(XdemandB*.003-2.533)+((ADvalueB>>4)*.003-2.533);
        VelocityB=(((ADvalueB>>4)*.003-2.533)-(XoldB*.003-
2.533))/(pacercount/freq);
 ControlB=(GainControlPB*XoffsetB+GainControlDB*.1*VelocityB+RefVoltsB);
        ControlVoltsB=(ControlB-2047)*5/4096.0;
        InVoltsB=((ADvalueB>>4)-2047)*20/4096.0;

        XoffsetC=-(XdemandC*.004-6.636)+((ADvalueC>>4)*.004-6.636);
        VelocityC=(((ADvalueC>>4)*.004-6.636)-(XoldC*.004-
6.636))/(pacercount/freq);
 ControlC=(GainControlPC*XoffsetC+GainControlDC*.1*VelocityC+RefVoltsC);
        ControlVoltsC=(ControlC-2047)*5/4096.0;
        InVoltsC=((ADvalueC>>4)-2047)*20/4096.0;

        XoffsetU=-(XdemandU*.004-6.636)+((ADvalueU>>4)*.004-6.636);
 VelocityU=(((ADvalueU>>4)*.004-6.636)-(XoldU*.004-6.636))/(pacercount/freq);
 ControlU=(GainControlPU*XoffsetU+GainControlDU*.1*VelocityU+RefVoltsU);
        ControlVoltsU=(ControlU-2047)*5/4096.0;
        InVoltsU=((ADvalueU>>4)-2047)*20/4096.0;

        XoffsetV=-(XdemandV*.004-6.636)+((ADvalueV>>4)*.004-6.636);
 VelocityV=(((ADvalueV>>4)*.004-6.636)-(XoldV*.004-6.636))/(pacercount/freq);
 ControlV=(GainControlPV*XoffsetV+GainControlDV*.1*VelocityV+RefVoltsV);
        ControlVoltsV=(ControlV-2047)*5/4096.0;
        InVoltsV=((ADvalueV>>4)-2047)*20/4096.0;

        highA=(ControlA/256);
        lowA=ControlA-high*256;
        outp(base+2*A,lowA);     /* Writes control output to Amplifier A*/
        outp(base+1+2*A,highA);  /* Using DDA-06 D/A Data acquisition Board*/
        XoldA=ADvalueA>>4;       /* saves old distance for velocity */
                                 /* calculations */

        highB=(ControlB/256);    /* same as above */
        lowB=ControlB-highB*256;
```

```
outp(base+2*B,lowB);
outp(base+1+2*B,highB);
XoldB=ADvalueB>>4;

highC=(ControlC/256);
lowC=ControlC-highC*256;
outp(base+2*C,lowC);
outp(base+1+2*C,highC);
XoldC=ADvalueC>>4;

highU=(ControlU/256);
lowU=ControlU-highU*256;
outp(base+2*U,lowU);
outp(base+1+2*U,highU);
XoldU=ADvalueU>>4;

highV=(ControlV/256);
lowV=ControlV-highV*256;
outp(base+2*V,lowV);
outp(base+1+2*V,highV);
XoldV=ADvalueV>>4;

highW=(ControlW/256);
lowW=ControlW-highW*256;
outp(base+2*W,lowW);
outp(base+1+2*W,highW);

if(i<=1000)
{
dXA[i]=XoffsetA;
current[i]=CurrentVolts;
Velocity[i]=VelocityA;
control[i]=ControlVoltsA;
}          /*   used for collecting displacement data.*/

/*Print statments are used to view diferent perameters while
  addusting the gain values, Xoffset, and the RefVolts of the
  coresponding MBA or amplifier.  To view the print values
  only view one block at a time by removing the comment
  characters from around the block of print statements.  */

/*    printf("GPA%2.2f ",GainControlPA);
      printf("GDA%2.2f ",GainControlDA);
      printf("InVA%dlof ",ADvalueA>>4);
      printf("ConA%d ",ControlA);
```

```
        printf("ConVA%1.3f ",ControlVoltsA);
        printf("dXA%1.3f ",XoffsetA);
        printf("VAab%2.3f\n ",VelocityA); */

    /*  printf("GPB%2.2f ",GainControlPB);
        printf("GDB%2.2f ",GainControlDB);
        printf("InVB%1.3f ",InVoltsB);
        printf("ConB%d  ",ControlB);
        printf("ConVB%1.3f ",ControlVoltsB);
        printf("dXB%1.3f ",XoffsetB);
        printf("VB%2.3f\n ",VelocityB);*/

     /* printf("GPC%2.3f ",GainControlPC);
        printf("GDC%2.3f ",GainControlDC);
        printf("InVC%1.3f",InVoltsC);
        printf("ConC%d ",ControlC);
        printf("ConVC%1.3f ",ControlVoltsC);
        printf("dXC%1.3f ",XoffsetC);
        printf("VC%2.3f\n",VelocityC); */

    /*  printf("RefU%d ",RefVoltsU);
        printf("dXU%1.3f\n ",XoffsetU); */
        printf("Running\n");

        /* This is the part in the program where the timer board is
           necessary to control the time the control loop is executed. */

        while (result<=(pacercount-1)) /*  Waits until Counter counts to result*/
         {
              keyboard();
              PA_WRITE_COMMAND(saveCounters,0x1);
              PA_READ_COUNTERS(1,1,&result);
           /* printf("%d",result); */
         }
         result=0;
         PA_WRITE_COMMAND(loadCounters,0x1);
}
       /* at this point the program returns to the top of the loop
          unless the ESC key has been hit.                  */

PA_RESET();          /* Resets timer to start up conditions*/

for(i=0;i<=5;++i)      /* Writes a  ero volt command to all amplifiers*/
      {              /* to put the amplifies in a no output state.  */
     high=(2047/256);
```

```
        low=2047-high*256;
        outp(base+2*i,low);
        outp(base+1+2*i,high);
        }
 if((data=fopen("C:\\dataout.asc","wt"))!=NULL)
 {
        for(i=0;i<=counter;++i)
        {
fprintf ( data,"%2.3f %2.3f %2.3f %2.3f
%2.3f\n",timer[i],dXA[i],current[i],Velocity[i],control[i]);
        }
        fclose(data);
 }
 else
        printf("Error: Couldn't create file.\n"); /*Only used to collect data*/
        /*  Final print of all Variables that can be changed while the
           program is running by key board inputs.                    */

        printf("BOARDS RESET\n");
        printf("XdemandA %d\n",XdemandA);
        printf("RefVoltsA %d\n",RefVoltsA);
        printf("GainPA %f\n",GainControlPA);
        printf("GainDA %f\n",GainControlDA);
        printf("XdemandB %d\n",XdemandB);
        printf("RefVoltsB %d\n",RefVoltsB);
        printf("GainPB %f\n",GainControlPB);
        printf("GainDB %f\n",GainControlDB);
        printf("XdemandC %d\n",XdemandC);
        printf("RefVoltsC %d\n",RefVoltsC);
        printf("GainPC %f\n",GainControlPC);
        printf("GainDC %f\n",GainControlDC);
        printf("RefV%d\n",RefVoltsV);
        printf("XdemandV %d\n",XdemandV);
        printf("RefU%d\n",RefVoltsU);
        printf("XdemandU %d\n",XdemandU);

        /* Setting up key board for inputs */
}
void keyboard(void)
{
    if(kbhit() !=0)
    {
    chin=getch();

                switch(chin)
```

```
{
case ESC:ch=ESC;
        break;
case UP:GainControlPA=GainControlPA+.1;
        break;
case DOWN:GainControlPA=GainControlPA-.1;
        break;
case RIGHT:GainControlDA=GainControlDA+.1;
        break;
case LEFT:GainControlDA=GainControlDA-.1;
        break;
case'c':case'C':RefVoltsA=RefVoltsA+1;
        break;
case'v':case'V':RefVoltsA=RefVoltsA-1;
        break;
case' ':case'Z':XdemandA=XdemandA+1;
        break;
case'x':case'X':XdemandA=XdemandA-1;
        break;

case'q':case'Q':GainControlPB=GainControlPB+.1;
        break;
case'w':case'W':GainControlPB=GainControlPB-.1;
        break;
case'e':case'E':GainControlDB=GainControlDB+.1;
        break;
case'r':case'R':GainControlDB=GainControlDB-.1;
        break;
case'a':case'A':RefVoltsB=RefVoltsB+1;
        break;
case's':case'S':RefVoltsB=RefVoltsB-1;
        break;
case'd':case'D':XdemandB=XdemandB+1;
        break;
case'f':case'F':XdemandB=XdemandB-1;
        break;

case't':case'T':GainControlPC=GainControlPC+.1;
        break;
case'y':case'Y':GainControlPC=GainControlPC-.1;
        break;
case'u':case'U':GainControlDC=GainControlDC+.1;
        break;
case'g':case'G':GainControlDC=GainControlDC-.1;
        break;
```

```
                case'b':case'B':RefVoltsC=RefVoltsC+1;
                        break;
                case'j':case'J':RefVoltsC=RefVoltsC-1;
                        break;
                case'o':case'O':XdemandC=XdemandC+1;
                        break;
                case'l':case'L':XdemandC=XdemandC-1;
                        break;
                case'[':RefVoltsU=RefVoltsU+1;
                        break;
                case']':RefVoltsU=RefVoltsU-1;
                        break;
                case';':XdemandU=XdemandU+1;
                        break;
                case'/':XdemandU=XdemandU-1;
                        break;

                }
        }
}
```

Appendix F

Calibration

F.1 Voltage to Distance relationship of proximity sensors

This section covers the calculations made to determine a relationship between the displacement of the rotor and the voltage signal from the proximity sensor electronics assembly. These calculations were performed using MathCad 5.0.

Calibration of Porximeter, Distance and Digital Count readings.

PROX A:

$$Ca := \begin{pmatrix} 700 \\ 1960 \\ 3271 \end{pmatrix} \quad Da := \begin{pmatrix} 0 \\ 3.41 \\ 7.30 \end{pmatrix}$$

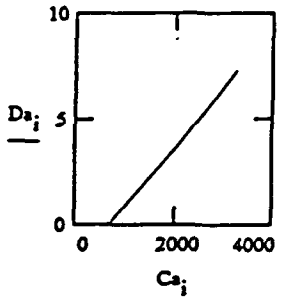

$Ma := slope(Ca, Da)$

$Ma = 0.003$

$Ya := intercept(Ca, Da)$

$Ya = -2.045$

PROX B:

$$Cb := \begin{pmatrix} 810 \\ 1951 \\ 3179 \end{pmatrix} \quad Db := \begin{pmatrix} 0 \\ 3.41 \\ 7.30 \end{pmatrix}$$

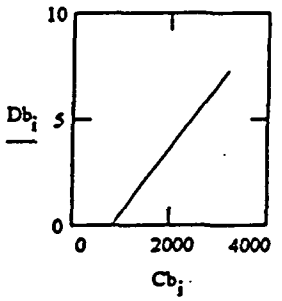

$Mb := slope(Cb, Db)$

$Mb = 0.003$

$Yb := intercept(Cb, Db)$

$Yb = -2.533$

PROX C:

$$Cc := \begin{pmatrix} 1645 \\ 2240 \\ 3385 \end{pmatrix} \quad Dc := \begin{pmatrix} 0 \\ 3.41 \\ 7.30 \end{pmatrix}$$

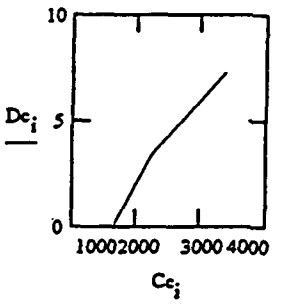

$Mc := slope(Cc, Dc)$

$Mc = 0.004$

$Yc := intercept(Cc, Dc)$

$Yc = -6.337$

PROX U:

$$Cu := \begin{pmatrix} 6184 \\ -1947 \end{pmatrix} \quad Du := \begin{pmatrix} 0 \\ 9.35 \end{pmatrix}$$

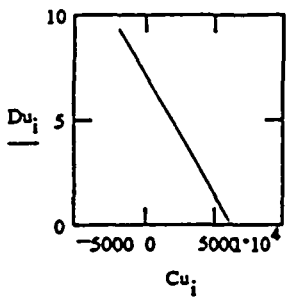

Mu slope(Cu,Du)

Mu = −0.001

Yu := intercept(Cu,Du)

Yu = 7.111

PROX V:

$$Cv := \begin{pmatrix} 5877 \\ -2766 \end{pmatrix} \quad Dv := \begin{pmatrix} 0 \\ 9.57 \end{pmatrix}$$

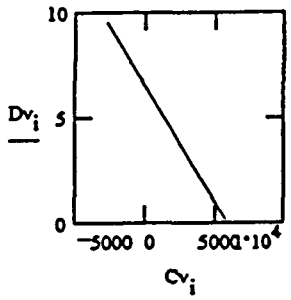

Mv slope(Cv,Dv)

Mv = −0.001

Yv := intercept(Cv,Dv)

Yv = 6.507

PROX W:

$$Cw := \begin{pmatrix} 4955 \\ -1414 \end{pmatrix} \quad Dw := \begin{pmatrix} 0 \\ 9.0 \end{pmatrix}$$

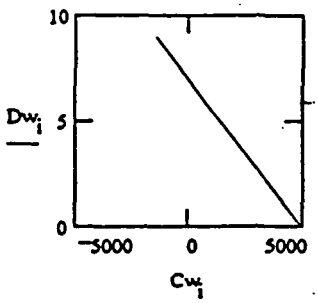

Mw slope(Cw,Dw)

Mw = −0.001

Yw := intercept(Cw,Dw)

Yw = 7.002

F.2 Current Monitor Voltage to Reference Voltage

The power amplifiers come equipped with a current monitoring signal. This signal is proportional to the amount of current being supplied to the magnetic actuator. To determine the relationship between these two quantities a plot of the relationship was plotted. From this a relationship was found. MathCad 5.0 was used in these calculations.

Relationship between current monitor voltage and reference voltage supplied to power amplifiers. This program reads data values from refvolt.dat and curentV.dat for the reference voltage readings and current monitor voltage readings respectively.

$i := 0..34$

Reference voltage:

$Vr_i := READ(refvolt)$

Current Monitor Voltage

$Vc_i := READ(curentV)$

Conversion from volts to Amperes

$I_i := Vc_i \cdot 2$ 2 Amps/Volt

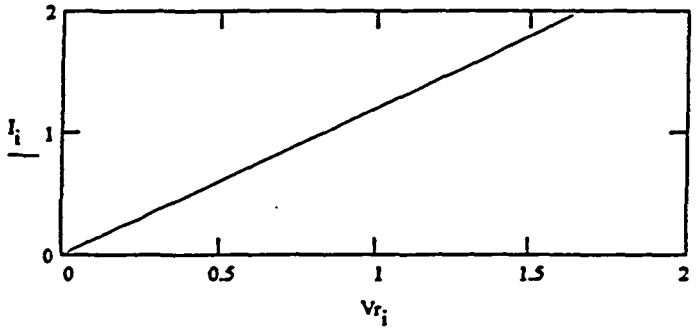

$m := slope(Vr, I)$ $m = 1.201$

The relationship between reference voltage and current supplied to the Magnetic bearing assemblies is as follows:

Current in MBA = 1.201 x *Voltage supplied to Amplifier Reference Signal.*

Ring Thickness: 7.58+/-.05 mm.
Gap between Top and Bottom poles of MBA's: 14.88 mm.
Maximum Ring Displacement along the X-axis: 9.35 mm.
Maximum Ring Displacement along the Y-axis: 9.57 mm.
Maximum Ring Displacement along the axis through the
center of the roll motor and the center of the ring: 9.0 mm.

Minumum current needed to suspend the ring at a gap of 3.41 mm at all MBA's: 1.03Amps.
Minumum current needed to suspend the ring at a gap of 0.00 mm at all MBA's: 0.17Amps.

Influence of Eddy Currents on the Dynamic Characteristics of Magnetic Suspensions and Magnetic Bearings

Dr. Colin P. Britcher

Associate Professor

Department of Aerospace Engineering

Old Dominion University

Norfolk, VA 23529-0247

804-683-4916, britcher@aero.odu.edu

ABSTRACT

Proper understanding and accurate modelling of eddy currents in magnetic bearings and magnetic suspensions is important if high-performance feedback controllers are to be employed. This paper first addresses the theoretical and computational modelling of the effects of eddy currents in a range of applications, encompassing small-gap (bearing-type) systems as well as large-gap (suspension and levitation-type) systems. Experimental results are presented for a large-gap system, the Large Angle Magnetic Suspension Test Fixture (LAMSTF), and a small-gap system, the Annular Suspension and Pointing System (ASPS), a prototype for a space payload pointing and vibration isolation system. Analysis of the effects of these eddy currents on the dynamic characteristics and control of each of these systems is also presented.

ACKNOWLEDGEMENTS

This work was supported by NASA Langley Research Center under Grant NAG-1-1056. The Technical Monitor was Nelson J. Groom of the Guidance and Control Branch, Flight Dynamics and Control Division. The author would also like to express gratitude to a number of graduate students who have contributed to this work, notably Mehran Ghofrani, Lucas Foster and Daniel Neff.

NOMENCLATURE

a	Outer radius, m
b	Thickness of plate, m
B	Magnetic flux density, T
G	Loop gain
H	Magnetic field strength, A/m
I	Current, A
J	Bessel function, first kind
K	Field coefficient, T/A (field) or T/Am (gradient)
r	Radius, m
R	Resistance, Ω
δ	Skin depth, m
μ_o	Permeability of free space, H/m
μ_r	Relative permeability
ρ	Resistivity, Ω
σ	Conductivity, 1/Ω
ϕ	Magnetic flux, Wb
ω	Angular frequency, rad/s

Subscripts

e	Eddy current
j	Electromagnet/coil number
m	Mutual (inductance)
s	Surface

Symbols

[ ]	Matrix

1. INTRODUCTION

Eddy currents are present whenever a time-varying magnetic flux penetrates a conducting medium. The direction of flow of the eddy current is such as to reduce the rate-of-change of flux. In feedback-controlled magnetic suspensions, this time-variation often represents the control effort necessary to maintain the required positioning or stability of the suspended object. It may, therefore, be important to develop an accurate mathematical model of the eddy currents, in order to configure an optimum controller. Analytic solutions for eddy currents are available for some simplified geometries, but eddy currents in complex geometries must be solved by computation, although it is only in recent years that such computations have been considered practical. In this paper, a state-of-the-art computer code "ELEKTRA" will be applied to the eddy current problem.

2. MODELLING OF EDDY CURRENTS

Two classes of problems have been addressed so far, classified by the relative penetration depth of eddy currents, the so-called "skin-depth", compared to the physical thicknesses of conducting material involved. The skin depth is given by the following formula :

$$\delta = \sqrt{\frac{2}{\mu_o \mu_r \sigma \omega}} \quad \text{or} \quad \sqrt{\frac{2\rho}{\mu_o \mu_r \omega}} \tag{1}$$

As an example, the skin depth for an aluminum conductor at 10Hz would be around 28mm. In iron regions, the value would be considerably less.

2.1 LARGE SKIN-DEPTH

A general form of a mathematical model for eddy currents can be established in this case, based on two assumptions, namely some a priori knowledge of the geometry of the eddy current circuit, and that the circuit geometry is independent of frequency. In practice, the first assumption requires that the eddy currents be constrained to flow around well-defined paths,

rather than through large plates or shells of conducting material. The second assumption requires that the skin depth be much greater than the local material thickness.

If the abovementioned assumptions are satisfied, the resulting model corresponds to that sometimes described in literature as the Single Time Constant Model. The derivation resembles the analysis of a transformer with a shorted secondary, as illustrated in Figure 1 :

$$V = IR + L\frac{dI}{dt} + L_m\frac{dI_e}{dt} \qquad 0 = I_eR_e + L_e\frac{dI_e}{dt} + L_m\frac{dI}{dt} \tag{2}$$

Multiple eddy current circuits are not considered here. The terminal characteristics of the driven coil are :

$$\frac{I}{V} = \left(\frac{1}{(R + Ls) - \frac{(L_m s)^2}{R_e + L_e s}} \right) \tag{3}$$

In large-gap applications, the field components generated at the suspended object will typically be expressed as :

$$B_j = K_jI + K_{e_j}I_e = K_jI\left(1 - \frac{K_{e_j}L_m s}{K_j(R_e + L_e s)}\right) \tag{4}$$

Now the factor K_{e_j} will, in general, be different for each field component, that is each field component will be a different proportion of the main electromagnet field. Therefore the eddy current effects in a large-gap system involving several electromagnets and eddy current circuits should be represented as follows :

$$[B_j] = [K_j][I] + [K_{j_e}][I_e] \tag{5}$$

If the eddy current circuit has similar geometry to the primary (for example the induced current in electromagnet cores), it can be argued that the relative effect on all field and field

gradient components at the suspended object will be similar. In this case, the representation can be considerably simplified by invoking a false current :

$$I' = \left(1 - \frac{K_e L_m s}{K_j (R_e + L_e s)} \right) I, \quad \text{where } B_j = K_j I' \tag{6}$$

It should be noted that the change in electromagnet terminal characteristics and the change in field at the suspended object are two separate effects and should be modelled as such.

2.2 SMALL SKIN DEPTHS

Analytic solutions are available for some simple geometries, which can be used to provide an insight into the correct form of eddy current models in the case of small skin-depth, where the eddy current circuit geometry varies with frequency. The classical problem of magnetization of an infinite flat sheet, illustrated in Figure 2, will now be reviewed. The solution can be found in numerous texts [1,2] :

$$B = B_s \left(\frac{\text{Cosh}(\alpha y)}{\text{Cosh}(\alpha b)} \right) \qquad \text{where } \alpha = \sqrt{(j\omega\sigma\mu_o\mu_r)} \tag{7}$$

Integrating the total flux across the conductor :

$$B_{total} = \frac{2B_s \,\text{Sinh}(\alpha b)}{\alpha \,\text{Cosh}(\alpha b)} = 2B_s b \left(\frac{1 + \frac{(\alpha b)^2}{3!} + \frac{(\alpha b)^4}{5!} + \frac{(\alpha b)^6}{7!} + \cdots}{1 + \frac{(\alpha b)^2}{2!} + \frac{(\alpha b)^4}{4!} + \frac{(\alpha b)^6}{6!} + \cdots} \right) \tag{8a,b}$$

It is recognized that equation 8b represents a pole-zero sequence, with a d.c. response of $2B_s b$. Similar results have been previously derived by other authors [3] The obvious approach to linear modelling is to approximate the expression using the first few terms of the series. Figure 3 shows the response for various numbers of terms. It is seen that large fluctuations in response occur at higher frequencies with larger numbers of terms. This is due to the generation of lightly damped, closely spaced poles, coupled with series truncation errors. In practice, only a few terms would be employed, to avoid excessive complexity in the model, so a

four- or five-term series may be a reasonable choice. It should also be noted that the limiting rate of roll-off (i.e. at high frequencies) is around 10db/decade and that the limiting phase lag is 45°. Both of these values are exactly half the corresponding value for a simple first-order pole.

A similar problem is the magnetization of an infinite cylindrical bar in a uniform axial field. Again, the solution can be found in numerous texts [1,2], and is of the form :

$$B = B_s \frac{J_o(j\alpha r)}{J_o(j\alpha a)} \tag{9}$$

This can be expressed as an infinite series and/or integrated across the bar, showing similar features as before, regarding limiting roll-off rates and phase lags :

$$B = \pi B_s a^2 \frac{1+\frac{(\alpha a/2)^2}{2.1!^2}+\frac{(\alpha a/2)^4}{3.2!^2}+\frac{(\alpha a/2)^6}{4.3!^2}}{1+\frac{(\alpha a/2)^2}{1!^2}+\frac{(\alpha a/2)^4}{2!^2}+} \tag{10}$$

3. COMPUTATIONAL APPROACHES

Magnetostatic fields in air are governed by Laplace's equation and can be described by simple potential functions. A difficulty arises exterior to current-carrying conductors, since the potential will be multi-valued. This difficulty can be overcome by splitting the field into two parts, one representing the field due to magnetized volumes, and another representing the contribution of current-carrying conductors. A "reduced potential" can be defined to represent the former, and a "total potential" to represent the combination. The total potential can now be made single-valued in regions exterior to current-carrying coils. The field due to currents is calculated in the reduced potential space using the Biot-Savart law.

For practical eddy current problems, the governing equations are the zero-frequency limit of Maxwell's equations. This implies that the wavelength of any electromagnetic wave is very long compared to the characteristic physical dimension of the problem. These equations can be solved using a "vector potential" formulation, where $\vec{B} = \nabla \times \vec{A}$. The region containing an eddy current problem can therefore be subdivided into reduced, total and vector

potential spaces as appropriate, with field continuity enforced on the boundaries between different formulations. The approach described is the one used in this work, but is not the only possibility.

3.1 OPERA-3D / TOSCA / ELEKTRA / VF-GFUN

OPERA-3D (OPerating environment for Electromagnetic Research and Analysis) comprises an interactive, graphically-based, pre-processor, for preparation of finite element problems, with a related post-processor, for analysis and display of results. Problems specified in the pre-processor are submitted to a variety of analysis packages for solution. These packages include TOSCA, for solution of magnetostatic and electrostatic problems using the finite-element method, VF/GFUN, for solution of magnetostatic problems using integral equation methods, and ELEKTRA, for solution of eddy current problems using the finite-element method.

4. THE LARGE-ANGLE MAGNETIC SUSPENSION TEST FIXTURE (LAMSTF)

In order to explore the technology required for the magnetic suspension of objects over large ranges of orientation, a small-scale laboratory development system, the Large Angle Magnetic Suspension Test Fixture (LAMSTF) has been constructed at NASA Langley Research Center. Possible applications for magnetic suspension systems of this general class include space payload pointing and manipulation, microgravity vibration isolation and wind tunnel model suspension. An important objective of this particular project is to investigate the dynamic modelling of large-gap magnetic suspension systems, so that future systems can be designed with higher confidence levels.

The general configuration [4] is illustrated in Figure 4. Five room temperature copper electromagnets are mounted on an aluminum plate, each electromagnet driven by a transistor switching power amplifier. The suspended element consists of Neodymium-Iron-Boron permanent magnet material inside an aluminum tube. The direction of magnetization is along the axis of the cylinder, which is horizontal when suspended. The suspension height is 0.1m,

measured from the axis of the suspended element to the top plane of the electromagnet conductor. Several different control systems have been developed and demonstrated, including several digital versions [5,6].

4.1 EDDY CURRENT EFFECTS IN LAMSTF

In the original design of LAMSTF, eddy-current circuits were deliberately introduced in three main areas: the position sensor structure, the electromagnet cores, and the aluminum baseplate. This was done so that it would be necessary to measure, analyze and model the eddy current effects, rather than attempting to avoid their influence, as would have been the conventional practice. The fact that stable suspension was initially achieved rather easily was taken to indicate that the eddy current effects were not very significant. However, a consistent discrepancy was discovered in the dynamic behaviour in the "pitch" degree-of-freedom [4], when the metallic baseplate and sensor frame were used. This led to a careful analysis of the effects of eddy currents, which were subsequently confirmed to be the cause of the anomaly.

4.2 COMPUTATIONS - LARGE SKIN DEPTHS

The OPERA code is used to calculate flux linkages, hence inductances, using:

$$\phi_{ij} = \frac{\phi_i}{I_j} = \frac{(\int\int B.ds)_i}{I_j} \tag{11}$$

By way of example, a series of calculations were made for a single LAMSTF electromagnet with a representation of one part of the position sensor assembly mounted on the same axis [7], as illustrated in Figure 5. Incorporating the estimated parameters in equation 4, and examining the axial (z-axis) field component, gives:

$$B_z = K_z I \left(1 - \frac{6.13\times10^{-4}\, s}{1+2.983\times10^{-3} s} \right) \tag{12}$$

It is seen that the predicted reasonant frequency of the eddy current circuit is around 53Hz, significantly higher than the system's open-loop natural frequencies, but still within the bandwidth of the controller.

4.3 COMPUTATIONS - SMALL SKIN DEPTHS

Direct computations of magnetic field due to a single electromagnet with a conducting ring on-axis (Figure 5) were made using ELEKTRA. Solutions provide the magnitude and phase of the on-axis field, the coil inductance (stored energy), power dissipation, and the magnetic field and eddy current distributions. Computations have also been carried out for the cases of a single coil on a conducting plate, and with an iron core. Here, especially in the latter case, the skin depth at higher frequencies is small with respect to the material thickness, resulting in increased dissipation and consequently attenuated field and increased phase lag. Results are shown in Figures 6 thru 8, with further explanation provided in the next section.

4.4 EXPERIMENTAL VERIFICATION

Actual measurements of the current to field transfer function, corresponding to equation 4, were made with an experimental set-up corresponding to that shown in Figure 5. Field components were measured with a Hall effect gaussmeter and the transfer function was measured directly with a frequency analyzer, with sine-sweep excitation. Figure 6 shows the measured transfer function for B_z, together with the predictions from equation 12, and ELEKTRA computations. The agreement is thought to be satisfactory, especially considering that the reasonant frequency of the eddy circuit depends on the material resistivity, which varies significantly between different aluminum alloys[1]. The values of most parameters in the linear model can be adjusted to give a better agreement with experiment, also shown in Figure 6. The only significant residual discrepancies are seen to occur at higher frequencies where the validity of the Single Time Constant Model is questionable. The adjusted form of equation 12 is :

---

[1] The resitivity of pure aluminum is around 2.65×10^8 Ωm, a high strength alloy could be around 5×10^8 Ωm

$$B_z = K_z I \left(1 - \frac{7.591 \times 10^{-4}\, s}{1 + 2.934 \times 10^{-3} s} \right) \tag{13}$$

If the electromagnet is mounted on the aluminum plate, a second eddy current circuit is added; when the iron core is inserted, a third is added. Experiments have indicated that the response may be characterized by multiple implementations of the linear model described above. However, as the complexity of the physical system increases, it becomes increasingly difficult to derive an accurate model. This is especially true when the iron core is present, since the core becomes highly dissipative at high frequencies, due to the small skin depth. This results in increased phase lag and reduced field strength at high frequencies. Representative results, shown in Figures 7 and 8, indicate the type of limiting roll-off behaviour suggested by equation 6.

4.5 EFFECT OF EDDY CURRENTS ON LAMSTF DYNAMICS

Mathematical models of LAMSTF have been derived previously [4]. The "pitch" degree-of-freedom can be decoupled from the other degrees-of-freedom to a first order, giving an effective plant transfer function resembling :

$$\frac{\theta_y}{\theta_{y_{demand}}} = G \frac{(1+0.01s)^2}{(1+0.001s)^2(1+0.0009s)(1+0.017s)(1-0.017s)} \tag{14}$$

The two zeros and the first two poles arise from the "Dual Phase Advance" controller used in early testing, the second pole from the electromagnet/power supply combinations, and the final two poles from the unstable "compass-needle" pitching mode [4]. G represents the controller gain, plus assorted component gains. With this transfer function, a value of G of around 10, gives reasonable response. If the transfer function of Equation 13 is appended, together with the (similar) functions representing the eddy current influence of the aluminum baseplate and the iron core, the damping ratio falls somewhat below this value, as shown in

Figure 9. The reduction in damping is of the same order as the observed discrepancy between predicted and experimental responses, thus the eddy currents in position sensor structure (and other parts of LAMSTF) can be concluded to be the primary source of the discrepancies.

In a later version of LAMSTF [8], most eddy currents were eliminated by replacing the position sensor structure and baseplate with non-conducting components. Correlation between predicted and observed responses is now quite good.

5. THE ANNULAR SUSPENSION AND POINTING SYSTEM

The Annular Suspension and Pointing System (ASPS) is a prototype for a high precision space payload pointing and vibration isolation system. A ferromagnetic rotor is magnetically suspended by five double-acting magnetic bearing stations, such that the orientation of the ring can be controlled in two "tilt" axes, with translational and rotational isolation of base vibrations. The general configuration is illustrated in Figure 10, with the geometry of one of the "axial" bearing stations shown in Figure 11. Considerable hardware upgrades have been made recently, and the system now utilizes transistor switching power amplifiers and a digital controller [9].

An effort to model, measure and compute the eddy current effects in each bearing station has begun. Early experimental results indicate steadily falling magnetic field intensity, with steadily increasing phase lag, in the air-gap with increasing frequency, as shown in Figure 12. The rate of roll-off is seen to be around 10 db/decade as predicted. There is also a strong indication of variations in relative amplitude and phase of the magnetic field across the air-gap, also shown in Figure 12. No quantitative computational results are shown, since the available results are limited and are not considered reliable at this stage. The variation of magnitude and phase of the magnetic field across the air-gap does occur in computations, however. Further, it should be noted that the computations require the specification of two material properties, namely magnetic permeability and electrical resitivity. Neither is easy to specify accurately for the nickel-iron alloy employed, partly due to the effect of heat-treatments.

The ASPS actuator bandwidth is seen to be around 30 Hz. This happens to be well above the design system bandwidth of around 1 Hz, so is not a serious performance limitation. The low design value is due to the massive payloads envisioned (at least 600 kg for the original specifications).

6. DISCUSSION

Eddy currents have been shown to significantly affect the dynamics of both a large-gap suspension system (LAMSTF) and a small-gap system (ASPS). Results appear to be consistent with other recent work [10 etc.], although much further study is called for.

The design choice of attempting to eliminate eddy current effects, typically by breaking loops of conducting material and using laminated iron cores, is not always available. For instance, large (low-T_c) superconducting electromagnets are generally contained in metallic dewars. In magnetic bearing applications, it is generally considered impractical to laminate the stators of thrust bearings, since the laminations would be required to be either radial or circumferential. In any application, the use of unlaminated material would be preferred on grounds of cost, provided that the penalty in dynamic response was small.

Contemporary software provides powerful tools for the analysis of eddy currents in magnetic suspensions and magnetic bearings. Early results compare reasonably well to experimental measurements, provided accurate material properties are available

7. CONCLUSIONS

The simplified circuit-based eddy current model proposed appears to predict the observed trends in the case of large eddy current circuits in conducting, non-magnetic material. Computations are capable of providing reasonable estimates of important parameters, with the option of refinement based on measurements of magnetic field or electromagnet terminal characteristics. A much more difficult case is seen to be that of eddy currents in magnetic material, or in non-magnetic material at higher frequencies, due to the smaller and frequency-dependent skin depths. Even here, the dissipative behaviour has been shown to yield at least

somewhat to linear modelling. Available computational tools are shown to be capable of providing the required information on fields, eddy currents etc., provided appropriate care is exercised.

REFERENCES

1. Stoll, R.L.: The Analysis of Eddy Currents. Clarendon, 1974
2. Binns, K.J.; Lawrenson, P.J.; Trowbridge, C.W.: The Analysis and Computation of Electric and Magnetic Fields. Wiley, 1992.
3. Zmood, R.B.; Anand, D.K.; Kirk, J.A.: The Influence of Eddy Currents on Magnetic Actuator Performance. IEEE Proceedings, Vol.75, No.2, February 1987.
4. Britcher, C.P.; Ghofrani, M.: A Magnetic Suspension System with a Large Angular Range. Review of Scientific Instruments, Volume 64, No. 7, July 1993.
5. Cox, D.E.; Groom, N.J.; Implementation of a Decoupled Controller for a Magnetic Suspension System using Electromagnets Mounted in a Planar Array. 2nd International Symposium on Magnetic Suspension Technology, Seattle, WA, Aug.1993. NASA CP-3247, May 1994.
6. Lim, K.; Cox. D.E.: Robust Tracking Control of a Magnetically Suspended Rigid Body. 2nd International Symposium on Magnetic Suspension Technology, Seattle, WA, Aug.1993. NASA CP-3247, May 1994.
7. Britcher, C.P.; Foster, L.: Some Further Developments in the Dynamic Modelling of the Large-Angle Magnetic Suspension Test Fixture. 2nd Int. Symposium on Magnetic Suspension Technology, Seattle, WA, Aug.1993. NASA CP-3247, May 1994.
8. Lim, Cox. IEEE
9. Britcher, C.P.; Groom, N.J.: Current and Future Development of the Annular Suspension and Pointing System, 4th International Symposium on Magnetic Bearings, ETH, Zurich, Aug.1994.
10. Palazzolo. MAG '95.

Figure 1 - Schematic of Circuit Model for Eddy Currents

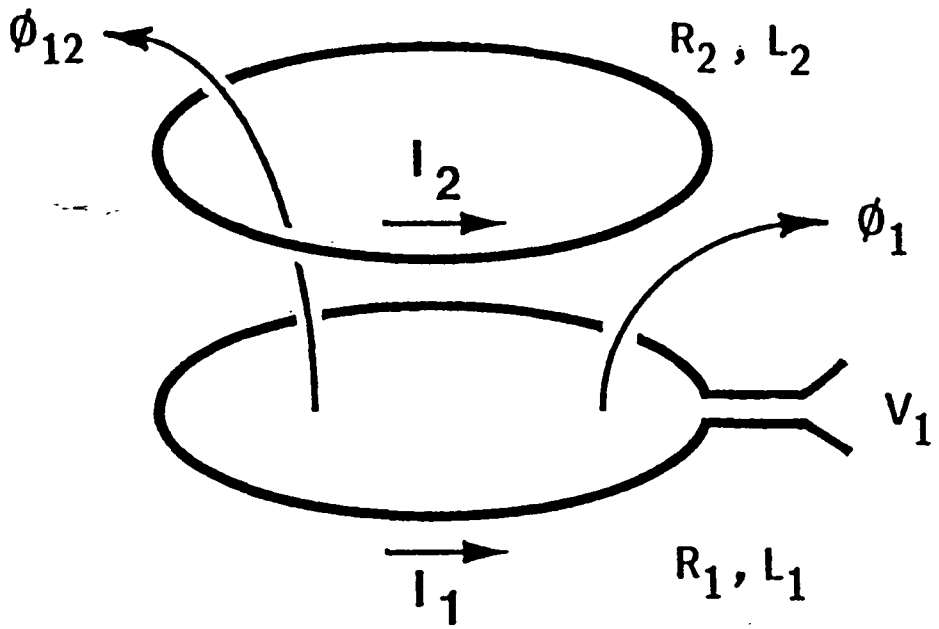

Figure 2 - Schematic of Infinite Flat Sheet Problem

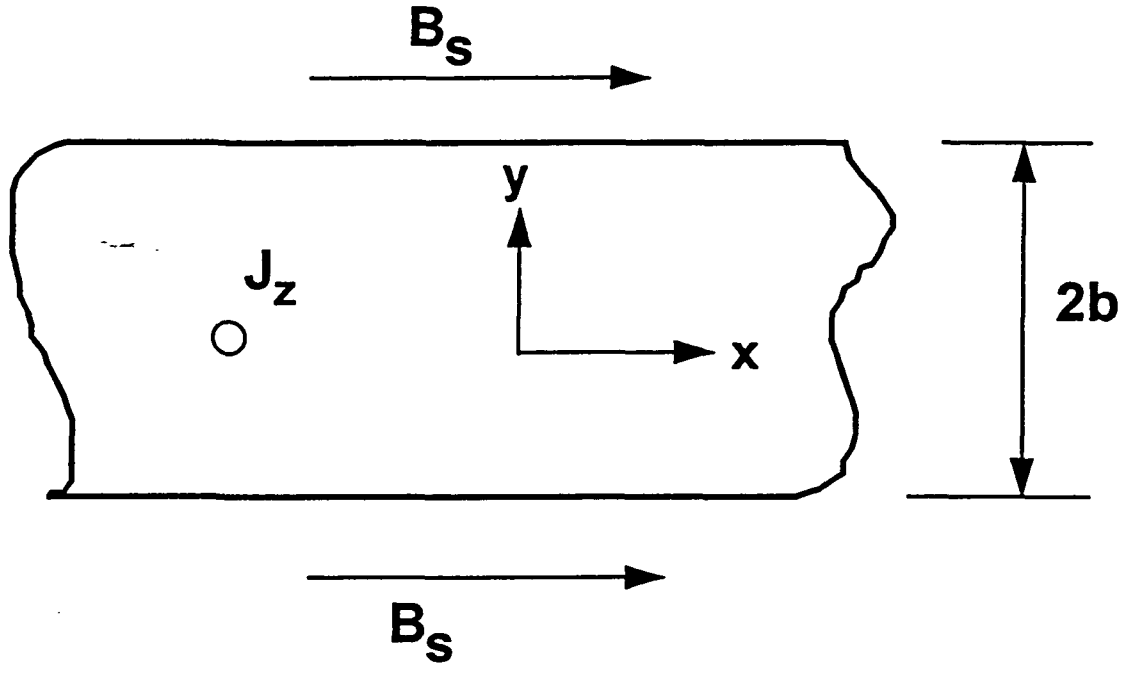

Figure 3 - Integrated Flux for Infinite Flat Sheet Problem

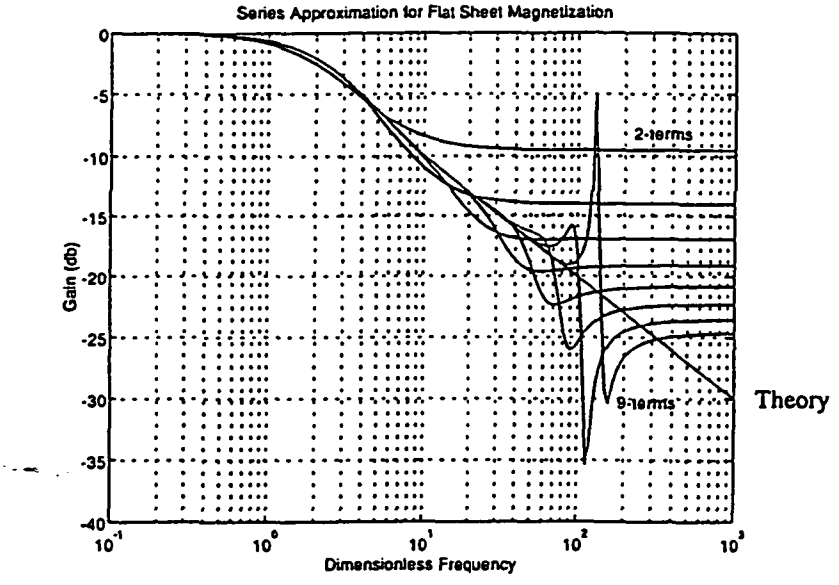

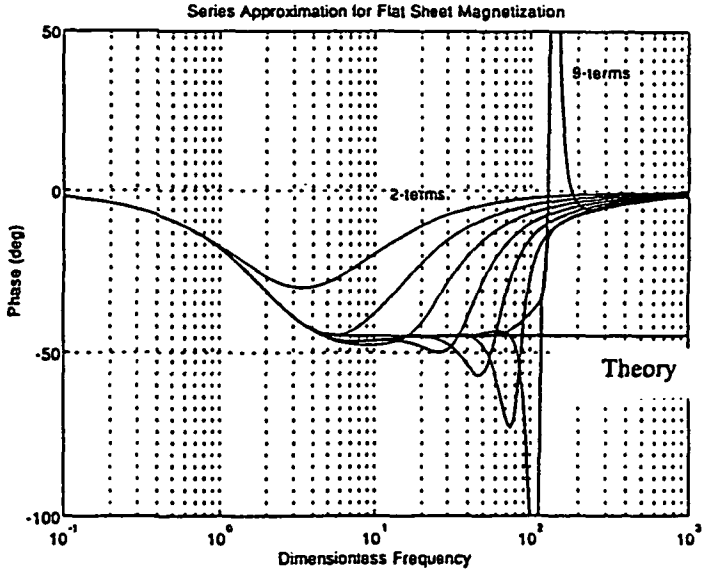

Figure 4 - General Arrangement of the Large Angle Magnetic Suspension Test Fixture

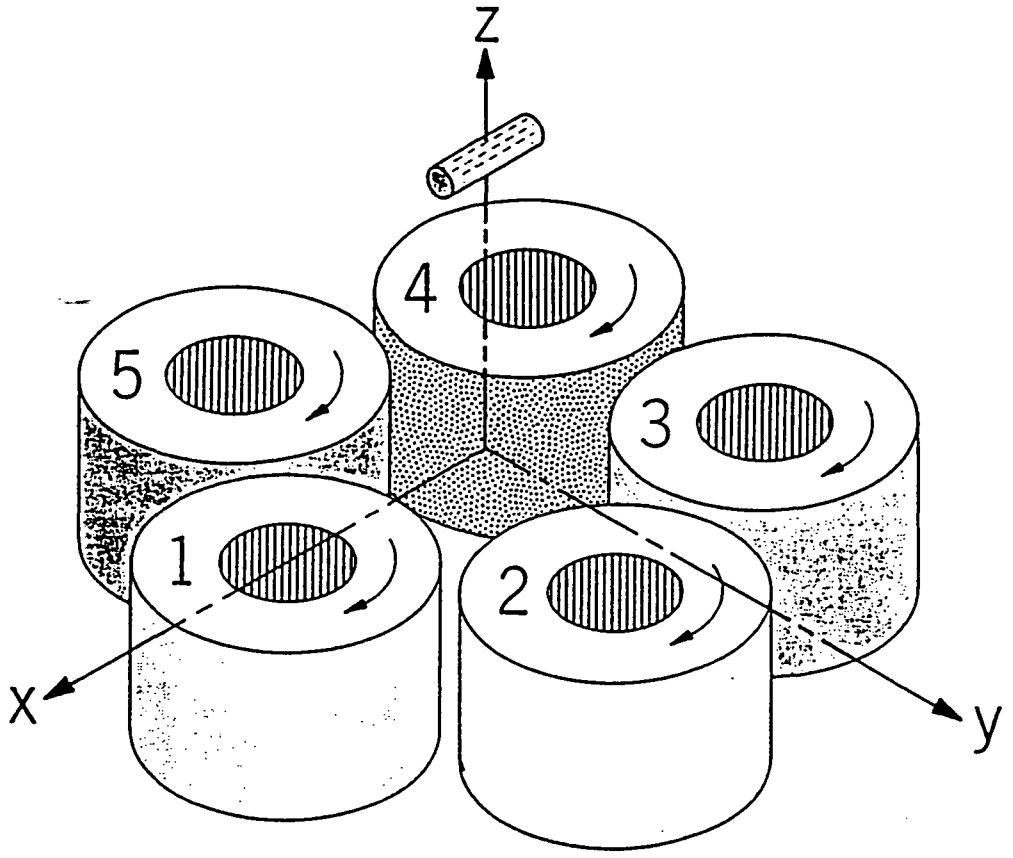

Figure 5 - Simplified Eddy Current Test Set-Up

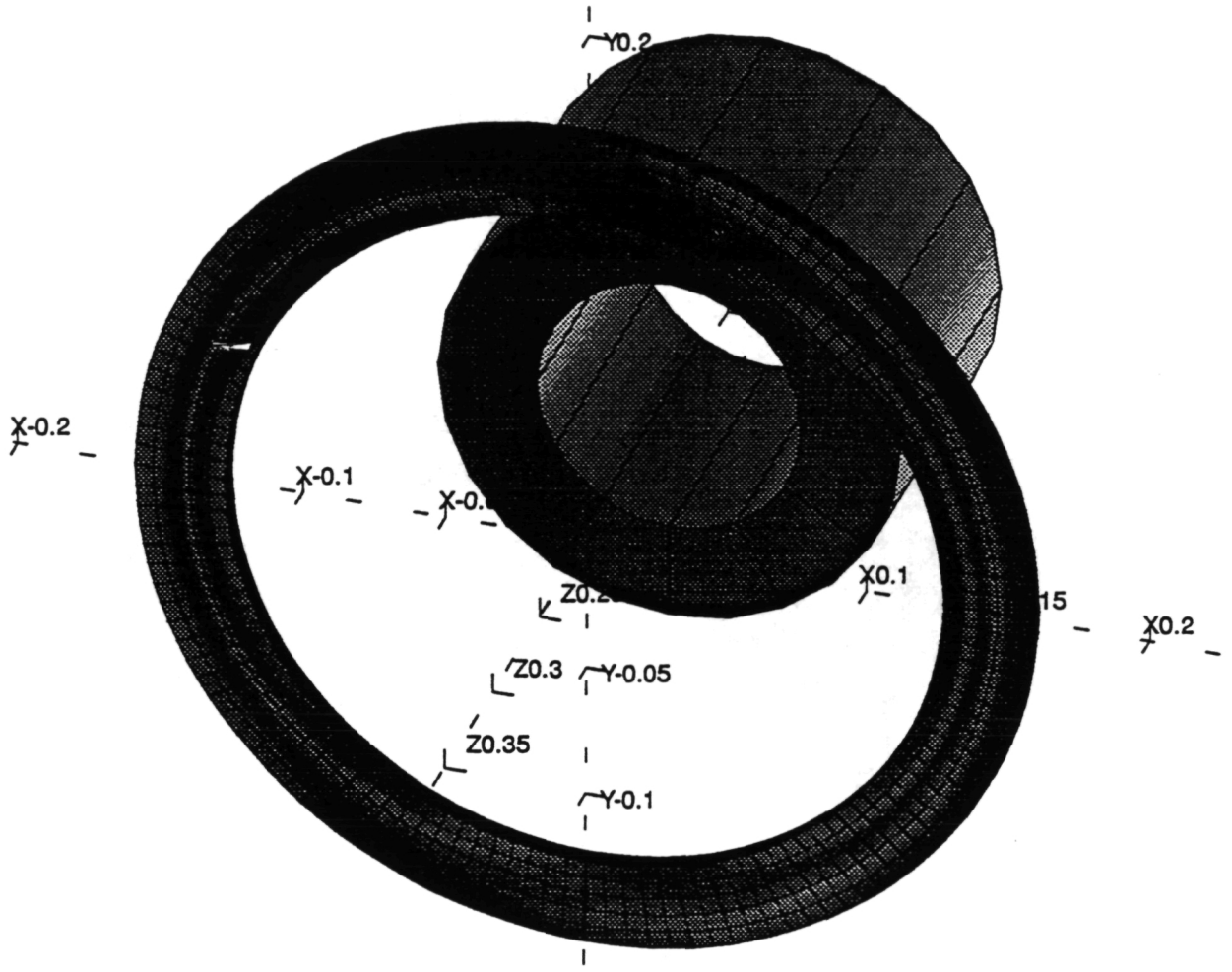

Figure 6 - Axial Field for Air-Cored Electromagnet and Dummy Sensor Ring

Showing axial field magnitude and phase at ring center

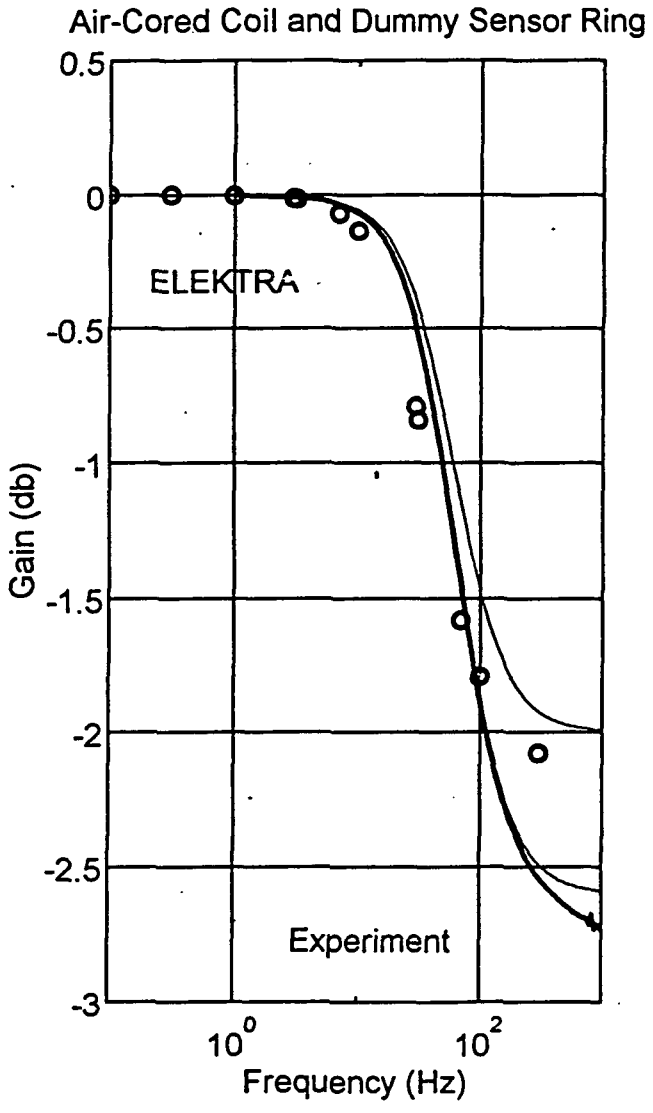

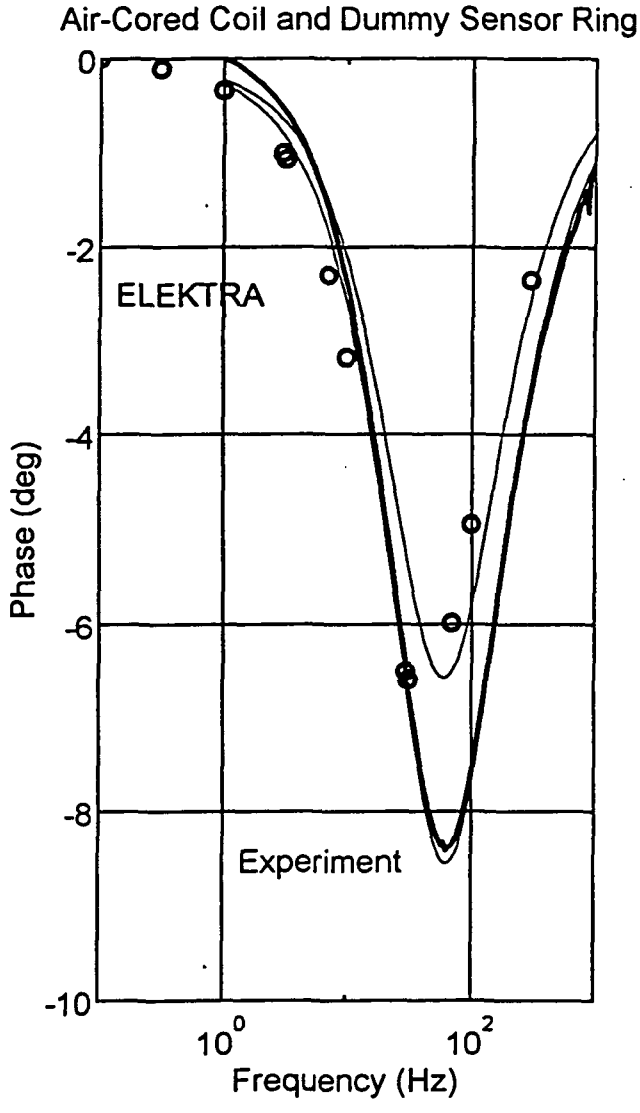

Figure 7 - Axial Field for Air-Cored Electromagnet on Conducting Plate

Showing axial field magnitude and phase 0.1m above the coil

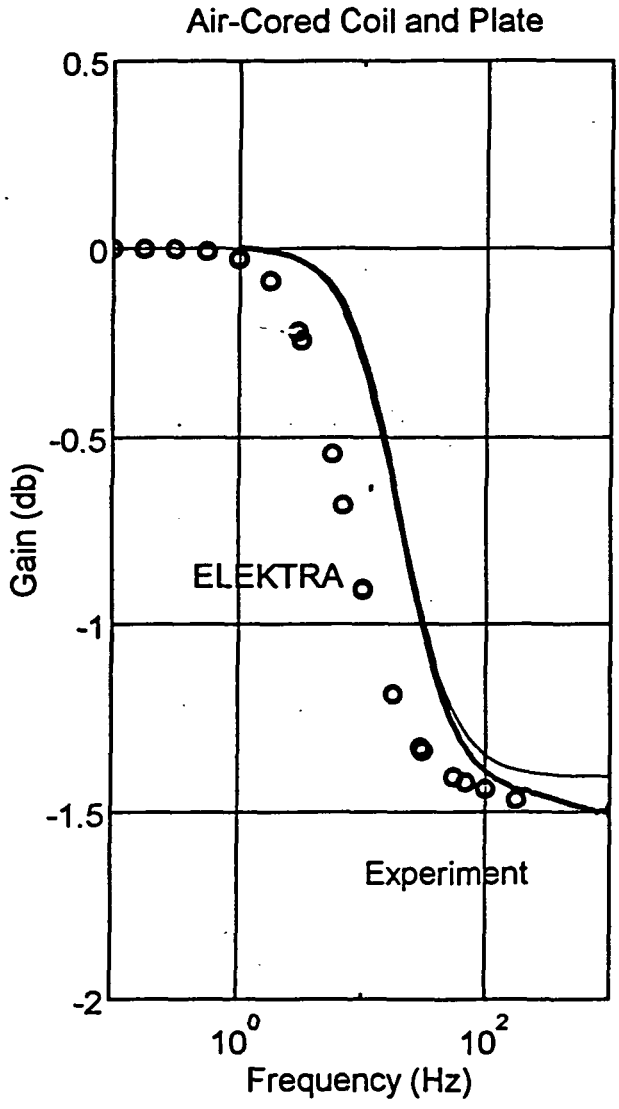

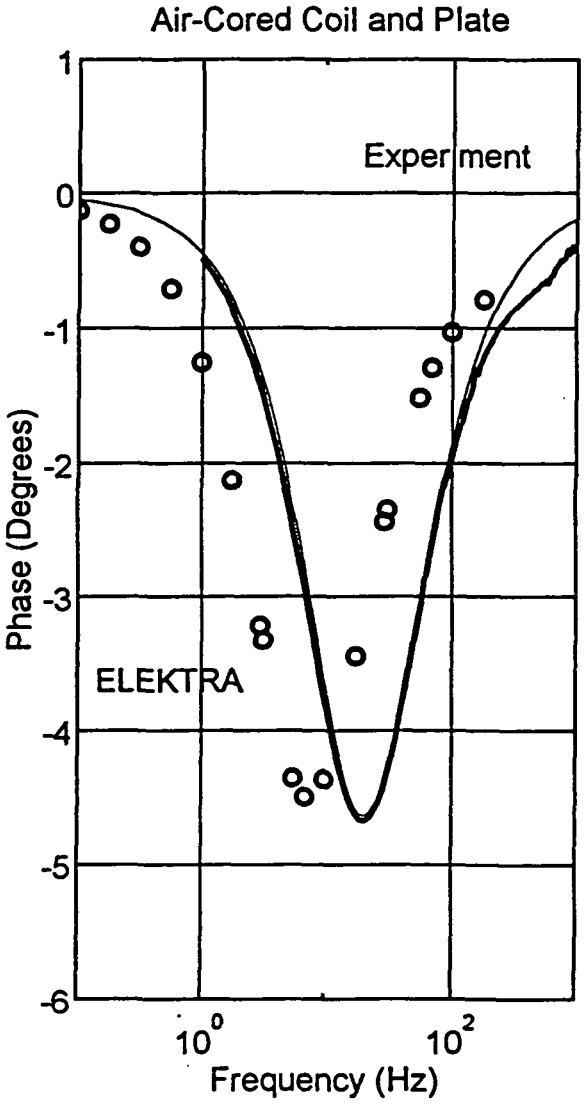

Figure 8 - Axial Field for Electromagnet with Iron Core

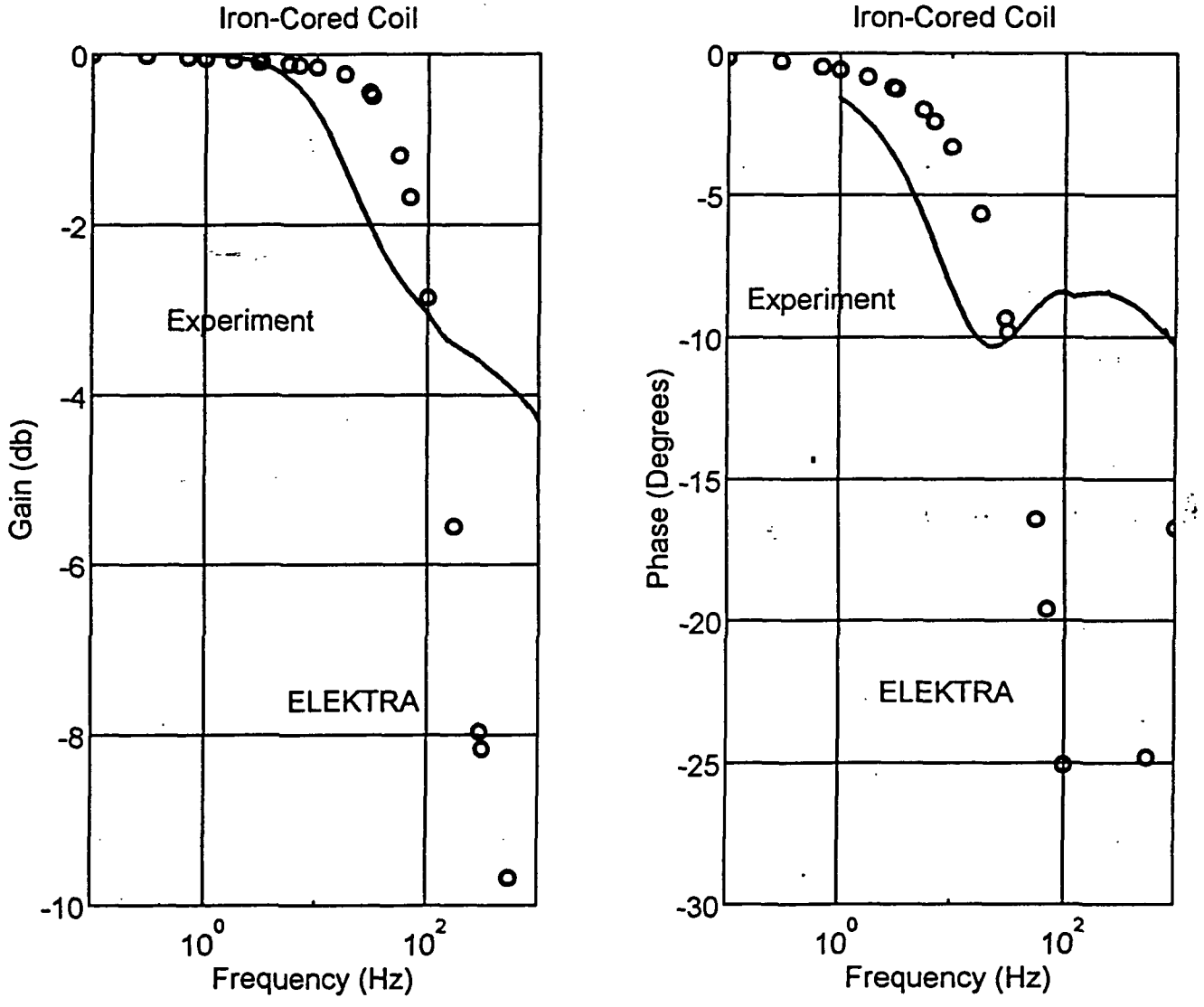

Figure 9 - Predicted Damping Ratios in Pitch, LAMSTF

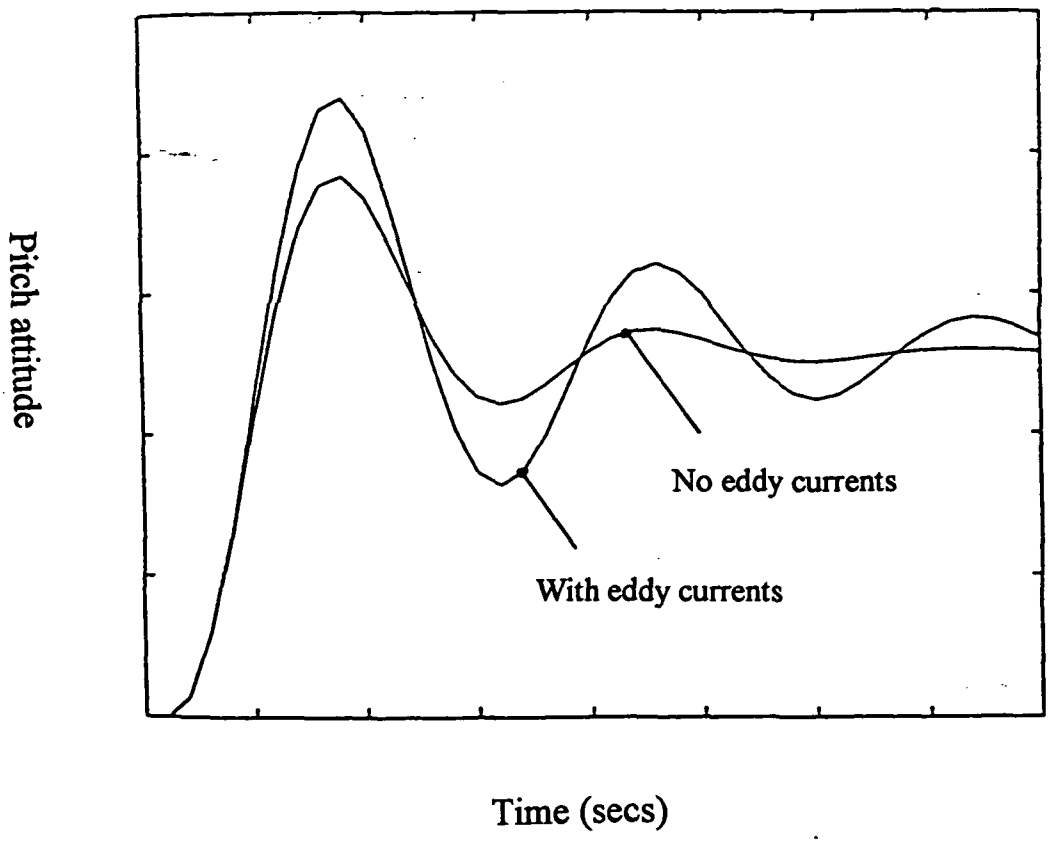

Figure 10 - Geometry of the Annular Suspension and Pointing System

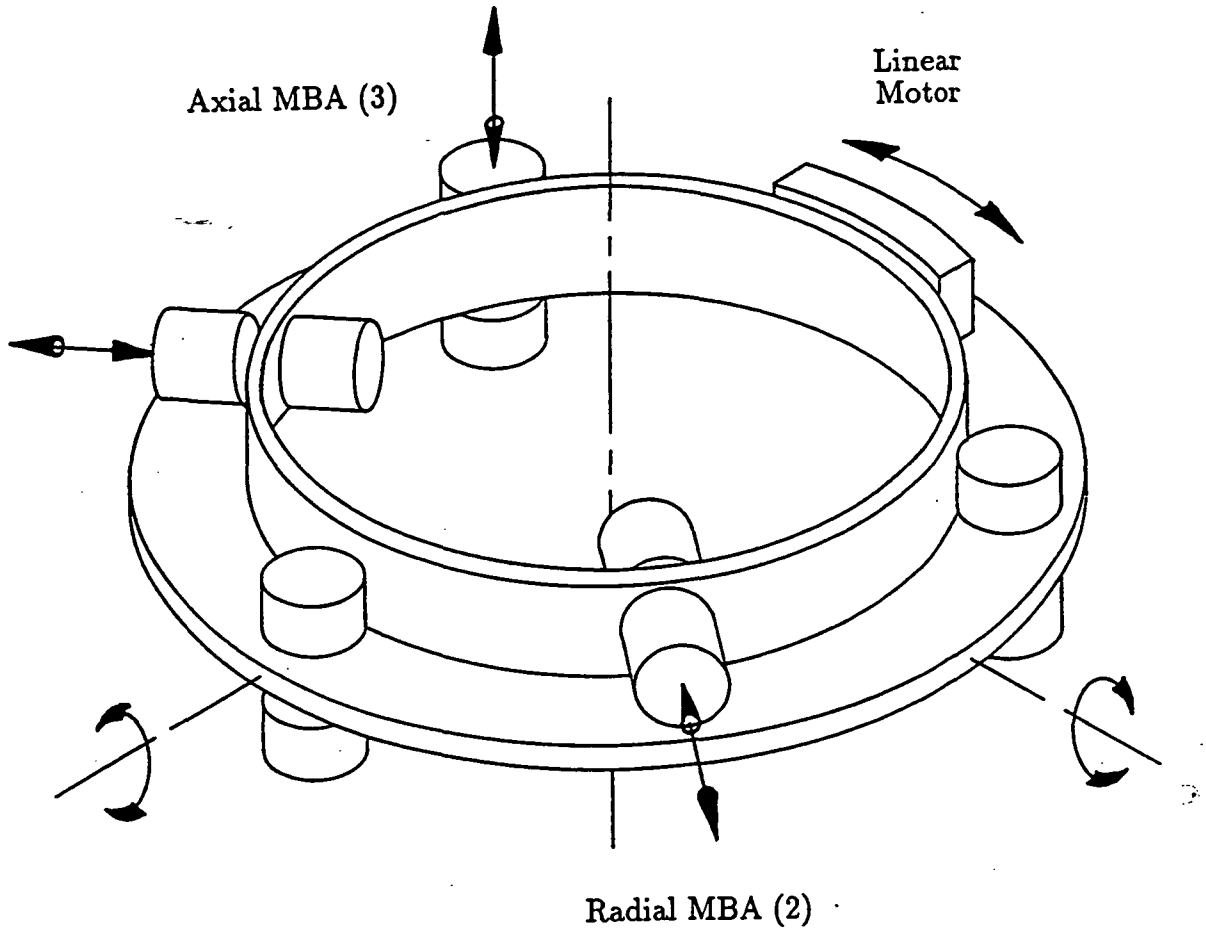

Figure 11 - ASPS Axial Bearing Station

(dimensions in inches)

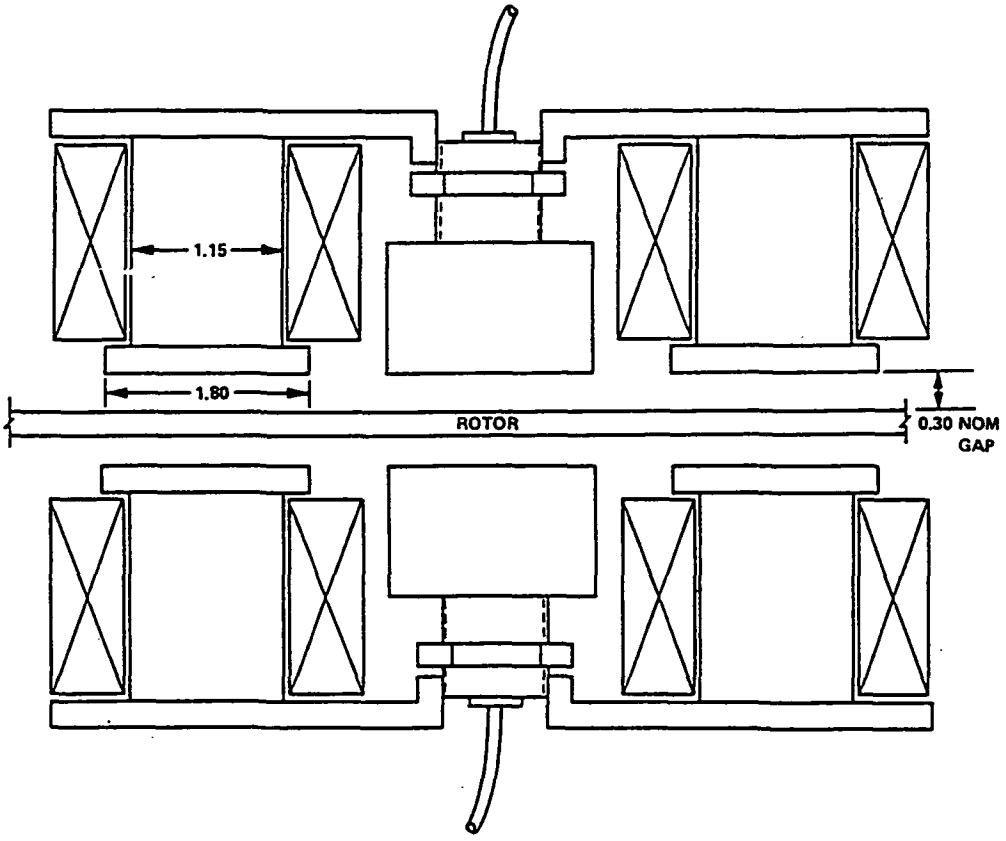

Figure 12 - Measured Magnetic Field in Air-Gap, ASPS Axial Station

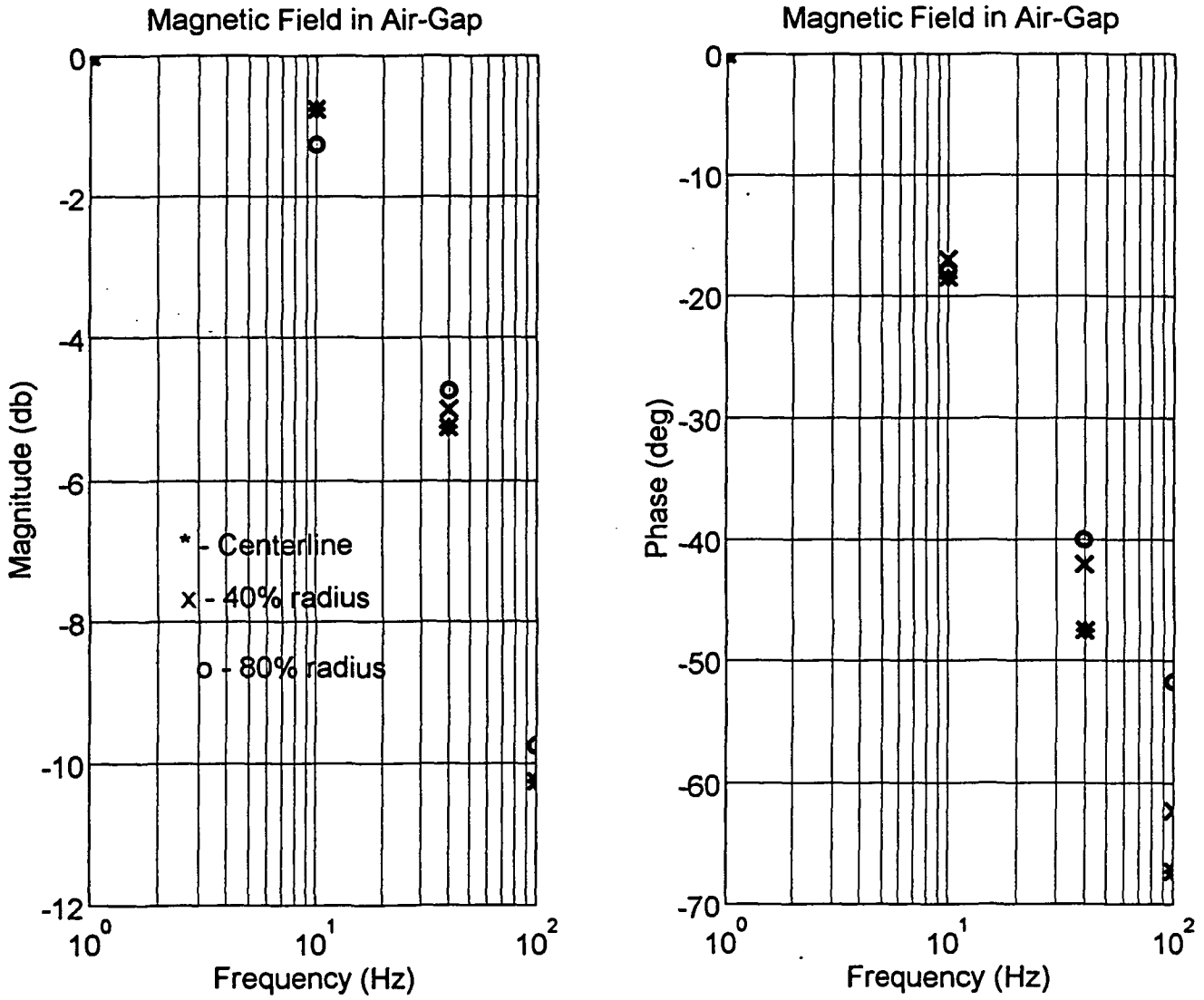

DESIGN AND IMPLEMENTATION OF A DIGITAL CONTROLLER FOR A VIBRATION ISOLATION AND VERNIER POINTING SYSTEM

Daniel J. Neff and Colin P. Britcher
Department of Aerospace Engineering
Old Dominion University
Norfolk, VA

SUMMARY

This paper discusses the recommissioning of the Annular Suspension and Pointing System (ASPS), originally developed in the mid 1970's for pointing and vibration isolation of space experiments. The hardware was developed for NASA Langley Research Center by Sperry Flight Systems (now Honeywell Satellite Systems), was delivered to NASA in 1983. Recently, the hardware was loaned to Old Dominion University (ODU). The ASPS includes coarse gimbal assemblies and a Vernier Pointing Assembly (VPA) that utilize magnetic suspension to provide noncontacting vibration isolation and vernier pointing of the payload. The VPA is the main focus of this research. At ODU, the system has been modified such that it can now be operated in a 1-g environment without a gravity offload. Suspension of the annular iron rotor in five degrees-of-freedom has been achieved with the use of modern switching power amplifiers and a digital controller implemented on a 486-class PC.

INTRODUCTION

The Annular Suspension and Pointing System (ASPS) is a precision payload pointing system designed for use on the space shuttle. In the early 1970's, NASA's Earth-Orbital Systems Technology group established a need to develop a multi-purpose experiment mounting platform to meet the needs of solar, stellar, and earth viewing experiments planned for the 1980's. The prototype hardware (ASPS) was developed for NASA Langley Research Center by Sperry Flight Systems (now Honeywell Satellite Systems). ASPS was delivered to NASA Langley Research Center in 1983, but was never recommissioned due to shifts in program priorities. In late 1992 the hardware was loaned to ODU so that it would be recommissioned and further developed.

GENERAL DESCRIPTION

The ASPS consisted of several systems, a payload mounting plate, the Vernier Pointing Assembly (VPA), two coarse gimbal assemblies, a mounting and jettison assembly, as shown in Figure 1, as well as a control electronics rack, various testing fixtures and assorted connection

hardware. The VPA contains an annular iron rotor with an L-shaped cross-section that supports the payload mounting plate. Five magnetic actuators, referred to as Magnetic Bearing Assemblies (MBA) that provide attractive magnetic forces to suspend the annular iron rotor in five degrees-of-freedom. The magnetic bearing assemblies control the payload tilt of ± 0.75 degrees (initial configuration). The VPA also contains a roll axis drive which can provide unlimited rotational motion about the axis perpendicular to the payload plate. Two coarse gimbal assemblies were stacked to form an elevation and a lateral gimbal pair, providing a mechanically limited travel of ± 100 degrees (from vertical) about the lower elevation gimbal axis, and ± 60 degrees about the upper lateral gimbal axis. The magnetic actuators were initially sized to accept payloads weighing up to 600 kg (later increased) with a center of mass positioned up to one and one half meters above the payload mounting plate [1].

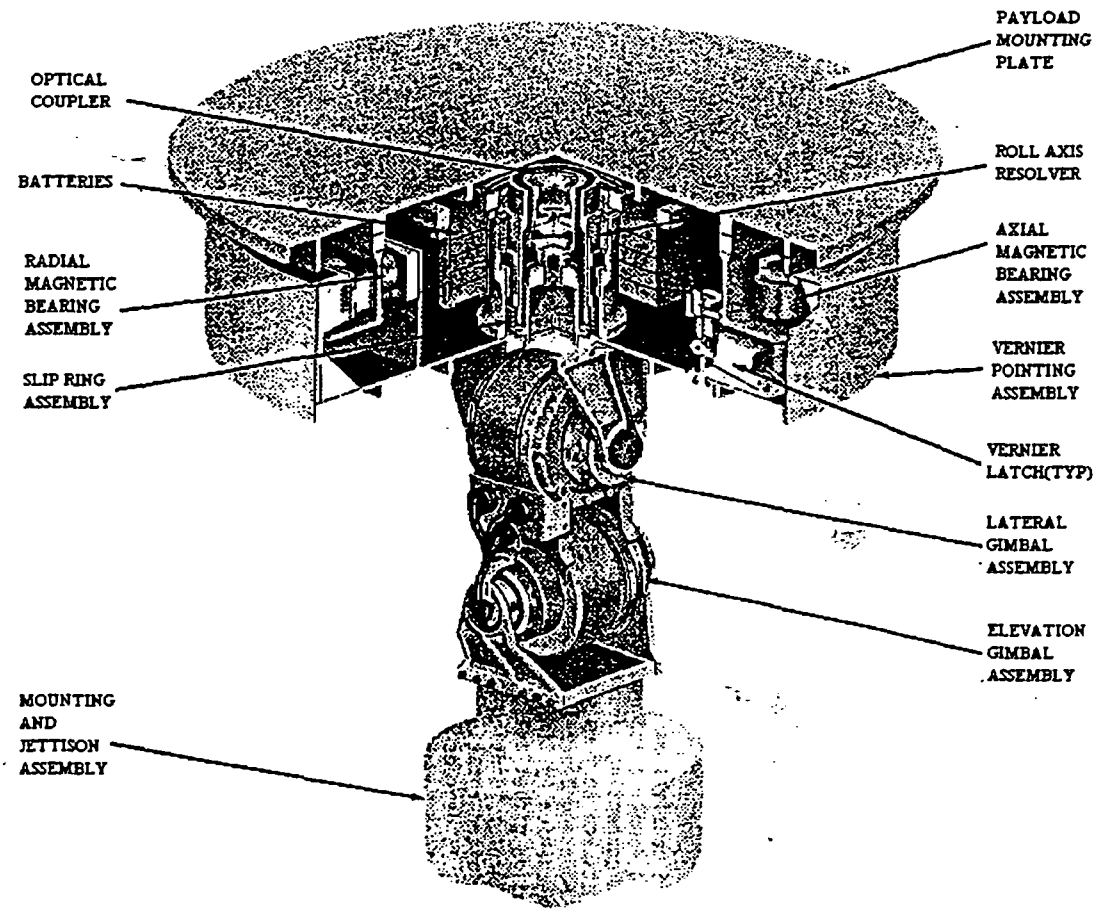

Figure 1 Annular Suspension and Pointing System

The mounting and jettison assembly supported the coarse gimbals and also contained pyrotechnics to jettison the ASPS (and payload) in the event of multiple failures which prevented stowage in orbit. The control electronics rack is an assembly of analog circuits made up of power amplifiers and data acquisition to control the vernier pointing assembly. The balance and testing fixture is a gravity off-load used to simulate a zero-gravity environment.

Hardware Status and Project Goals

Of the systems described above, only the VPA, control electronics rack, and balance and testing fixture were loaned to ODU. The goal of this project was to develop a modern digital control system to suspend the annular iron rotor against gravity in five degrees-of-freedom, and to develop the necessary hardware and software. Once the system became operational, future work could concentrate on improved control algorithms and hardware upgrades, with the objective of steadily improving performance [2].

COMPONENT DESCRIPTIONS

Vernier Pointing Assembly

The VPA provides the ASPS with its high resolution pointing capability. The VPA originally comprised of an annular iron rotor, three axial magnetic bearing assemblies, two radial magnetic bearing assemblies, a roll motor, a total of twelve proximity sensors, five vernier latches, a roll resolver and rotary transformer, and standby battery packs, as shown in Figure 2. However, the rotary transformer and standby batteries were not fully developed [1]. The three axial MBAs, two radial MBAs and roll motor actively control the six degrees-of-freedom of the annular iron rotor, whose mass is 21.59 kg. The axial MBAs control the translation and angular rotation of the payload about two axis and the radial MBAs control the lateral position, providing radial centering. The roll motor controls the sixth degree-of-freedom about the axis perpendicular to the payload plate. The axial MBAs react against the horizontal surface and the radial MBAs react against the vertical surface of the annular iron rotor. The displacements of the rotor are sensed by proximity sensors. Each axial and radial MBA incorporates a pair of proximity sensors. The roll motor has two pairs of proximity sensors to assist in compensating for stray forces and torques produced by the roll motor.

Magnetic Bearing Assembly

The electrical and mechanical descriptions of the axial MBAs is contained in Figure 3. The force capacity of the axial and radial magnetic bearing assemblies are ± 28.9N and ± 14.2N respectively. The operating range of the axial and radial assemblies were ± 5.6mm and

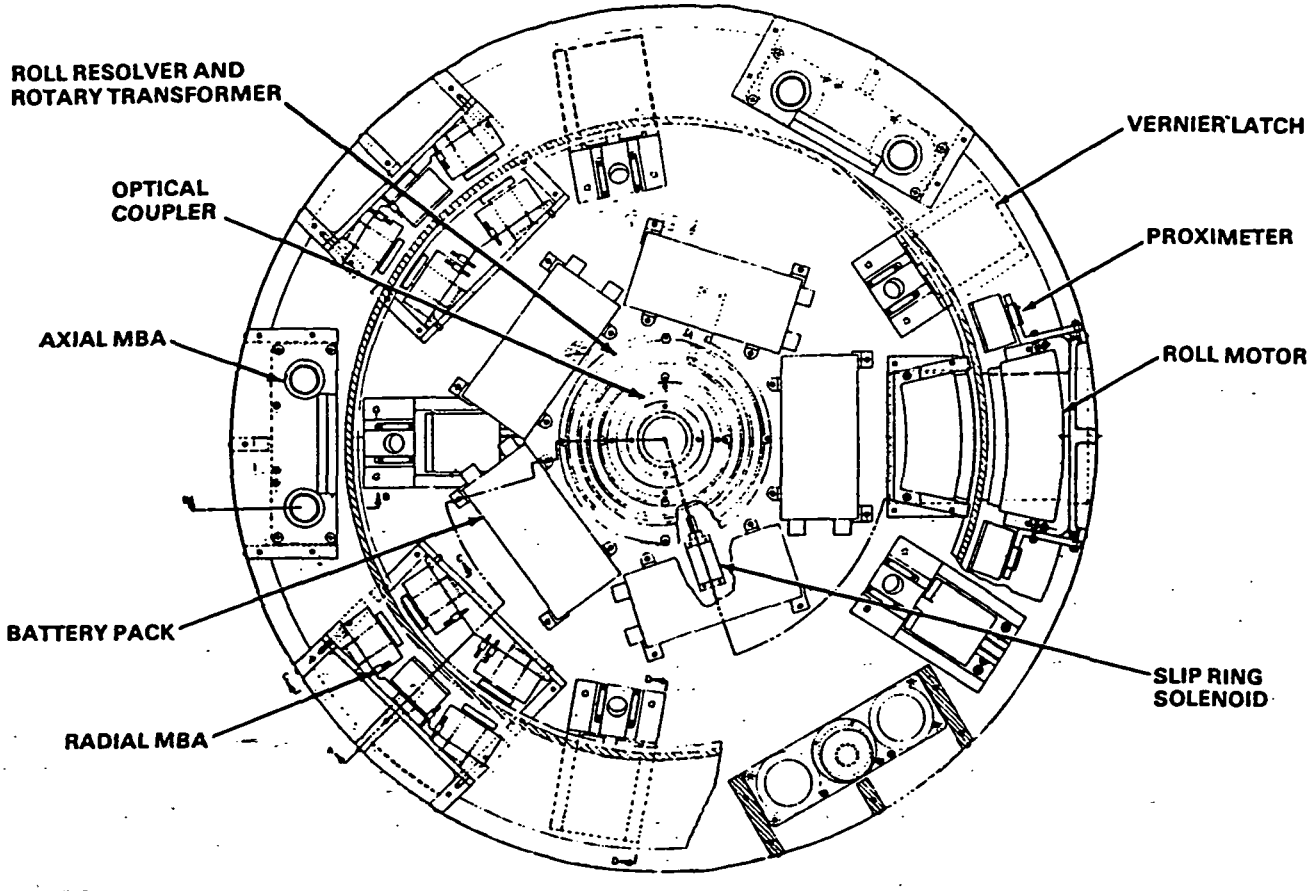

Figure 2 - The Vernier Pointing Assembly

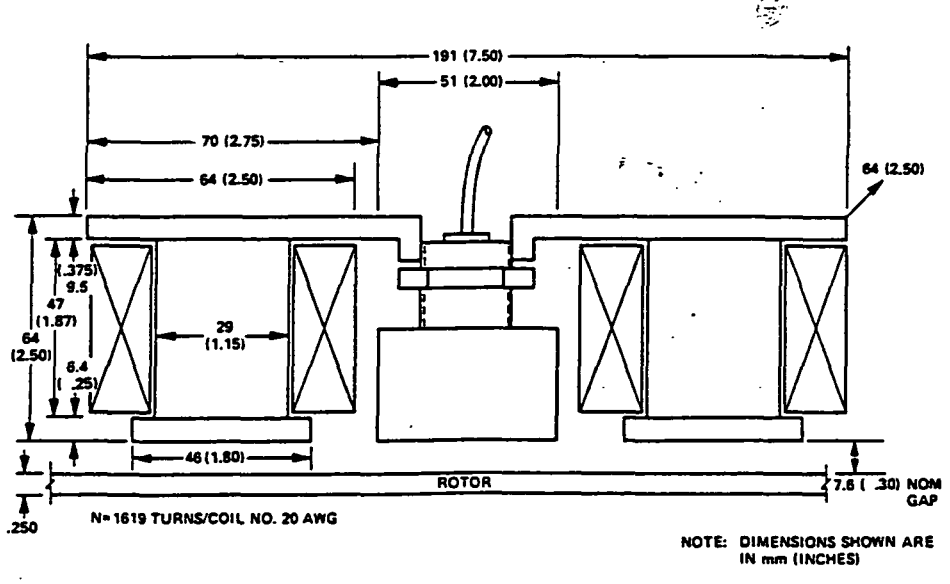

Figure 3 - Axial MBA Configuration (lower coils omitted for clarity)

$\pm$ 5.1mm respectively*. The magnetic actuators consist of a wire-wound magnetic coil and a core material manufactured out of 50% Nickel-Iron. The magnetic coils for the axial and radial MBAs are wound with 810 $\pm$ 1 turns of #20 AWG, HML insulated copper wire and 863 $\pm$ 1 turns of #22 AWG, HML insulated copper wire, respectively, with two coils connected in series.

Proximity sensors

The proximity sensors used on the ASPS were developed by Kaman Instrumentation, and are still commercially available. These noncontacting sensors use the principle of variable impedance caused by eddy currents that are induced in the conductive target by the sensor coil. Table 1 is a list of sensor characteristics. The coil in the sensor is driven by a 10 MHz crystal-controlled oscillator. Excitation of the sensor coil generates an electromagnetic field that couples with the target. The gap between the sensor and target affects the strength of the electromagnetic coupling. The changing gap causes the impedance of the coil to vary, which unbalances the bridge network in the electronic package. The MBAs use two sensors one on each side of the iron rotor. The signals from each sensor are demodulated and differenced in an electronic package mounted on the VPA under one of the radial MBAs.

Roll Motor

The roll motor used on the ASPS is an AC Linear Induction Motor [1]. The motor also incorporates proximity sensors to permit compensation for the radial attractive forces produced in the two motor segment windings. The roll motor produces a maximum of 0.677 Nm of torque in its high excitation mode of operation. The radial force associated with the maximum torque is less then 1.56 N.

Vernier Latches

Five vernier latches, located on the baseplate of the VPA, support the iron rotor for launch and recovery maneuvers. The latches locate and lock the rotor into a center position. Locking the rotor down prevents damage to the MBAs, proximity sensors, and data transfer electronics during maneuvering.

Control Electronics Rack

The control electronic rack was a free standing rack that connected to the VPA through flexible cables, but was intended for laboratory test use only. The electronic assembly contains

*The axial MBA's have had the gap modified from a nominal gap of 7.6mm to 4.31mm in order to suspend the rotor in a one-g enviornment.

the nessesary hardware to drive the actuators, position sensors, and roll motor of the vernier pointing assembly. One of the major goals of the current work was to replace this system with up-to-date hardware, which will be discussed in more detail shortly.

Balance and Testing Fixture

The balance and testing fixture was used to simulate a zero-gravity environment. The apparatus consists of a counter-balancing system to unload the payload mounting plate and vernier pointing assembly in an attempt to simulate orbiter conditions. Tests using this fixture were performed on servo dynamics, decoupling control, stability during cross-axis disturbances, and a variety of other parameters [1,3].

HARDWARE ANALYSIS AND MODIFICATIONS

Magnetic Circuit Analysis

To estimate the force between the MBAs and the rotor the method of Virtual Work was used. Calculation of the change in magnetic energy in a device in which there are moving parts is a simple method of calculating the forces on moving parts in the device [4]. Simply stated, the change in energy, ΔW is equal to the force, F multiplied by the displacement of the body, Δd ($\Delta W = F\Delta d$). Assuming the permeability of Nickel-Iron to be infinite and that the permeability in the air gap remains constant as the body is displaced through a distance Δd, then the energy W is equal to

$$W = \frac{1}{2}\int_v \mu_o H^2 dV \approx \mu_o H^2 Sl$$

where H is the field intensity in the gap. Using Ampere's law for magnetic coils the field intensity can be found from $H2\ell = NI$ where N is the number of turns in the magnetic coils, I is the current in the coil, and ℓ is the length of the air gap. To calculate the force exerted on the rotor, shown in Figure 4 :

$$W_1 = \tfrac{1}{2}\mu_o H_1^2 S\ell_1 2 = \left(\frac{NI}{2\ell_1}\right)^2 S\ell_1 \quad \text{and} \quad W_2 = \left(\frac{NI}{2\ell_2}\right)^2 S\ell_2$$

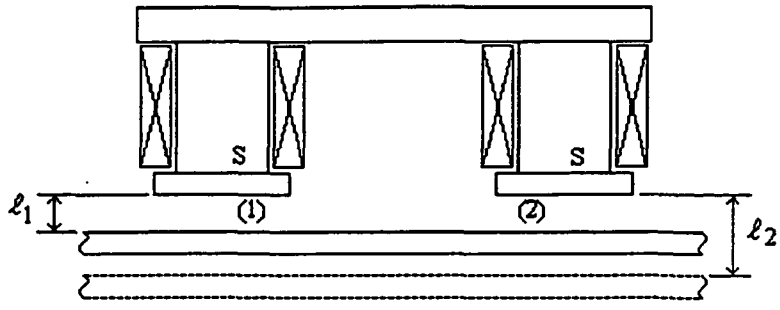

Figure 4 - Magnetic Circuit of an MBA with Movable Rotor.

The force between the rotor and the fixed part of the actuator can then be found by :

$$F = \frac{(W_2\text{-}W_1)}{(\ell_2\text{-}\ell_1)} = \frac{\mu_o N^2 I^2 S}{4\ell_1\ell_2}$$

Where $\ell_1 = \ell_2 = 3.41\ mm$; $S = 1.58 \times 10^{-3}\ m^2$; $N = 1620$. By rearranging the above equation for current, I gives the following :

$$I = \frac{1}{N}\sqrt{\frac{\ell_1\ell_2 F}{\mu_o S}} = \frac{1}{N}\sqrt{\frac{g^2 F}{\mu_o S}}$$

Where $F = \frac{1}{3}M$, where M is equal to the mass of the rotor, the current needed to suspend the rotor at an air gap of $g = 3.41mm$ is found to be 0.794 Amps. Alternative calculations using the more traditional circuit model give nearly identical results.

Control Approach

A block diagram of the proposed control system is shown in Figure 5. If the time interval between each input sample is small compared to the time constant of the actuator and process (high sampling rate), the system essentially acts as a continuous system [5]. This allows the A/D and D/A converters to be transparent in the preliminary control system design. The initial controller will be a simple proportional-derivative (PD) type. The plant comprises power amplifiers, the actuators, and the suspended mass. Feedback in the control loop is a measure of suspended mass (rotor) displacement from steady state conditions. In order to predetermine the proportional gain, K_p, and the derivative gain, K_D, the accurate plant models are required. This is straightforward except for the MBAs, where the traditional linearized model is employed :

$$F \approx \frac{\mu_o N^2 I_o^2 S}{g^2} + \frac{2\mu_o N^2 I_o S}{g^2} i = F_o + \frac{\partial F}{\partial i} i \qquad \text{where} \qquad I^2 \approx I_o^2 + 2I_o i$$

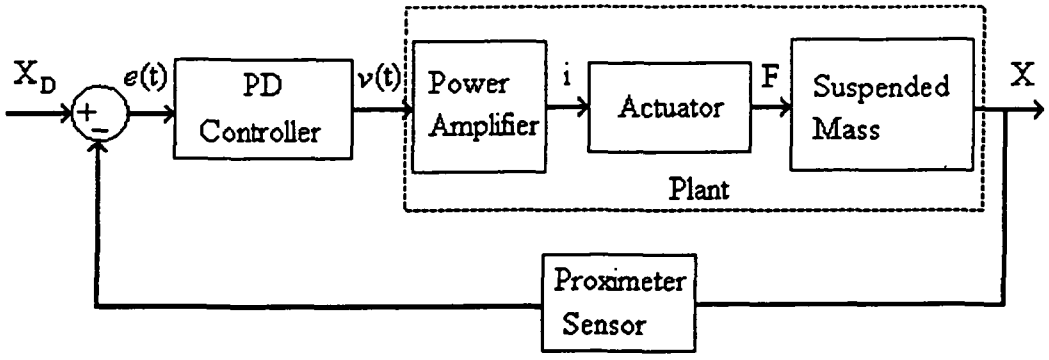

Figure 5 - Block diagram of the ASPS control system.

Figure 6 shows the control system transfer functions :

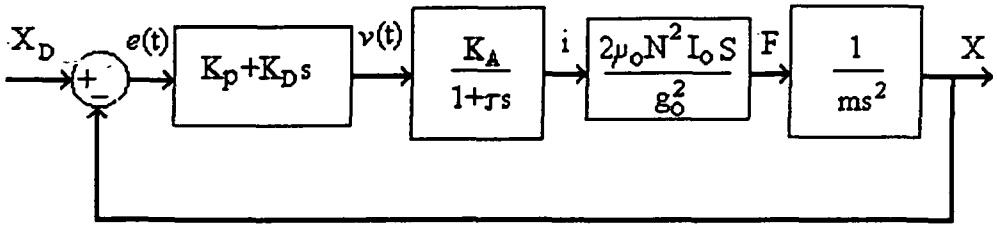

Figure 6 - ASPS component transfer functions

Finally, the transfer function representing the power amplifiers was verified by frequency response analysis of the amplifier using a signal analyzer. A break frequency of approximately 35 Hz was established. Table 1 summarizes all the required constants :

K_A	1.201 $\frac{\text{Amps}}{\text{volt}}$
τ	.00455 sec
μ_o	$4\pi \times 10^{-7} \frac{\text{H}}{\text{m}}$
N	$810 \frac{\text{turns}}{\text{coil}}$
I_o	1.25 amps*
S	1641.7 mm^2
g_o	3.41 mm
m	7.19 kg

Table 1 - Summary of constants used in transfer functions.

*Experimentally determined value.

With a ratio of $\frac{K_D}{K_p}$=0.1 the closed-loop transfer function of the system shown in Figure 6 is as follows :

$$K \frac{34.949\ s + 349.49}{0.0327\ s^3 + 7.19\ s^2}$$

The root locus plot of this system shows that the system is stable for a range of K from 0 to 10. An overall gain of 4.5 corresponding to a damping ratio of 0.7 can be determine graphically from Figure 7.

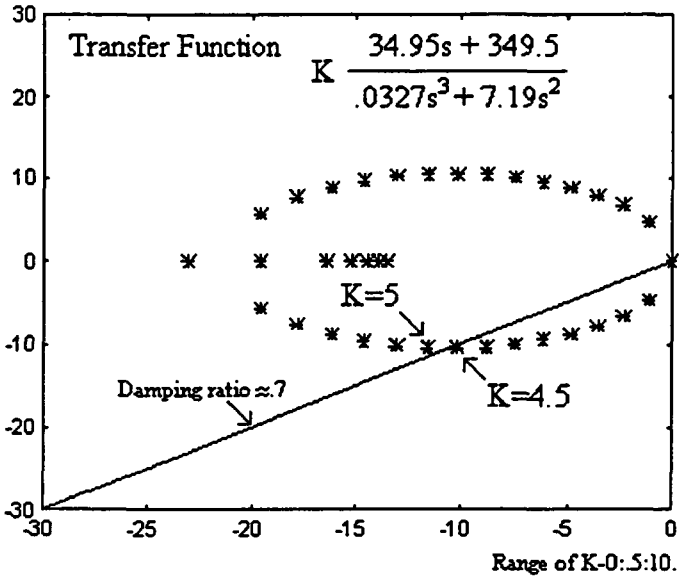

Figure 7 - Root locus for the PD controller.

Modifications to the Magnetic Bearing Assemblies

The first step in recommissioning the VPA was to modify the three axial MBAs so that the rotor could be suspended in a 1-g environment. To accomplish this the gap between the magnetic actuators and the rotor was reduced 54.5%, such that the current needed to suspend the rotor at the new gap was predicted (and verified by testing) to be low enough not to cause overheating of the magnetic coils. To implement the new air-gap, the top plate as shown in Figure 8 was remanufactured with a thickness change from 6.35 mm to 9.53 mm. This new thickness would extend the core material of the magnetic bearing assembly, and reduce the air gap between the top plate and the iron rotor from 7.62 mm to 3.41 mm. The radial magnetic bearing assemblies were not modified.

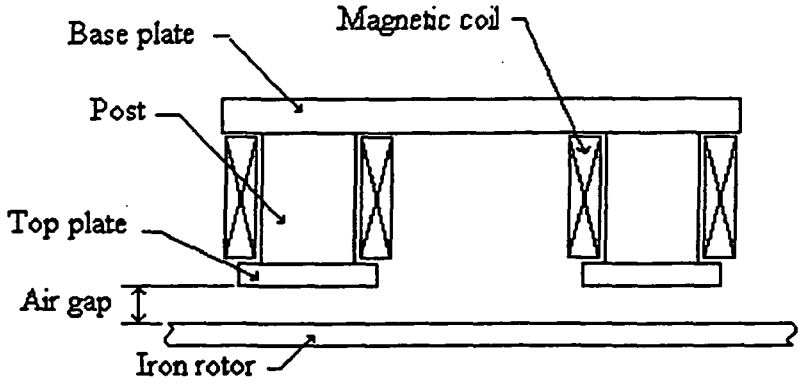

Figure 8 - Magnetic Bearing Assembly.

Digital Controller

The controller hardware comprises a 486DX4-33 PC with 12-bit A/D and D/A boards [6,7]. A counter/timer board was installed to interrupt the main program in order to perform the input/output at a regularly scheduled time interval. The power amplifiers selected to provide power to the magnetic actuators are commercial PWM types [8]. The switching frequency is 22kHz. The controller software was written using Microsoft Quick C and implemented the simple PD controller described earlier. Rate information is estimated by simple differencing of succesive position samples. A block diagram of the new hardware is shown in Figure 9.

Each bearing station is controlled independantly. This is possible since each has similar dynamics, and the geometry of the system is such that cross-coupling between actuators and system degrees-of-freedom is minimized. It should be noted that extensive coupling is introduced with a payload added, due to the large C.G. offset. Further, the magnetic actuators are quite non-linear, requiring a superior linearizing strategy if operation over the full range of displacements or tilt angles is anticipated. The original control system design incoporated many linearizing, mixing, and feedforward stages for these reasons [1].

OPERATION

The system is operational, with a typical time history from axial MBA station C shown in Figure 10. The large transient around 3 seconds corresponds to the release of the vernier latch at that station. As can be seen, excessive sensor noise currently hampers performance somewhat, but this appears to be due to improper wiring, grounding and shielding practices. Additional signal conditioning is currently being studied.

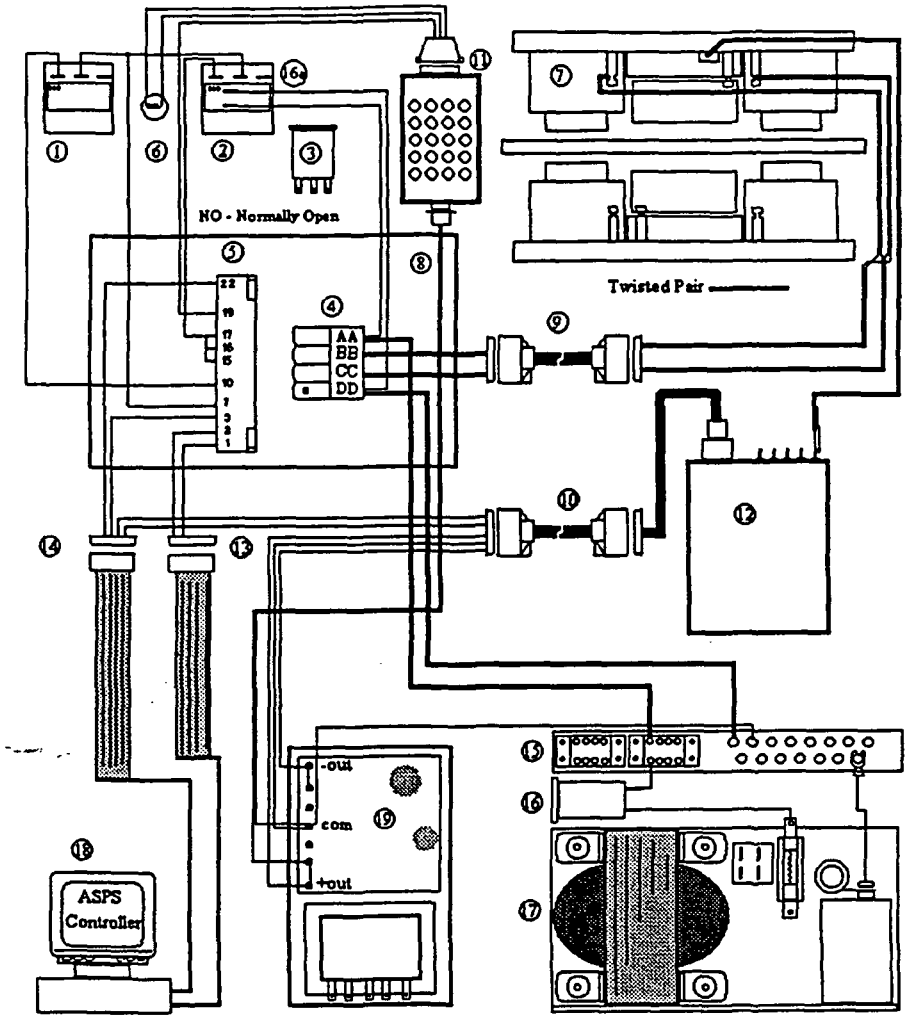

Figure 9 - Schematic Diagram of Revised ASPS Controller and Supporting Hardware

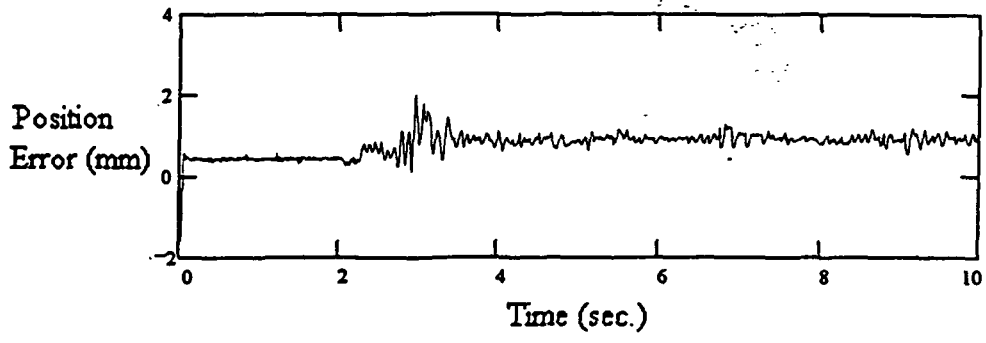

Figure 10 - Typical Time History, MBA station C, showing "launch" transient

CONCLUSIONS

The VPA has been successfully recommissioned and operated with five degree-of-freedom control.

ACKNOWLEDGEMENTS

This work was partially supported by NASA Grant NAG-1-1056, Technical Monitor Nelson J. Groom, and by the NASA/USRA Advanced Design Program administered by the Universities Space Research Association.

REFERENCES

1 Cunningham, D.C., et al. Design of the Annular Suspension and Pointing System (ASPS). NASA CR-3343, October 1980.

2 Britcher, C.P., Groom, N.J., Current and Future Development of the Annular Suspension and Pointing System. 4th International Symposium on Magnetic Bearings, Zurich, Switzerland, August 1994.

3 Final Report "The Development of the ASPS Vernier System", Sperry Corporation Flight Systems Phonix, AZ. Contract No.NAS1-15008, June 1983.

4 Ida, Bastos,"Electromagnetics and Calculations of Fields", Copy right 1992, Springer-Verlag, New York, Inc.

5 Richard C. Dorf,"Modern Control Systems",Sixth Edition, Addison-Wesley Publishing Company, 1992.

6 *Users Guide of the DAS-1402 Data Acquisition Boards, Keithley MetraByte Corporation.*

7 Users Guide of the DDA-06 Data Acquisition Board, Keithley MetraByte Corporation.

8 PWM Amplifier Catalog, Copley Controls Corporation.